TR- 104 Vol 2
1980

Heat Transport in Groundwater Systems – Laboratory Model

D.B. Reed
D.L. Reddell

Texas Water Resources Institute

Texas A&M University

RESEARCH PROJECT COMPLETION REPORT

Project Number A-039-TEX
(July 1, 1976 - December 31, 1978)

Agreement Numbers
14-34-0001-7091
14-34-0001-7092
14-34-0001-8046

HEAT TRANSPORT IN GROUNDWATER SYSTEMS
VOL. II - LABORATORY MODEL

David Bryan Reed
Donald L. Reddell

The work on which this publication is based was supported in part by funds provided by the Office of Water Research and Technology (Project A-039-TEX), U.S. Department of the Interior, Washington, D.C., as authorized by the Water Research and Development Act of 1978.

Technical Report No. 104 - Vol. II
Texas Water Resources Institute
Texas A&M University

August 1980

ABSTRACT

Heat Transport in Groundwater Systems

Vol. II - Laboratory Model

by

David Bryan Reed

and

Donald L. Reddell

Solar energy is a promising alternate energy source for space heating. A method of economic long term solar energy storage is needed. Researchers have proposed storing solar energy by injecting hot water heated using solar collectors into groundwater aquifers for long term energy storage. Analytical solutions are available that predict water temperatures as hot water is injected into a groundwater aquifer, but little field and laboratory data are available to verify these models. The objectives of this study were to construct a laboratory model to simulate hot water injection into a confined aquifer, to use data from the model to verify analytical solutions modeling this process, and to evaluate the effects of physical properties and design parameters on thermal recovery efficiency.

Initial studies of hot water injection into underground reservoirs were done by the petroleum industry while studying secondary and tertiary oil recovery methods. These studies involved small laboratory models. Advances in computer technology made it possible to model these systems numerically. Many assumptions must be made to predict temperature distributions and thermal efficiencies using analytical

models which are not required in numerical solutions.

To simulate hot water injection into a confined aquifer, a laboratory model (a 1.8288 m deep, 0.2 radian sector tank, that was 7.01 m in the radial direction) was constructed. There were 39 temperature and 15 fluid pressure measuring locations through the model. Water was supplied to the model at a constant temperature and flow rate. The flow layer was composed of a fine grained Texblast blasting sand. Four runs were made. During the initial run, no heat transfer took place and the hydraulic conductivity was measured. Three runs were made where the heat transfer was monitored.

Water level data from the heat transfer runs showed that as the temperature of the aquifer increased, the hydraulic conductivity increased. Temperature data indicated that the three radii closest to the well bore reached thermal equilibrium. The equilibrium temperature decreased as radius increased. From Run 1 to Run 2, the equilibrium temperature increased at each radius because a larger flow rate was used. A vertical thermal gradient existed in the flow layer with the less dense warm water floating out over the cooler more dense water initially in the model. During the pumping cycle, the temperatures gradually decreased.

The temperature of the water as it was pumped out of the model was measured and the energy recovered was computed using the initial temperature as a reference. Various other temperatures were used as a base reference to calculate recovery efficiency.

There were heat losses out the sides of the model. The assumption of angular symmetry made in all analytical solutions was there-

fore not met. For this reason, the analytical solutions showed adequate, but not great, agreement with the experimental temperature distributions.

Using the analytical solutions, the effects of changing system design parameters were evaluated. Increasing thermal conductivity in the flow layer caused the temperature distribution to spread out but had no effect on thermal efficiency. Increasing the thermal conductivity in the confining layers caused the temperature profile to not move as far from the well, and decreased thermal efficiency. Injection rates are only indirectly related to thermal efficiency. The physical parameter having the greatest effect on thermal efficiency was the flow layer thickness. As thickness increased, thermal efficiency increased.

ACKNOWLEDGEMENTS

The authors wish to express appreciation to Dr. Terry A. Howell, Dr. John L. Nieber, Dr. Jack R. Runkles, and Dr. David J. Norton for their review of the manuscript and their helpful comments and corrections. A special thanks goes to Phil Barnes and Lynn Ebeling who were always a help in solving problems that arose, and to Steve Raabe, Howard Frerich, Jerry Richardson, John Bonn, Charles Bordovsky, and Annette Vaandrager who aided in data collection and presentation. The help of Karen Hall is greatly appreciated.

The authors are also grateful to the Department of Agricultural Engineering (Dr. E. A. Hiler, Head), the Texas Water Resources Institute (Dr. J. R. Runkles, Director), and the Center for Energy and Mineral Resources (Dr. Spencer R. Baen, Director) at Texas A&M University for providing the financial assistance for this study.

TABLE OF CONTENTS

TABLE OF CONTENTS (continued)

LIST OF TABLES

LIST OF FIGURES

LIST OF FIGURES (continued)

LIST OF FIGURES (continued)

CHAPTER I

INTRODUCTION

The Arab oil embargo of 1974 and the resulting rise in energy costs have made people in the United States realize the need for developing alternate energy sources. The harsh winters of 1976-77 and 1977-78 made people even more aware of the need to find alternate energy sources for space heating. Kenward (1976) cited coal, nuclear fission, fusion, geothermal energy, and solar energy as potential alternate energy sources to replace natural gas and oil. Of these, solar energy is one of the most promising alternate energy sources for space heating and cooling.

Solar energy is not a new energy source. Meinel and Meinel (1976) reported the use of solar energy to power furnaces before the time of Christ. The eighteenth and nineteenth century saw the development of solar motors and several patents were issued for this invention. By the beginning of the twentieth century, solar energy was generally considered economical only in extremely remote areas.

With the recent price escalation of conventional energy sources, interest in developing economical solar energy systems has increased. Kenward (1976) estimated that the sun supplies more energy to the Earth in one day than will be used in 25,000 years at our present rate of consumption. The primary problem in utilizing this vast energy resource is that solar insolation is at a maximum during the summer when energy

for space heating is needed least. Conversely, it is a minimum during the winter when most needed.

A method of storing solar energy for long periods of time is needed. According to Duffie and Beckman (1976), the current methods of storing solar energy are:

1. An insulated tank for a liquid system,
2. Pebble beds for an air system, and
3. Latent heat from a phase transition of a chemical compound.

The third system holds possibilities for long term solar energy storage but much more research is needed. Air and liquid systems allow only limited storage which results in the need for a conventional auxiliary heating system to back up the solar heating system during prolonged periods of cold weather with little sunshine. Because of the increased initial cost of an auxiliary system, much of the attractiveness of a solar heating system is eliminated. To overcome this problem, a method of storing solar energy for extended periods of time is needed.

In most areas of the Earth, groundwater aquifers underlie the ground surface. These aquifers have the ability to receive or yield large volumes of water but vary greatly in depth, porosity, and water quality. Combining aquifer availability with the knowledge that the Earth is a good insulator and water has a relatively high specific heat gives the basis for long term solar energy storage by injecting hot water into groundwater aquifers.

To use groundwater aquifers effectively for thermal energy storage, models to predict temperature profiles and heat losses from the aquifer are required. Numerical models and mathematical models are available for predicting water pressures and temperatures in confined aquifers when

water at a given temperature is injected into an aquifer with a different water temperature. However, limited field and laboratory data are available to verify these models. Thus, the objectives of this study are:

1. To design, construct, and instrument a physical laboratory model of a confined aquifer and simulate the injection and pumping of hot water into the aquifer,
2. To collect water temperature and pressure data from the physical model and compare these data with predictions obtained from existing mathematical models, and
3. To evaluate the effects of parameters such as injection rate, injection temperature, and aquifer thickness on thermal energy storage and the efficiency of energy recovery.

The physical laboratory model, coupled with mathematical and numerical models, will be very valuable in evaluating the effect of important system design parameters on the efficiency of storing thermal energy in groundwater aquifers.

CHAPTER II

REVIEW OF LITERATURE

Meyer and Todd (1973) were among the first to suggest thermal energy storage by injecting hot water into groundwater aquifers. Their calculations were based on injecting 99°C water at a rate of 0.05 m^3s^{-1}. They simulated five 90 day injection-pumping cycles into a 33 m thick confined aquifer. They assumed the hot water would float above the more dense cooler water in the aquifer, and form an inverted cone with a top radius of from 180 to 210 m. After the fifth injection cycle, 86 percent of the heat was recovered at a temperature greater than 82°C. The first four cycles were less efficient because some thermal energy was required to bring the aquifer to the temperature of the injected water. Above ground storage of energy recovered during their fifth injection cycle would have required a tank 33 m high and 130 m in diameter, plus insulation. This represented 2.8×10^{13}J of usuable energy for space heating.

Davison et al. (1975) proposed the "Solaterre" system which would use solar heaters to heat water during the summer. The resulting hot water would be stored in an aquifer until winter and would then be used for space heating. Using a utility-type distribution system, a large number of homes could be heated with the stored hot water. The "Solaterre" system also included a chilling pond to cool water during the winter. The cold water would be stored in the aquifer and used to cool homes in the summer. The distribution system used for heating would also be used for cooling. The aquifer was divided into four separate zones; two for heating and two for cooling. In a study of the

"Solaterre" system at Lubbock, Texas, Martin et al. (1974) found the system to be economically feasible.

Hot water injected into a groundwater aquifer can be 1/6 as viscous and 10 percent less dense than the natural groundwater. The hot water will tend to float over the cooler and more dense natural groundwater. Mass flow will be affected by the density and viscosity differences. Heat flow in the permeable flow region will be by both conduction and convection. Determining how hot water will move through a porous aquifer is a difficult process. At the present time, little work has been done in evaluating heat flow in a confined aquifer system. Even less work has been done in evaluating the thermal storage efficiency and the eventual thermal recovery efficiency.

Initial studies of hot fluid injection into underground reservoirs were done by the oil and gas industry developing secondary and tertiary oil recovery by hot water flooding and steam injection. Design work involved laboratory studies on core samples similar to those described by Breston and Pearman (1953) for the Pembian oil fields in Canada. Their design also included a trial and error procedure.

Preston and Hazen (1954) were among the first to publish laboratory results of hot water injection into an unconsolidated sand. The laboratory model consisted of a 7.62 cm (3 in) diameter column which varied in length from 15.32 cm (6.03 in) to 60.96 cm (24 in). Hot water was forced vertically downward at a constant rate and temperature. By measuring the temperature at the outlet port, Preston and Hazen (1954) were able to calculate a heat transfer coefficient between sand and water using an analytical solution by Schumann (1929).

Malofeev (1959) experimentally studied hot water injection in a linear laboratory model. The flow area was 2.54 cm (1 in) thick, 22.86 cm (9 in) wide, and 71.12 cm (28 in) long. The impermeable strata above and below were simulated by a clay layer 12.70 cm (5 in) thick. Pore water velocities ranged from 0.16 m/hr (0.52 ft/hr) to 1.27 m/hr (4.14 ft/hr). With thermocouples in the sand and clay layers, temperature distributions were measured as a function of time. Thermal efficiencies were calculated and found to agree with the analytical solution presented by Lauwerier (1955).

Baker (1967) studied hot fluid injection in a laboratory model and compared results with analytical solutions by Lauwerier (1955), Marx and Langheim (1959), and Rubinshtein (1959) and a computer simulation by Spillette (1965). The laboratory model simulated plane radial flow in a confined sand aquifer with a 10.16 cm (4 in) thick flow area and a maximum radial extent of 91.44 cm (36 in). To simplify the model the caprock and bedrock were composed of a saturated sand separated from the confined flow region by a 3.3 mm (0.013 in) thick layer of mylar plastic. The injection rates were kept constant during each run, and the injection temperature was 76.7°C (170°F). Temperatures were measured in the caprock, bedrock, and flow area using thermocouples. In the flow area, temperature distributions in the model compared favorably with those predicted by the analytical solutions. Predicted thermal efficiencies and heat losses using analytical solutions were in poor agreement with the laboratory data. Results indicated that thermal efficiency is dependent on flow rate. Baker (1969) later showed that heat losses from steam injection into a laboratory model agreed closely with the predicted values from analytical solutions.

Chappelear and Volek (1969) modeled steady state mass flow and unsteady state heat flow in a rectangular laboratory model composed of sand. The flow region was 10.24 cm (4 in) thick, 10.24 cm (4 in) wide, and 91.44 cm (36 in) long. The caprock and bedrock were simulated by dry limestone. Temperatures were measured with thermocouples. The system was modeled numerically, and results compared favorably with laboratory data. A comparison with the analytical solution by Lauwerier (1955) showed poor agreement.

Rabbimov et al. (1974b) constructed a linear laboratory model to simulate long term energy storage by injecting water heated by solar collectors into a groundwater aquifer. The flow area, composed of sand, was 10 cm (3.94 in) thick and 1 m (39.37 in) long. The confining layers consisted of clay, and temperatures were measured using thermocouples. Fluid fluxes ranged from 15.8×10^{-2} m/hr (5.184×10^{-2} ft/hr) to 79×10^{-2} m/hr (25.92×10^{-2}).

According to Spillette (1965), the differential equation governing heat transport in a porous media is:

$$\nabla \cdot K \nabla T - \nabla \cdot (\rho_f C_f \overline{V} T) = \frac{\partial}{\partial t}(\rho_l C_l T) \qquad (1)$$

where $\rho_l C_l = \phi(\rho_f C_f) + (1.0-\phi)\rho_r C_r$;

T = temperature (deg);

K = thermal conductivity ($FT^{-1}deg^{-1}$);

ρ = density (ML^{-3});

C = specific heat ($FLM^{-1}deg^{-1}$);

$\overline{V}$ = fluid pore water velocity vector (LT^{-1});

t = time (T);

ϕ = porosity (fraction); and

∇ = vector "del" operator (L^{-1}).

The subscripts denote the following media properties:

f = flowing fluid properties;

r = porous media or rock properties; and

1 = combined porous media and fluid properties.

Equation (1) is valid for any coordinate system, contains both conductive and convective heat transfer, and is valid for a non-homogenous, anisotropic porous media. One assumption inherent in this equation is that an instantaneous thermal equilibrium exists between the water and porous media; i.e., a grain of sand instantaneously reaches the temperature of the surrounding fluid. This assumption is made in all useful mathematical and numerical models of heat transport in porous media.

In obtaining analytical solutions for the hot water injection problem, additional simplifying assumptions are necessary. Incompressible, one-dimensional mass flow, two-dimensional heat flow, with constant physical properties are the only cases for which analytical solutions are available. In many cases, assumptions concerning thermal conductivity are made to restrict heat flow to certain directions; thus simplifying the problem. Theoretical developments and analytical solutions are discussed in Chapter 3.

Before the recent advances in computer technology, mathematical models were the only practical way to analyze a problem as complex as combined heat and mass transfer in porous media. Recent advances in computer technology have made it possible to numerically analyze problems as complicated as Equation (1). Simplifications necessary to solve

Equation (1) analytically are not necessary in existing computer simulations. Numerical models can analyze heat transfer and fluid flow in anisotropic, non-homogenous aquifer in all three directions. Mass flow does not have to be considered separately from heat transfer as is required in analytical solutions.

Fournier (1965) used the Buckley-Leverett displacement theory and an analytical solution by Lauwerier (1955) to derive a differential equation describing hot water injection for oil recovery in a radial system. Using Milne's predictor-corrector scheme to solve the finite difference equations, Fournier (1965) was able to calculate water saturations and temperatures in the reservoir.

Gottfried (1965) developed a sophisticated numerical model to simulate thermal oil recovery in a linear system. In his three-phase (oil, gas, water) flow model, seven non-linear partial differential equations with variable coefficients were used to solve for temperatures, pressures, saturations, and mass fractions as functions of time and space.

Using an analytical solution, Davidson et al. (1967) evaluated temperatures after the injection and condensation cycles in a cyclic steam injection process. The production or backflow cycle was modeled numerically to calculate oil recovery and temperature.

Spillette (1965) modeled hot water injection in a groundwater aquifer using a one-dimensional radial mass flow model and a two-dimensional heat transfer model. The thermal properties and the injection temperature were held constant, but they could easily have been functions of time and temperature. The energy balance equation was solved by the method of characteristics. Results compared favorably with Rubinshtein's

(1959) analytical solution for thermal efficiency and the temperature distribution obtained in a laboratory study by Malofeev (1959).

Flock et al. (1967) developed a one-dimensional incompressible mass flow model and a heat flow model for the radial and vertical directions. To simulate steam injection, a step function approach like Marx and Langheim (1959) was used. All thermal conductivities had finite values except the vertical thermal conductivity in the flow layer which was assumed infinite. Numerical results, considering two-dimensional heat flow in the strata above and below the aquifer, compared favorably with Marx and Langheim's (1959) analytical solution.

Chappelear and Volek (1969) modeled hot water injection into a saturated sand layer surrounded by two impermeable layers using a numerical model and a laboratory model. Assuming incompressible mass flow, the elliptic mass flow equation was solved by successive over relaxation (SOR) and the parabolic heat flow equation was solved by an explicit approximation. Viscosity was a function of temperature. The numerical results compared more favorably to the laboratory results than did the analytical solution of Marx and Langheim (1955).

Weinstein (1972) used a semi-analytic approach to solve for temperature distributions in an aquifer and its confining layers during hot fluid injection. Solving the mass and energy balance equations simultaneously, excessive computer storage and computation time were avoided. The semi-analytic method approximates the overburden temperature as a function of height above the aquifer. This temperature function is combined with finite difference equations for temperature and pressure in the aquifer to determine the temperature distribution in the confining

layers. This method resulted in a 40 percent saving in computer time as compared to a fully finite difference technique. Answers were within 15 percent of a fully finite difference technique.

Ebeling and Reddell (1976) studied several aspects of the hot water injection and storage problem and the "Solaterre" system proposed by Davison et al. (1975). Possible aquifer sites were investigated for several locations in Texas. The volumes of hot water capable of being produced by solar collectors at several locations in Texas were computed using a numerical model. They also developed a three-dimensional numerical model in cylindrical coordinates to simulate hot water injection into an anisotropic, non-homogenous, confined aquifer. The media and fluid properties were considered functions of both pressure and temperature. The problem was set up in finite difference form and solved using an unconditionally stable Crank-Nicholson method.

Reed (1977) modeled hot water injection into a confined aquifer with one-dimensional mass flow and "pseudo" two-dimensional heat flow. Density varied with temperature and pressure while all other properties were held constant. Temperatures were constant in the vertical direction in the aquifer. "Pseudo" two-dimensional heat flow refers to the fact that heat losses out the top and bottom of the aquifer were calculated using a heat loss coefficient as employed by Rabbimov et al. (1974a).

Numerical modeling is important in studying hot water and steam injection into underground reservoirs. Fluid physical and thermal properties can be made functions of both temperature and pressure. However, excessive storage requirements and computation time are needed to solve coupled mass and heat flow problems. Numerical models combined with analytical solutions can reduce storage requirements and computer

time, and yet be very useful in determining how parameters such as injection rate, injection temperature, aquifer thickness, and fluid properties affect thermal energy storage in aquifers.

CHAPTER III

THEORETICAL DEVELOPMENTS

Theoretical studies of hot fluid injection into confined aquifers involve predicting temperature as a function of time and space within the aquifer. Ramey (1967) indicated that the usual procedure was to consider heat and fluid flow separately. Baker (1967) justified the separate treatment of heat and mass transfer by assuming that only a single fluid exists in the porous media. If two fluids are present, the fluid is assumed to be a mixture of the two.

According to Spillette (1965), the differential equation governing heat transfer in a porous media is:

$$\nabla \cdot K \nabla T - \nabla \cdot (\rho_f C_f \bar{V} T) = \frac{\partial}{\partial t}(\rho_1 C_1 T) \qquad (2)$$

where $\rho_1 C_1 = \phi(\rho_f C_f) + (1.0-\phi)\rho_r C_r$ $(FL^{-2}deg^{-1})$;

T = temperature (deg);

K = thermal conductivity $(FT^{-1}deg^{-1})$;

ρ = density (ML^{-3});

C = specific heat $(FLM^{-1}deg^{-1})$;

$\bar{V}$ = fluid pore water velocity vector (LT^{-1});

t = time (T);

ϕ = porosity fraction; and

∇ = vector "del" operator.

The subscripts denote the following media properties:

f = flowing fluid ;

r = porous media or rock properties; and

1 = combined porous media and fluid properties.

To obtain a solution to Equation (2), many simplifying assumptions in addition to instantaneous thermal equilibrium must be made. Assuming one-dimensional mass flow, two-dimensional heat flow, constant fluid physical properties, and a homogenous and isotropic porous media for a cylindrical coordinate system, Equation (2) becomes:

$$K \frac{\partial^2 T}{\partial r^2} + K \frac{\partial^2 T}{\partial z^2} + \frac{1}{r} \left(K - \frac{Q \rho_w C_w}{2\pi h} \right) \frac{\partial T}{\partial r} = \rho_1 c_1 \frac{\partial T}{\partial t} \quad , \tag{3}$$

where r = radial distance from well (L);

Q = injection rate ($L^3 T^{-1}$);

h = aquifer thickness (L); and

z = vertical distance (L).

All other symbols have been previously defined. Equation (3) is derived in detail in Appendix A.

Additional simplifications of Equation (3) can be made by making assumptions concerning the thermal conductivity. Assuming that the acquifer has an infinite vertical thermal conductivity results in no temperature gradient vertically throughout the aquifer. The resulting temperature distribution will correspond to an average temperature at a given radius from the well. If the radial thermal conductivity in the flow area is assumed zero, then heat flow in the flow region is restricted to convective flow only. In the confining layers above and

below the aquifer, heat flow is restricted to vertical conduction by assuming that the radial thermal conductivity and mass flow in these layers is zero.

An early analytical study of hot fluid injection into a porous media was made by Schumann (1929) in which he assumed incompressible mass flow with constant fluid physical properties. However, Schumann (1929) did not assume an instantaneous thermal equilibrium between the sand and water. Thus, his solution required a heat transfer coefficient to evaluate the heat exchange between the fluid and porous media. Baker (1967) stated that the analytical work by Schumann (1929) and laboratory studies by Preston and Hazen (1954) justified the assumption that an instantaneous thermal equilibrium is reached between the fluid and the sand grain. All recent works have incorporated this assumption.

Lauwerier (1955) obtained an analytical solution to a hot water injection problem for incompressible flow in a linear system. He assumed no horizontal conduction in both the sand layer and the confining layers. Vertical thermal conductivity was assumed finite in the confining layers but infinite in the sand layer. For a constant injection rate and temperature, Lauwerier's (1955) solution for the temperature distribution in the flow area is:

$$\overline{T} = \text{erfc}\left[\frac{\xi/\theta}{2\sqrt{\tau/\theta-\xi/\theta}}\right] U(\tau-\xi) \qquad (4)$$

where $$\overline{T} = \frac{T - T_o}{T_i - T_o} \quad ;$$

$$\xi = \frac{4K_2 x}{h^2 \rho_f C_f V} \quad ;$$

$$\tau = \frac{4K_2 t}{h^2 \rho_1 C_1} \quad ;$$

$$\theta = \frac{\rho_1 C_1}{\rho_2 C_2} \quad ;$$

x = distance from injection interface (L);

V = fluid flux (LT^{-1});

T = aquifer temperature at x (deg);

T_i = injection temperature (deg);

T_o = initial aquifer temperature (deg);

erfc = complimentary error function;

U = unit step function defined as $U(\tau-\xi)=0$ when $\tau-\xi \leq 0$ and $U(\tau-\xi)=1$ when $\tau-\xi>0$, and

subscript 2 denotes properties of the confining strata above and below the aquifer. All other variables are as previously defined.

Marx and Langheim (1959) modeled the injection of steam or hot water into underground reservoirs. Using a step function approach, they were able to determine the expected heated area following thermal injection. Making the same assumptions as Lauwerier (1955), oil recovery was calculated. However, their solution is more applicable to steam injection than to hot fluid injection. Ramey (1959) expanded this concept and calculated the temperature distribution for underground combustion in a reservoir with a varying fuel injection rate. Landrum et al. (1960) analyzed a linear injection system and computed steam areas, hot water areas, and cold water areas using the Buckley-Leverett displacement theory. William et al. (1961) also used the Buckley-Leverett displacement theory and applied it to a radial system. However, they were

unable to separate the injection region into steam, hot water, and cold water regions.

The Russians have been very active in formulating mathematical models of thermal injection into groundwater reservoirs. Malofeev (1960) used Lauwerier's (1955) solution for a linear system and made it applicable to a radial coordinate system by changing the dimensionless parameter, ξ, to:

$$\xi = \frac{4K_2\pi r^2}{h\rho_f C_f Q}$$

where Q = injection rate (L^3T^{-1}); and

r = radial distance from the well (L).

Assuming a non-zero horizontal thermal conductivity (K_1) in the sand layer, Avdonin (1964) obtained a solution for the temperature distribution in a radial coordinate system. His solution was:

$$\overline{T} = \frac{1}{\Gamma(\nu)}\left(\frac{R}{4\lambda\tau}\right)^{\nu}\int_0^1 \exp\left(\frac{-R^2}{4\lambda\tau y}\right)\operatorname{erfc}\left(\frac{y\sqrt{\tau/\lambda}}{2a\sqrt{1-y}}\right)\frac{dy}{y^{\nu+1}} \qquad (5)$$

where $\nu = \frac{Q\rho_f C_f}{4\pi h K_1}$;

K_1 = horizontal thermal conductivity in the aquifer ($FT^{-1}deg^{-1}$) ;

$\lambda = \frac{K_1}{K_2}$;

$a = \sqrt{\frac{K_2\rho_1 C_1}{K_1\rho_2 C_2}}$

$R = \frac{2r}{h}$; and

y = an integration parameter.

The term, $\Gamma(\nu)$, is the gamma function of ν. All other terms were previously defined.

Thermal efficiency, ε, is defined as a fraction of the injected energy which remains in the aquifer at a given time after injection. This is very important when evaluating the total energy recovery from an injection pumping cycle. Assuming a constant isotropic thermal conductivity in both the flow layer and confining strata, Rubinshtein (1959) was able to solve the energy equation for thermal efficiency but not for the temperature distribution. His solution for thermal efficiency in a homogenous isotropic sand with confining layers of caprock and bedrock are:

$$\varepsilon = 1-(1-\alpha)\left\{\frac{2}{3}\sqrt{\frac{\lambda\tau}{\pi}}\left[1-(1-\alpha)\sum_{n=1}^{\infty}\alpha^{n-1}\left(1+\frac{n^2}{\lambda\tau}\right)e^{-\frac{n^2}{\lambda\tau}}\right]\right.$$

$$\left. + (1-\alpha)\sum_{n=1}^{\infty} n\alpha^{n-1}\left(1+\frac{2n^2}{3\lambda\tau}\right)\operatorname{erfc}\left(\frac{n}{\sqrt{\lambda\tau}}\right)\right\} , \qquad (6)$$

where ε = thermal efficiency (fraction); and

$\alpha = \frac{\lambda a-1}{\lambda a+1}$.

All other parameters were previously defined. Ramey (1964) presented a solution for thermal efficiency as derived from the temperature distribution of Lauwerier (1955). The solution was:

$$\epsilon = \frac{\theta}{\tau}\left[2\sqrt{\frac{\tau}{\theta\pi}} - 1+e^{\tau/\theta}\,\mathrm{erfc}\sqrt{\frac{\tau}{\theta}}\right] \quad . \tag{7}$$

An examination of Equations (6) and (7) indicates that thermal efficiency is not directly dependent upon flowrate or injection temperature. However, it is a function of time, aquifer thickness, and the ratios of thermal conductivity, density, and specific heat in the aquifer and confining layers. However, the injection rate is indirectly involved in the time of injection. For example, if a given amount of heat energy is injected, then the flow rate could be increased and the time of injection decreased, resulting in less heat energy loss.

Thomas (1964) modeled conduction heating in underground systems with little or no permeability. This corresponded to underground reservoirs with thick heavy oils where convective heat transfer was negligible. Making thermal conductivities a function of temperature, the temperature distribution was calculated for a constant heat injection rate using a step-function approach. Thomas (1967) obtained three solutions for hot water injection into a confined aquifer. All three solutions assumed convective heat transfer would dominate and neglected conduction in the sand layer. The range of validity for such an assumption was evaluated. The first solution was obtained by mapping the problem into a new coordinate system, the second solution was obtained by a weighted residuals method, and the third solution was obtained by using Laplace transforms. The first solution was the simplest and was considered the best of the three because it more closely matched computer data of Spillette (1965).

Rabbimov et al. (1974a) mathematically studied solar energy accumulation by injecting hot water into a groundwater aquifer. Heat losses to the confining layers were assumed proportional to the difference between the present aquifer temperature and its initial temperature. The proportionality factor was defined as a heat loss coefficient. His solution was for a pair of wells, one injecting and one pumping simultaneously, called a doublet.

Gringarten and Sauty (1975) modeled steady state mass flow and unsteady state heat flow while injecting hot water into a confined aquifer. They neglected the horizontal thermal conductivity in the aquifer and assumed an infinite vertical thermal conductivity in the flow region. Holding all physical properties constant, they used Lauwerier's (1955) approach to obtain a solution in radial coordinates for a single injection well. By modifying the solution for a single well, the temperature distribution for a doublet was determined. Resulting temperatures at the pumping well were also obtained.

In designing systems for storing energy by injecting hot water into groundwater aquifers, mathematical models can play an important part. With mathematical models, design parameters are more easily identified and the effects evaluated. Because simplifying assumptions are required to solve the problem analytically, work is needed to determine the validity of these solutions and assumptions and incorporate these solutions into design procedures.

CHAPTER IV

LABORATORY MODEL

A laboratory model was constructed to simulate the injecting or pumping of hot water into a confined aquifer. Instrumentation monitored movement of the heat front as hot water moved through the model. The model, in the shape of a sector tank of 0.2 radians (11.46°), was constructed of 0.64 cm (1/4 in) steel plates, 182.9 cm (6 ft) high, and 7.57 m (24 ft) in length (radial direction) as shown in Figure 1. The model simulated two-dimensional heat flow in the vertical and radial direction and one-dimensional plane radial flow for a cylindrical coordinate system. Symmetry was assumed in the angular direction.

The well was 0.3048 m (1 ft) in radius and located at the apex of the sector. Water was supplied to the well through a 1.91 cm (3/4 in) nominal size pipe with 0.64 cm (1/4 in) holes drilled 6.35 cm (2 1/2 in) apart along the length of the pipe. The holes were covered with 100 mesh wire screen. A storage tank 0.3048 m (1 ft) wide, was located at the outer boundary of the sector tank and maintained at a constant head. Water pressures were maintained at a sufficient level to assure that the flow area would always be saturated. The model was insulated with 0.1524 m (6 in) of Owens Corning* Fiberglass insulation with an R value of 2.28 $m^2°C/w$ (19 $hrft^2°F/Btu$).

*Trade names are used in this paper solely for the purpose of providing specific information. Mention of trade names does not constitute a guarantee or warranty of the product by the Texas A&M System or an endorsement by the University over other products not mentioned.

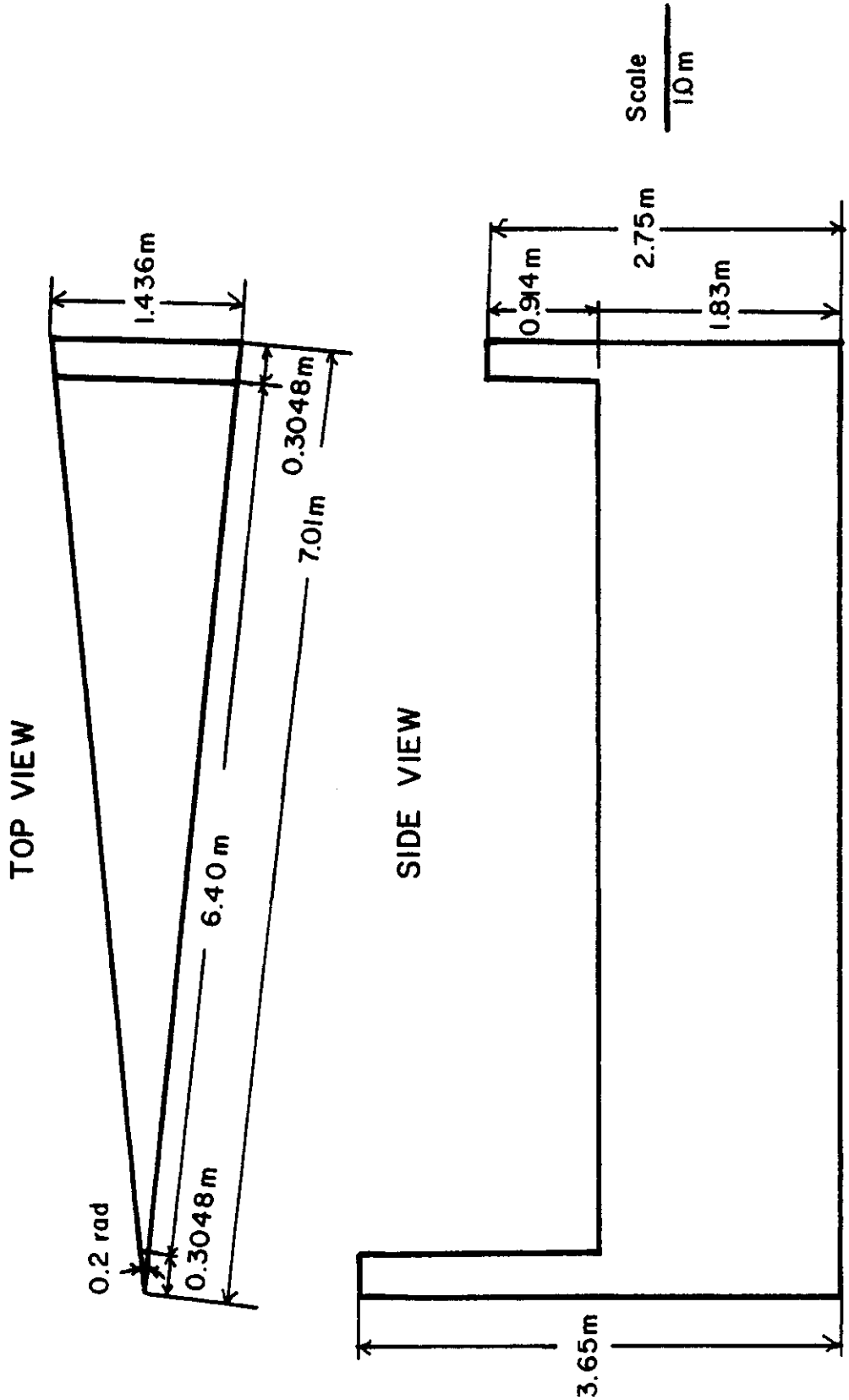

Figure 1. Schematic of the laboratory model.

Water was supplied to the model at a constant temperature and flowrate. The water was initially heated to approximately 60°C (140°F) by a 0.11 m^3 (30 gal) Jackson hot water heater with two 4500 watt heating elements and injected into a constant temperature bath where the temperature was controlled by a Polyscience Model 1266 immersion circulator-controller. Using a Masterflex Tubing Pump #7545, water was supplied to the apex of the well at a constant flowrate. The flowrate was measured by a Brooks Micro-Oval II pulsing flowmeter. For each 5 cm^3 of flow, the flowmeter gave an electrical pulse which was counted by a frequency counter. As the water entered the model, the temperature was measured using a thermistor.

Water pressures were measured using piezometer tubes. Since only positive gage pressures were measured, open port pressure taps were used. Holes for a 1.58 cm (5/8 in) bolt were drilled and tapped into the side of the model. For open port pressure taps, 1.58 cm (5/8 in) bolts were milled out and covered with 100 mesh wire screen as shown in Figure 2.

Fifteen water pressure measuring locations were established, three vertically at each of five different radii. Water pressures were measured at heights of 0.4572 m (18 in), 0.7620 m (30 in), and 1.0668 m (42 in) above the bottom of the confined layer and at radii of 0.4572 m (1 1/2 ft), 0.6096 m (2 ft), 1.829 m (6 ft), 3.581 m (11.75), and 4.801 m (15.75 ft). All pressure measuring locations are shown in Figure 3.

Temperatures were measured using Fenwal GB32J2 glass bead thermistors. For protection, each thermistor was encased in 6.35 mm (1/4 in) plexiglass tubing and sealed using industrial epoxy. The glass bead thermistor protruded slightly from the epoxy used to seal the

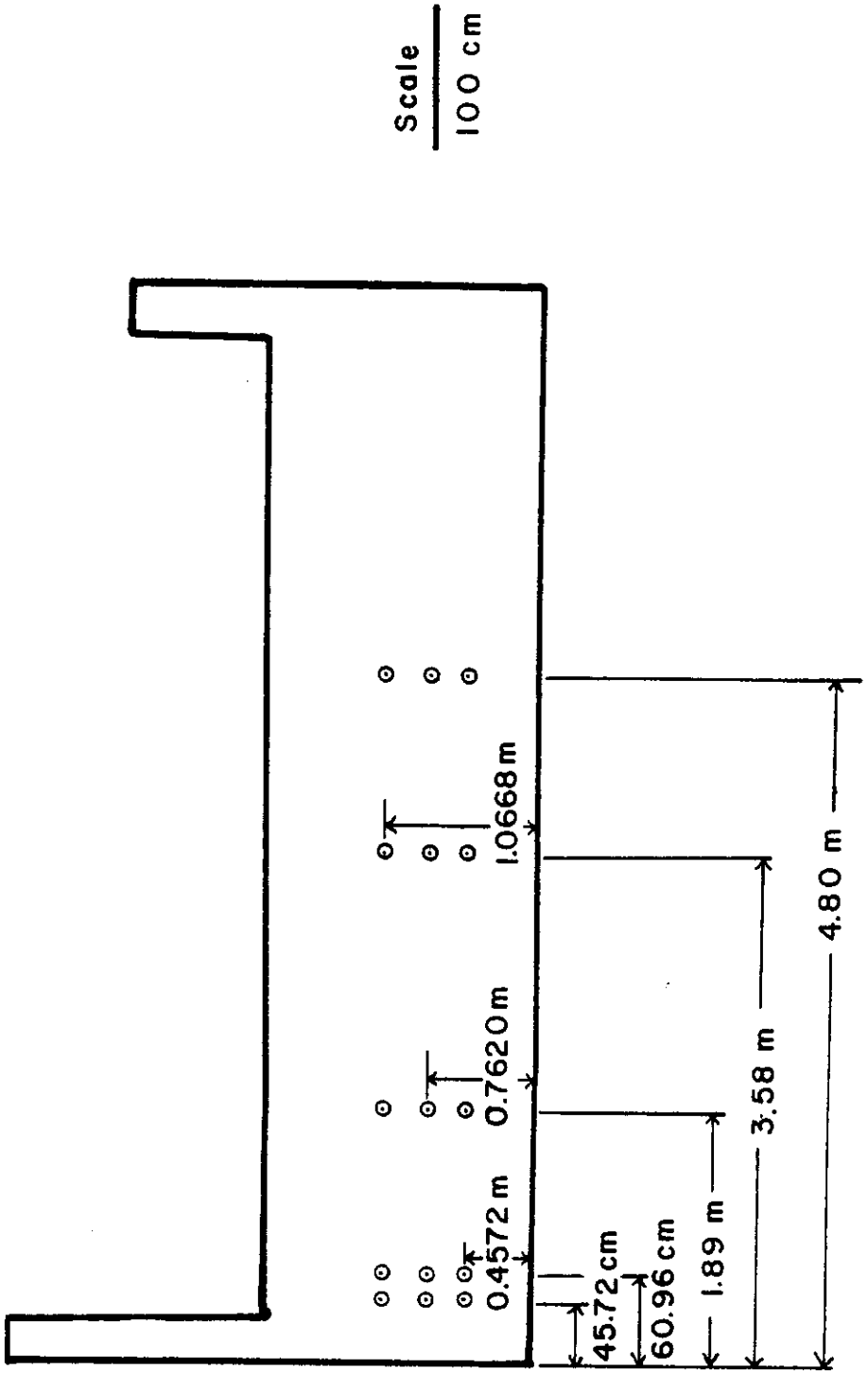

Figure 3. Location of pressure measuring locations.

plexiglass tubing as shown in Figure 4. Each thermistor was connected to one of two contact switches. Resistance readings were measured using a Fluke Digital Multimeter and recorded manually.

The resistance of each thermistor varies non-linearly with temperature as shown by a typical calibration curve in Figure 5. Each thermistor was calibrated by placing it in a constant temperature bath. Temperatures in the bath were measured using a copper-constantan thermocouple. At 10 temperatures ranging from 5°C to 75°C, the resistance of each thermistor was measured and recorded. Using a least squares curve fit, a fifth order calibration curve with temperature as a function of resistance was calculated for each thermistor. Using the correct calibration curve, the temperature of each thermistor could be determined by measuring its resistance.

Temperatures were measured at six radial distances and seven heights above the bottom of the flow layer. The six radial distances were: 0.3048 m (1 ft), 0.6096 m (2 ft), 1.524 m (5 ft), 3.048 m (10 ft), 4.57 m (15 ft), and 6.10 m (20 ft). The seven heights were: 0.0762 m (3 in), 0.3048 m (1 ft), 0.6096 m (2 ft), 0.7620 m (2 1/2 ft), 0.9144 m (3 ft), 1.2192 m (4 ft), and 1.4478 m (4 3/4 ft). All temperature measuring locations are shown in Figure 6.

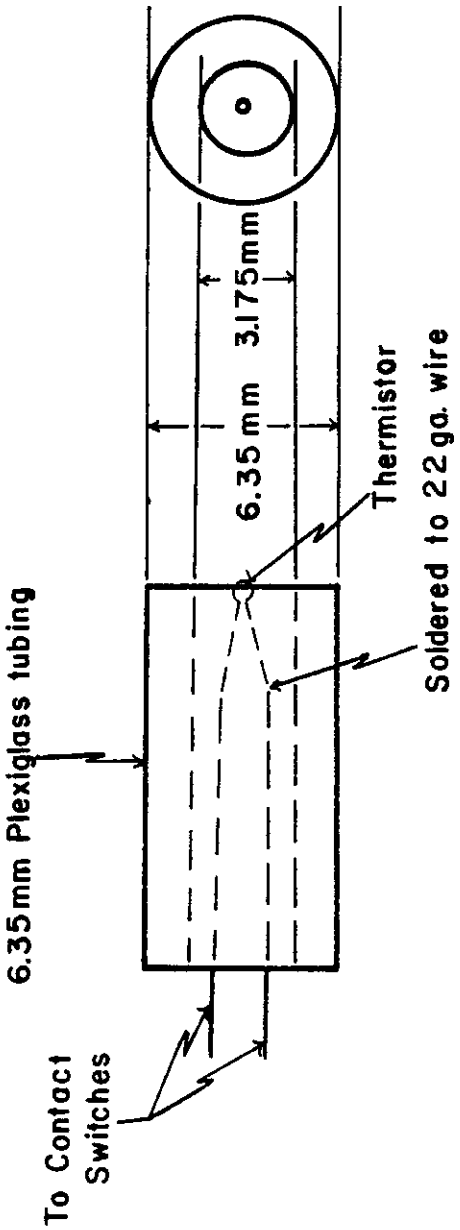

Figure 4. Fenwal GB32J2 thermistor encased in plexiglass.

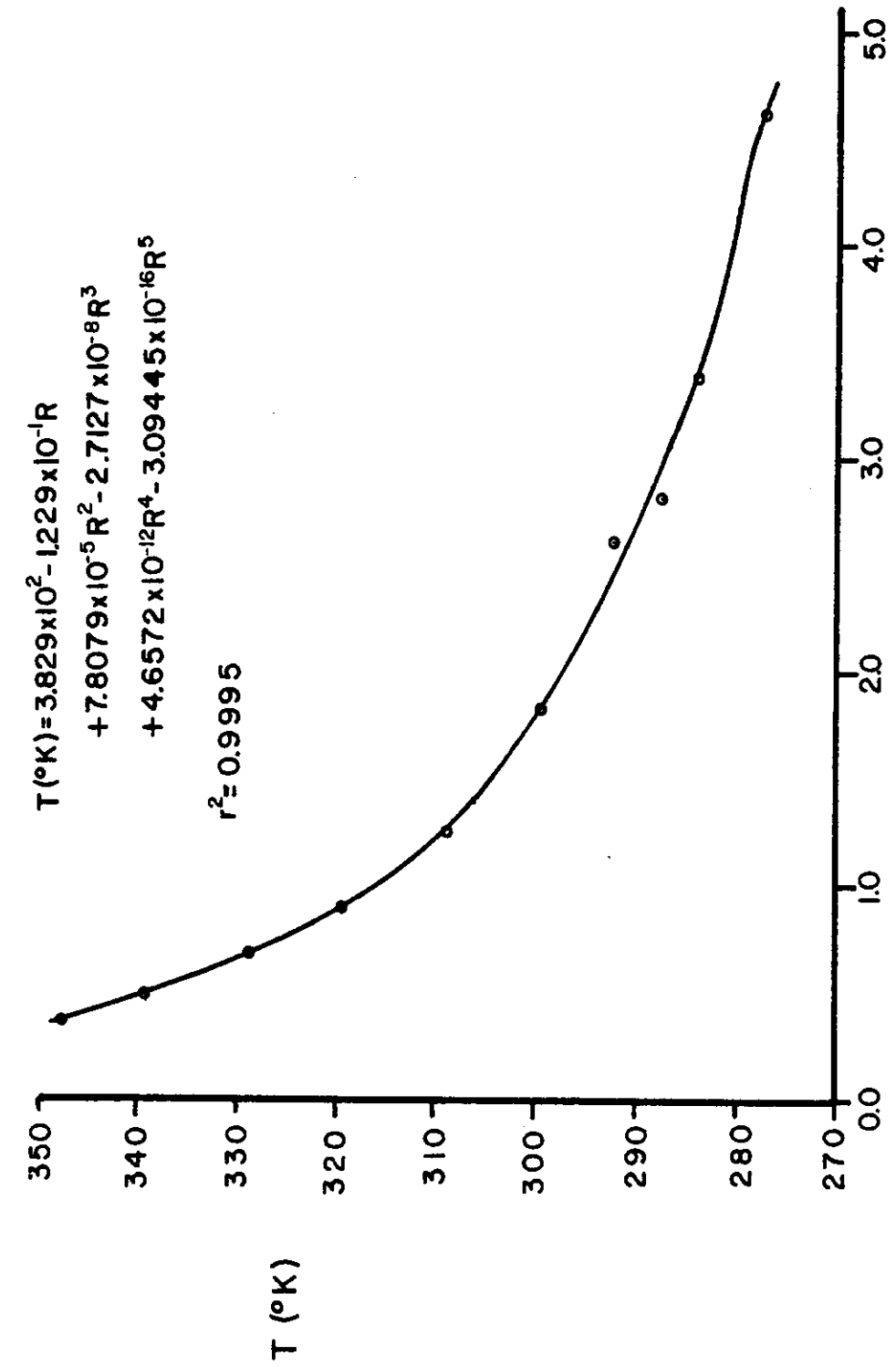

Figure 5. Calibration curve for a Fenwal GB32J2 thermistor.

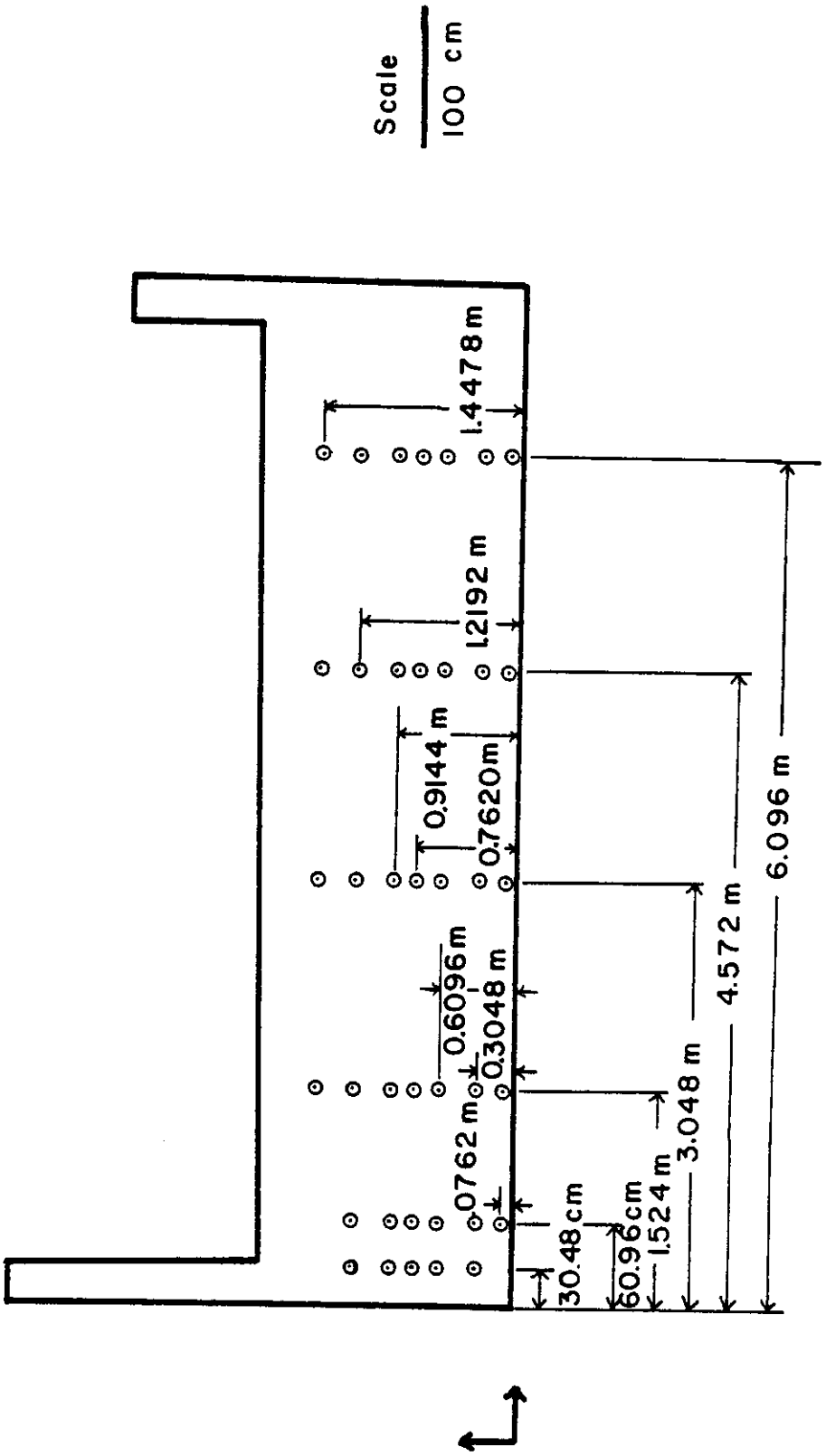

Figure 6. Location of temperature sensors.

CHAPTER V

PROCEDURE

After the model was filled with sand and saturated, a 2.66 mm (0.1064 in) steel plate top was bolted on top of the model and sealed. A head of 1.2192 m (4 ft) of water was applied to the model to check for water leaks. Leaky pressure and temperature sensors were replaced and all leaks were sealed before the test was initiated.

Before the injection cycle of each run, the water supply system was operated until thermal equilibrium was achieved and a constant water temperature was supplied at the injection well. To accomplish this, the supply valve to the model was closed and a bleed-off valve was opened. With the constant temperature bath full of water at 60°C (140°F), hot water was pumped through the supply system (described in Chapter 4) and routed through the bleed-off valve where the temperature was measured using a thermistor. When the temperature at the bleed-off valve became constant, the hot water system and the environment had reached thermal equilibrium.

Before the injection cycle, the pump controller was set so that the tubing pump would operate at the desired flowrate. This was accomplished while the hot water supply system was reaching thermal equilibrium. For Run 1, the desired flowrate for the 0.2 radian sector was 963.84 cm^3/min, which is equivalent to injecting 5.05 x 10^{-4} m^3/sec (8 gpm) into a full 360° circle. This flowrate corresponded to a pulse rate of 193 pulses per minute from the pump, as counted by a frequency counter. While counting the pulses per minute using a frequency counter, the pump

controller was varied until the desired pulses per minute were obtained. The average injection rate for Run 1 was 957.3 cm^3/min.

When the hot water supply system reached thermal equilibrium and the pump was operating at the proper flowrate, the injection cycle was ready to be initiated. The resistance of each thermistor and the water level in each piezometer tube was measured and recorded. The pump was turned off (very briefly), the bleed-off valve closed, the supply valve to the model opened, and the frequency counter reading recorded. The pump was then turned back on to initiate the injection cycle.

When the pump was turned on, two people manually recorded water level readings every two minutes for the first 40 minutes and then every 5 minutes until the end of the first hour. The time between water level readings was gradually increased to about one hour. When the injection cycle was completed and the pumping cycle began, this procedure was repeated. Two people read water levels and recorded them every two minutes and gradually increased the time between readings to approximately one hour.

The frequency of temperature measurements was dependant on the location of the thermistors. Thermistors that measured air temperatures were read approximately every 90 minutes. Sensors at the 0.3048 m (1 ft) radius were read every 2 minutes for the first 100 minutes. The time between readings was then gradually increased to 30 minutes. At the 0.6096 m (2 ft) radius, temperature measurements were made at 10 minutes after the injection cycle started and then every 2 minutes for the next 180 minutes. The time interval between readings was eventually increased to 30 minutes. At all other radii, temperature measurements were made every 30 minutes until the hydraulic front reached that radii. Readings

were then taken at 5 minute intervals and gradually increased as the temperature change slowed down. When the injection cycle began, the water temperature entering the well was measured at 2 minute intervals. This temperature remained stable, so that these measurements were eventually made only every 15 minutes.

During the pumping cycle, temperature readings were taken at 4 minute intervals initially. Because the readings changed so slowly, they were eventually taken at 10 minute intervals. As the temperatures at the outer radii approached their initial values, readings were taken less frequently. During the pumping cycle, the temperature of the water removed from the model was initially measured every 2 minutes. The reading times were soon lengthened to 10 minutes.

On Run 1, the injection cycle lasted 29 hours and was followed by a pumping cycle of 24 hours. To go from injecting to pumping, the pump was turned off and the supply valve closed. After reversing the pump and flowmeter in the line, the supply valve to the model was reopened. The pumping cycle began by starting the pump at the same speed as before. The average pumping cycle flowrate was 1044.5 cm^3/min.

Between the first and second run, a second 0.1524 m (6 in) thick layer of insulation was applied to the first 3.048 m (10 ft) of the model. This was done because temperature measurements at the first two radii (0.3048 m and 0.6096 m) during Run 1 showed temperature fluctuations resulting from changes in air temperature within the building. Insualtion was added to reduce this effect. Also during this interval of time, two aborted attempts were made to run the model. Both runs were aborted because of a malfunction in the water heater.

Run 2 was set up to simulate 2 complete injection-pumping cycles (36 hours injecting - 36 hours pumping - 36 hours injecting - 36 hours pumping). However, 12 hours into the second injection cycle, the tubing pump that supplied water to the model broke down, and the test was halted at that time. The target sector flowrate was 1442 cm^3/min, which is equivalent to injecting 7.57 x 10^{-4} m^3/sec (12 gpm) into a full 360° circle. Compared to Run 1, a higher flowrate and longer injection cycle were used in Run 2 because, in Run 1, the hydraulic front reached only about 5 m (16.4 ft) and the thermal front was barely noticeable at the 3.048 m (10 ft) radius.

The procedure for Run 2 was the same as for Run 1. The only differences were that Run 2 was at a higher flowrate and temperature data collection was more efficient for Run 2 because of the experience gained from Run 1. The average injection rate for Run 2 was 1482 cc/min and the pumping rate was 1246 cc/min.

Upon completion of Run 2, all data were punched on computer cards. A calibration curve for each thermistor had been obtained in the laboratory by placing the thermistors in a constant temperature bath and calibrating them using a copper-constantan thermocouple as a standard. For each location in the model, the correct calibration curve was known and used to convert from resistance to temperature.

CHAPTER VI

RESULTS AND DISCUSSION

Physical Properties

The physical properties of the porous media used in the laboratory model were determined by standard procedures, and the values are listed in Table 1. The porous media was a fine grained Texblast blasting sand from Lone Star Industries.

According to Brady (1974), bulk density (d_b) is defined as:

$$\text{Bulk Density} = \frac{\text{Mass of soil}}{\text{Bulk volume of soil}} \quad . \tag{8}$$

The mass of sand put into the model was measured and the bulk density was calculated to be 1.61 x $10^3 kg/m^3$. The porosity (ϕ) is related to bulk density by

$$\phi = 1. - (d_b/\rho_p) \tag{9}$$

where ϕ = porosity (fraction);

d_b = bulk density (ML^{-3}); and

ρ_p = particle density (ML^{-3}).

The particle density was measured to be 2.65 x $10^3 kg/m^3$ using an air pycnometer. From Equation 9, the porosity was calculated to be 0.392.

A sieve analysis, as described by Johnson Division, UOP Inc. (1975), was run on the sand placed in the model. The sand would be classified as a fine to medium grained sand. A mean particle diameter of 4.064 x 10^{-4}m (0.016 in) and an effective grain size of 2.743 x 10^{-4}m

Table 1. Physical Properties of the Porous Media used in the laboratory model

Bulk Density	$1.61 \times 10^3 kg/m^3$
Porosity	0.392
Mean Particle Diameter	$4.064 \times 10^{-4} m$ (0.016 in)
Effective Size	$2.743 \times 10^{-4} m$ (0.0108 in)
Uniformity Coefficient	1.65
Hydraulic Conductivity (at 25°C)	8.40×10^{-4} m/sec
Intrinsic Permeability	$7.69 \times 10^{-11} m^2$
Stagnant Thermal Conductivity	2.65 w(m°K)
Sand Density	2.65×10^3 kg/m^3
Specific Heat of Sand	0.825×10^3 J/(kg°K)
Volumetric Heat Capacity of Sand	2.186×10^6 J/(m^3°K)
Combined Volumetric Heat Capacity	2.98×10^6 J/(m^3°K)
Thermal Diffusivity	2.782×10^{-7} m^2/sec

(0.0108 in) were obtained from the particle size distribution curve shown in Figure 7. The uniformity coefficient, defined and calculated as the quotient of the 40 percent retained size of sand divided by the 90 percent retained size, was calculated to be 1.65.

Thermal Properties

The specific heat of the sand (C_r) was 0.825 x 10^3 J/(kg°K) as measured using a bomb calorimeter. The density of the porous media (ρ_r) is the same as the particle density (ρ_p), and was measured using an air pycnometer. The density (ρ_w) and specific heat (C_w) of water were assumed to be 1000 kg/m^3 and 4.186 x 10^3 J/(kg°K) respectively. The volumetric heat capacity of a fluid or solid is defined as the product of the density and specific heat of the fluid or solid. The combined volumetric heat capacity of the porous media and water ($\rho_1 C_1$) is

$$\rho_1 C_1 = \phi \rho_w C_w + (1.0 - \phi)\, \rho_r C_r \quad . \tag{10}$$

All variables were previously defined. The combined volumetric heat capacity of the porous media and water was calculated to be 2.98 x 10^6 J/(m^3°K).

According to Bear (1972), the modes of heat transfer in a porous media, in addition to convection, are

a. conduction in the solid phase,

b. conduction in the fluid phase, and

c. heat dispersion in the fluid phase.

The stagnant thermal conductivity (K_o) of a porous media is the result of the first two modes mentioned above, and occurs without any fluid

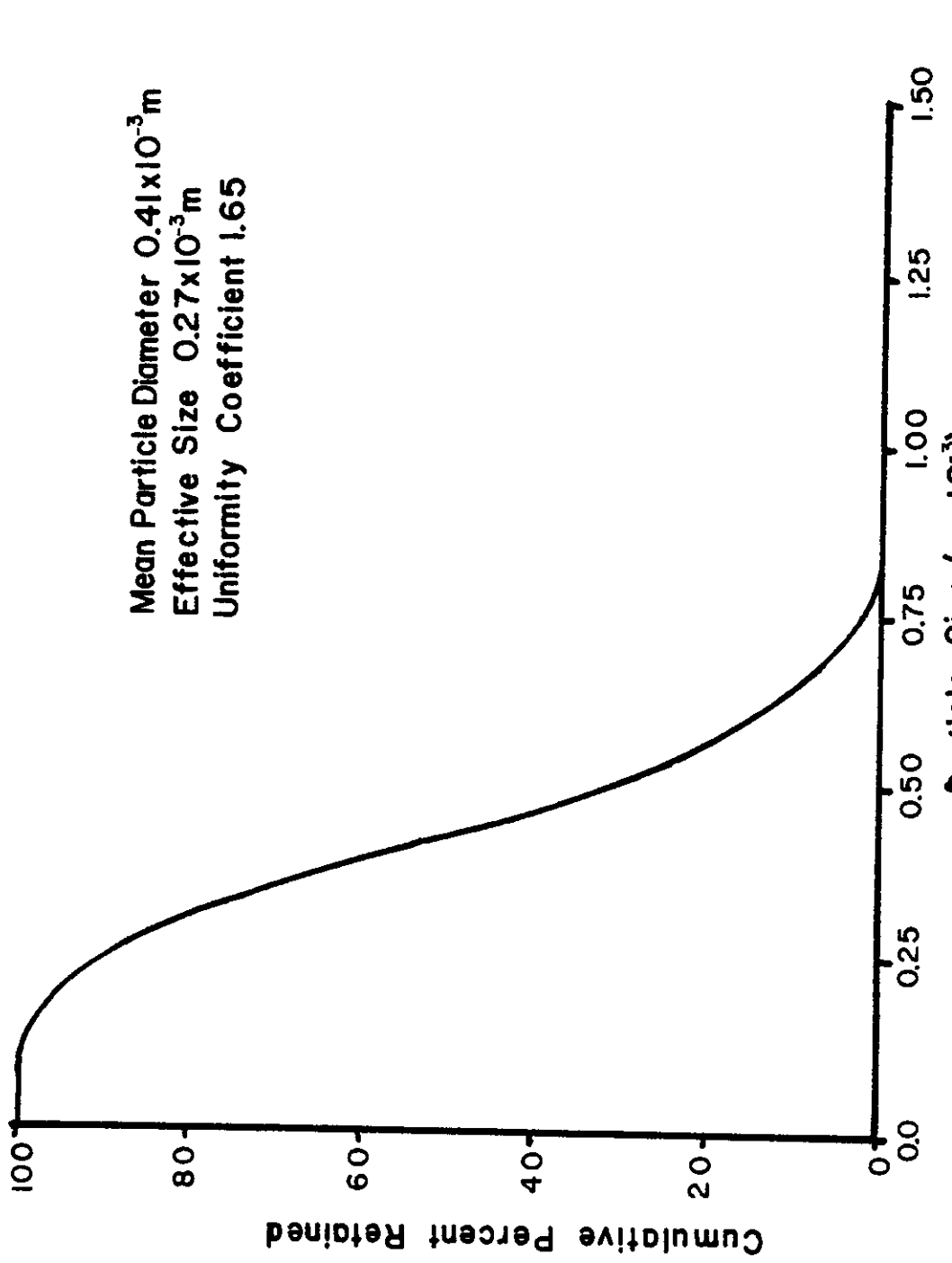

Figure 7. Particle size distribution curve for sand used in flow layer of the laboratory model.

motion. Using a probe and procedure by Sweat (1976), the stagnant thermal conductivity was measured to be 2.65 w/(m°K).

According to Green et al. (1964), heat transfer by dispersion is dependant on fluid velocity and is called eddy dispersion. The effective thermal conductivity, K_1, is the sum of the stagnant thermal conductivity and eddy dispersion. Values of all thermal conductivities used in analytical solutions describing heat flow through porous media are the values of effective thermal conductivity.

Values of eddy dispersion were obtained from data by Green et al. (1964). A plot of K_1/K_o versus a modified heat transfer Peclet number was prepared using data from Green et al. (1964) and is shown in Figure 8. The modified heat transfer Peclet number is defined as

$$Pe = \frac{V\, d_p}{\alpha_1} \quad , \tag{11}$$

where Pe = Peclet number;

V = fluid pore water velocity (LT^{-1});

d_p = mean particle diameter (L); and

α_1 = thermal diffusivity of the porous media (L^2T^{-1}).

The thermal diffusivity is calculated using the stagnant thermal conductivity, i.e.

$$\alpha_1 = \frac{K_o}{\rho_1 C_1} \quad , \tag{12}$$

where K_o = stagnant thermal conductivity ($FT^{-1}deg^{-1}$); and

$\rho_1 C_1$ = combined porous media and water volumetric heat capacity ($FL^{-2}deg^{-1}$).

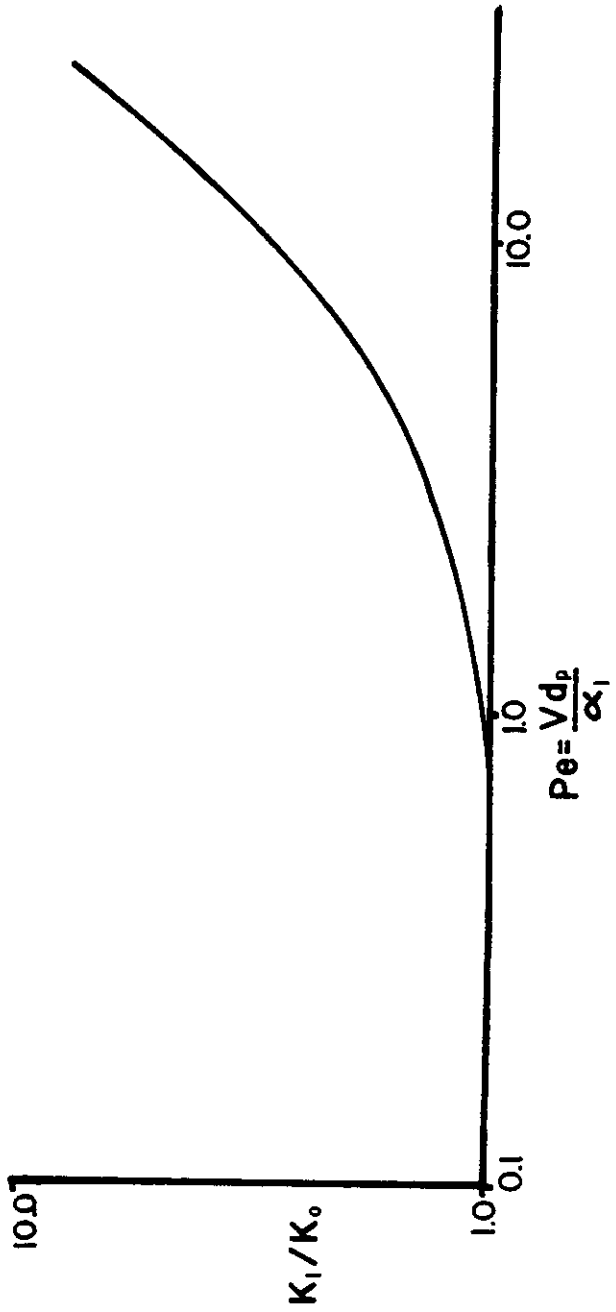

Figure 8. Ratio of effective thermal conductivity to stagnant thermal conductivity (K_1/K_0) versus heat transfer Peclet number from Green et al. (1964).

The fluid pore water velocity is a function of radius, i.e.

$$V = \frac{Q}{2\pi r h \phi} \tag{13}$$

where Q = injection rate (L^3T^{-1});

r = radial distance from well (L); and

h = thickness of flow layer (L).

Using the physical properties in Table 1 and the flow rates for Run 1 and Run 2, the Peclet number as a function of radius, r, in meters, is

$$Pe = 5.2101 \times 10^{-2}/r \quad \text{and} \tag{14a}$$

$$Pe = 8.0693 \times 10^{-2}/r \tag{14b}$$

for Runs 1 and 2 respectively. These relationships showing the Peclet number as a function of radius are given in Figure 9. Thus, over the entire length of the model, the Peclet numbers are less than 1. Entering Figure 8 with $Pe \leq 1$, $K_1/K_o = 1$. Therefore, the effective thermal conductivity is essentially equal to the stagnant thermal conductivity for all values of radius in both Runs 1 and 2.

Pressure Data

The hydraulic conductivity, P, was measured in the laboratory model during an injection cycle where there was no heat transfer and only water level data were collected. Water was injected until the water levels reached equilibrium. At that time, the hydraulic conductivity was calculated using the equilibrium well formula

$$P = \frac{Q \ln(r_2/r_1)}{2\ b(h_2-h_1)} \quad , \tag{15}$$

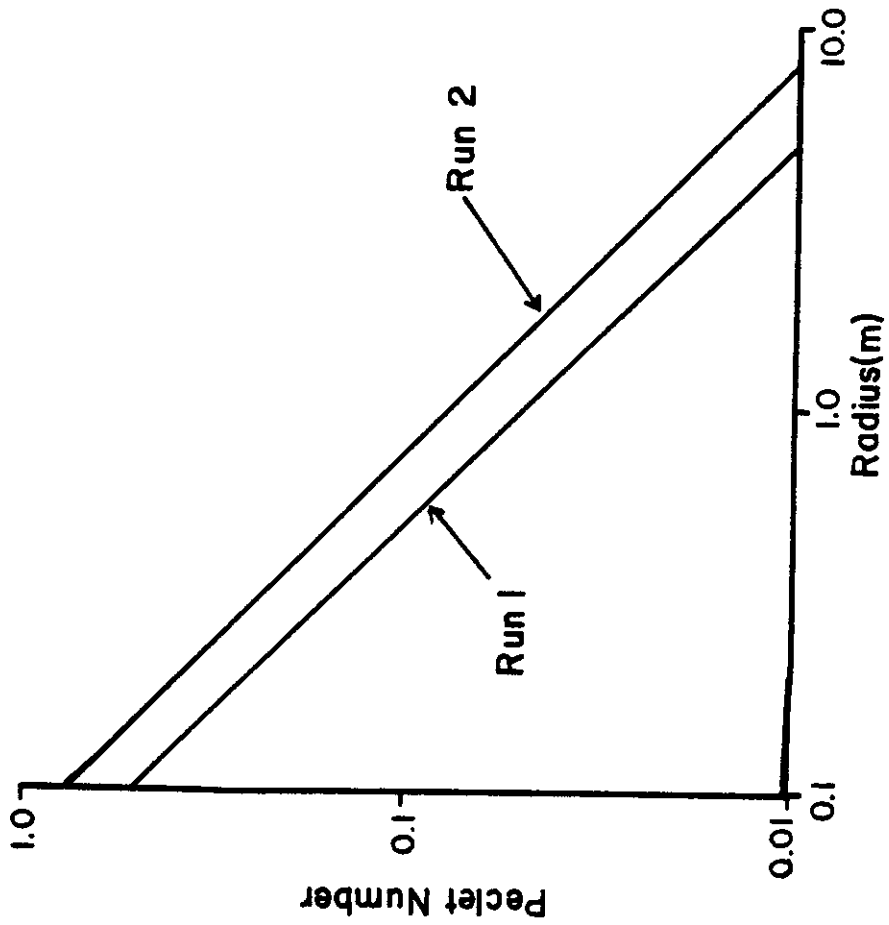

Figure 9. Heat transfer Peclet number as a function of radius for Run 1 and Run 2.

where P = hydraulic conductivity (LT^{-1});

Q = injection rate (L^3T^{-1});

b = flow layer thickness (L);

r = radial distance from well (L);

h_1 = water level measured at radius r_1(L); and

h_2 = water level measured at radius r_2(L).

For the run with no heat transfer, the equilibrium water levels are shown in Figure 10 and a hydraulic conductivity of 8.40×10^{-4} m/sec was calculated.

The assumed steady state changes in water levels for Runs 1 and 2 50 minutes after injection began are also shown in Figure 10. Hydraulic conductivities of 8.85×10^{-4} m/sec and 5.76×10^{-4} m/sec were calculated for Runs 1 and 2 respectively using the equilibrium well formula. For Run 1, the hydraulic conductivity is only slightly larger than the one measured with no heat transfer. However, the hydraulic conductivity for Run 2 was significantly less than the hydraulic conductivity for Run 1.

During the time interval between Runs 1 and 2, one of the pressure sensors began to leak and the model was drained to repair this leak. After resaturating the model, some air was apparently entrained in the model during Run 2, which effectively reduced the hydraulic conductivity for Run 2.

According to Todd (1964), hydraulic conductivity is a function of both flowing fluid and media properties, i.e.

$$P = \frac{k_i \rho_f g}{\mu_f} \quad , \tag{16}$$

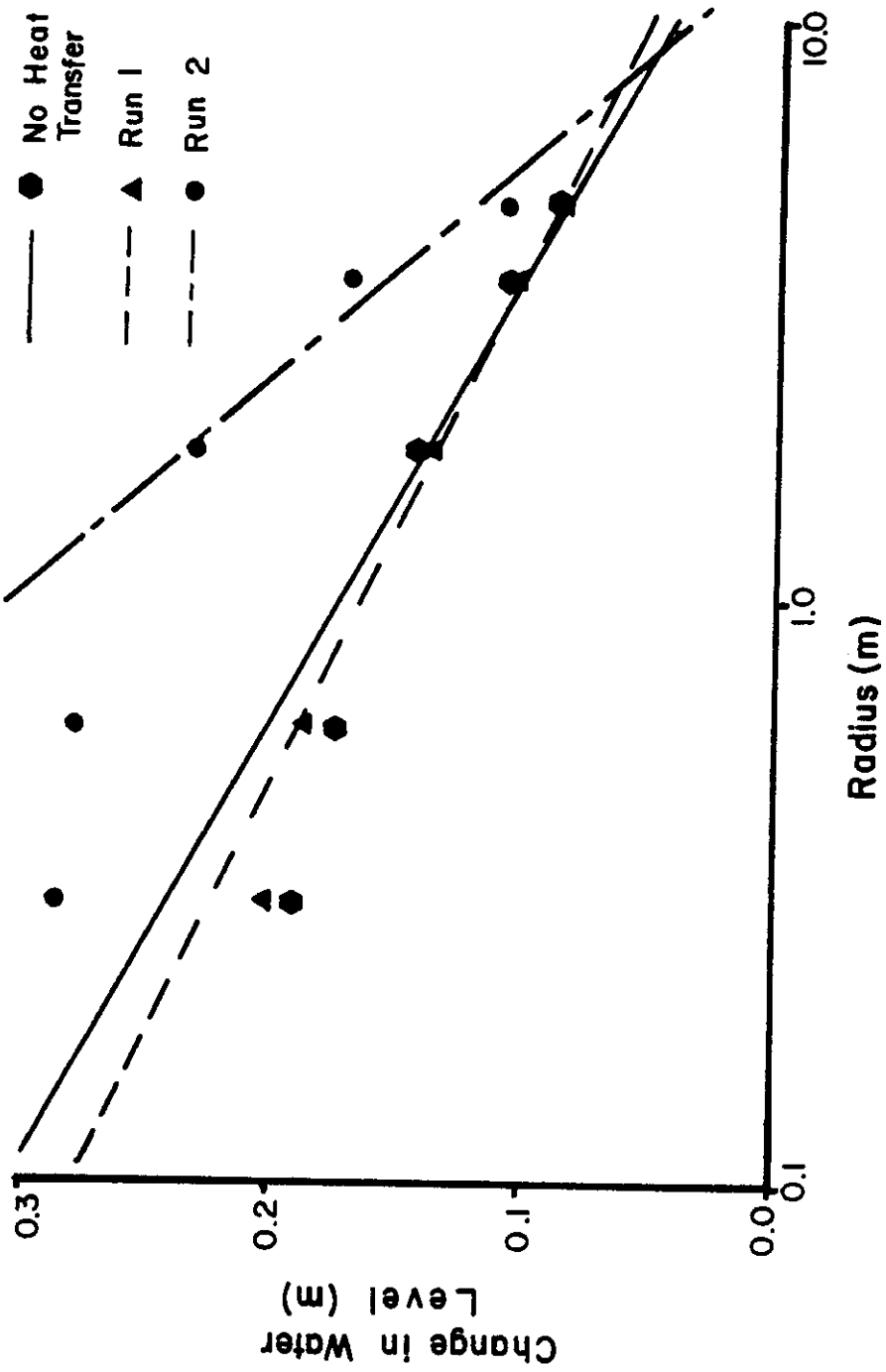

Figure 10. Steady state change in water level for the run with no heat transfer, Run 1 and Run 2.

where k_i = intrinsic permeability (L^2);

ρ_f = density of fluid (ML^{-3});

g = acceleration of gravity (LT^{-2}); and

μ = viscosity of fluid ($ML^{-1}T^{-1}$).

The intrinsic permeability is a unique pore area governing flow. Density and viscosity are fluid properties and a function of temperature. Both properties decrease with an increase in temperature. However, viscosity decreases more than density and a net increase in hydraulic conductivity results. As hot water is injected into the model, temperature increases and the hydraulic conductivity increases behind the thermal front.

Figure 11 shows the effects of the increasing aquifer temperature on water levels and hydraulic conductivity during Run 1. As the slope of the lines in Figure 11 decreases, the hydraulic conductivity increases. The increase in hydraulic conductivity resulting from temperature increases in the flow layer are quite large. Initially the flow layer was at a temperature of approximately 298.16°K(25°C). From Streeter and Wylie (1974), the viscosity and density of water are 0.894×10^{-3}kg/(m sec) and 997.1 kg/m^3 respectively. The intrinsic permeability of the porous media (from Equation 16) will be 8.09×10^{-11}m^2 based on a hydraulic conductivity of 8.85×10^{-4}m/sec. For water at 328.16°K(55°C), the density and viscosity are 985.7 kg/m^3 and 0.506×10^{-3} kg/(m sec) respectively. Using an intrinsic permeability value of 8.09×10^{-11}m^2 and the physical properties of water at 328.16°K, the hydraulic conductivity is 1.54×10^{-3}m/sec. Thus, a 75 percent increase in hydraulic conductivity occurs because of an increase in water temperature from 298.16°K(25°C) to 328.16°K(55°C). For this

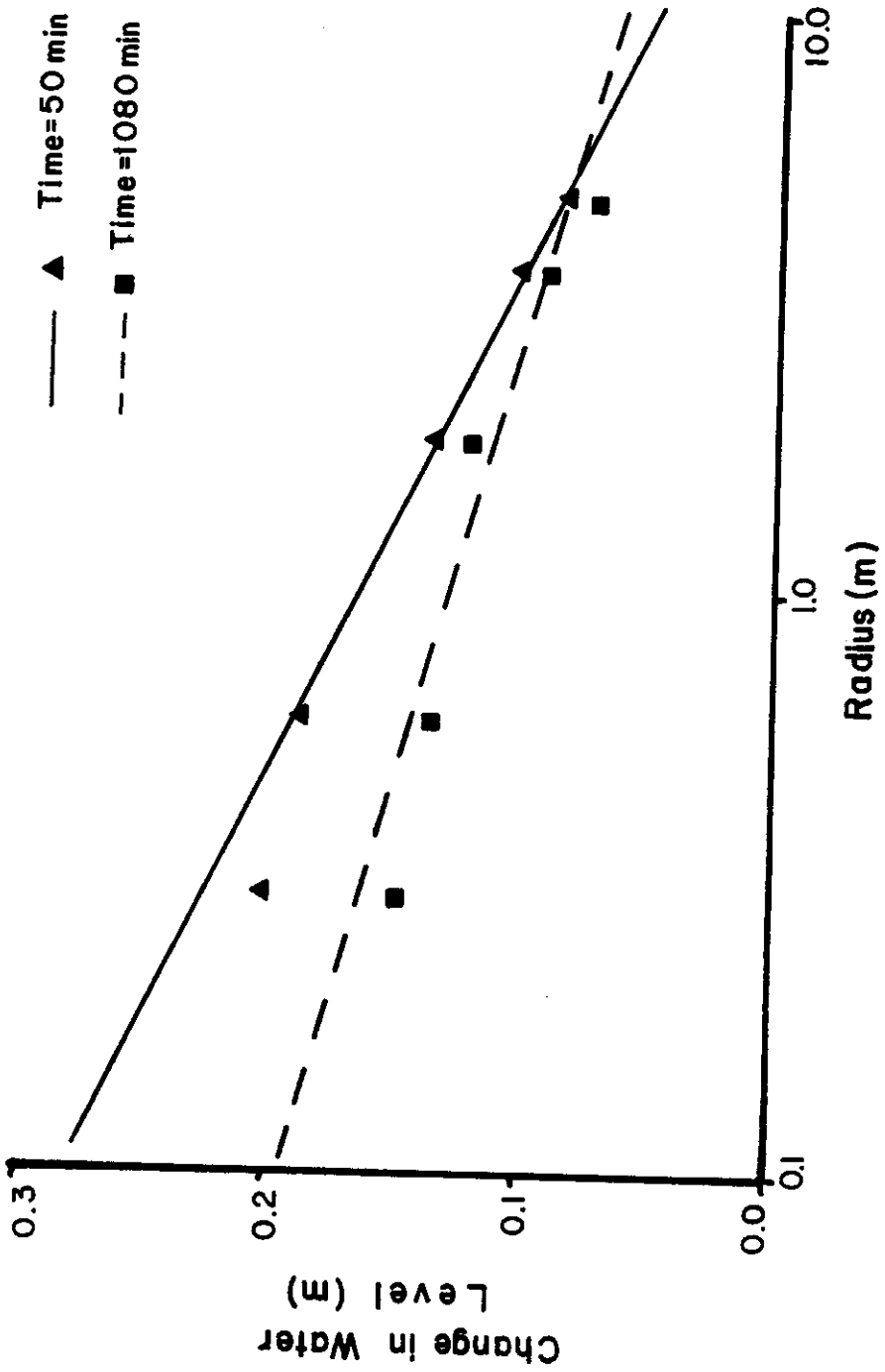

Figure 11. Water levels during Run 1 showing the effect of increasing flow layer temperature.

reason, the hydraulic conductivity in the model increased with time, and the water levels declined as the thermal front moved through the aquifer. This is shown in Figure 11 by comparing the water levels 1080 minutes after Run 1 was initiated with the water levels 50 minutes after Run 1 was initiated. The hydraulic conductivity calculated from the experimental data at 1080 minutes was 1.53×10^{-3} m/sec, a 74 percent increase over the value of the hydraulic conductivity calculated from the experimental data at 50 minutes. This was certainly in line with theoretical expectations.

Temperature Measurement

Two laboratory runs were made that involved heat transfer in the porous media. For Run 1, the average injection rate was 957.34 cm^3/min for the 0.2 radian sector which is equivalent to injecting 0.50126×10^{-3} m^3/sec in a full 360°, and the injection cycle lasted 29 hours. This was followed by a 24 hour pumping cycle at an average pumping rate of 1044.5 cm^3/min for 0.2 radians or 0.5469×10^{-3} m^3/sec for a full 360° circle. Run 2 was designed to be two full injection-pumping cycles (36 hrs injecting - 36 hrs pumping - 36 hrs injecting - 36 hrs pumping). The first injection cycle lasted 36 hours at an average rate of 1482 cm^3/min followed by a 36 hour pumping cycle at an average flowrate of 1245.9 cm^3/min. This injection-pumping cycle will be referred to as Run 2. Twelve hours into the second injection cycle of Run 2, the tubing pump broke, and the test was stopped. For convenience and clarity, this 12 hour injection cycle will be referred to as Run 3. The average injection rate for Run 3 was 1574.1 cm^3/min.

Temperatures were measured and recorded manually for the injection and pumping cycles of all runs. The average injection temperature was 332.65°K(54.49°C) for Run 1 and 332.49°K(59.12°C) for Run 2. The injection temperature ranged from 331.13°K(59.97) to 333.64°K(60.48°C) during Run 1 and from 329.89°K(56.73°C) to 333.89°K(60.73°C) during Run 2. A representative sample of the temperature data is shown in Appendix B.

For Run 1, the temperatures 0.762 m above the bottom of the model for the first four radii (0.3048 m, 0.6096 m, 1.524 m, and 3.048 m) are plotted versus time in Figure 12. All the curves have the general shape of breakthrough curves experienced when recording the movement of a mass tracer through a porous media. At the end of the injection phase of Run 1, the hydraulic front had reached 4.8 m (15.7 ft) radially. At the same time, the temperature 0.7620 m above the bottom of the flow layer were 309.33°K(36.17°C) and 298.43°K(25.27°C) at the 3.048 m and 4.572 m radii, respectively. The temperature at the 3.048 m radius had not reached thermal equilibrium. Therefore, the thermal front was located close to the 3.048 m radius and lagged far behind the hydraulic front.

From Figure 12, temperatures at radii of 0.3048 m and 0.6096 m reached a peak after about 300 minutes and then began decreasing. These temperatures decreased because the air temperature surrounding the model was lowered. An additional 0.152 m thick layer of insulation was added to the first 3.048 m radius of the model after Run 1 to reduce this effect.

The effects of fluctuating air temperatures were apparent at the 0.3048 m and 0.0696 m radii but were not noticeable at the larger radii (1.524 m, 3.048 m, 4.572 m, and 6.096 m). The ratio of heat transfers

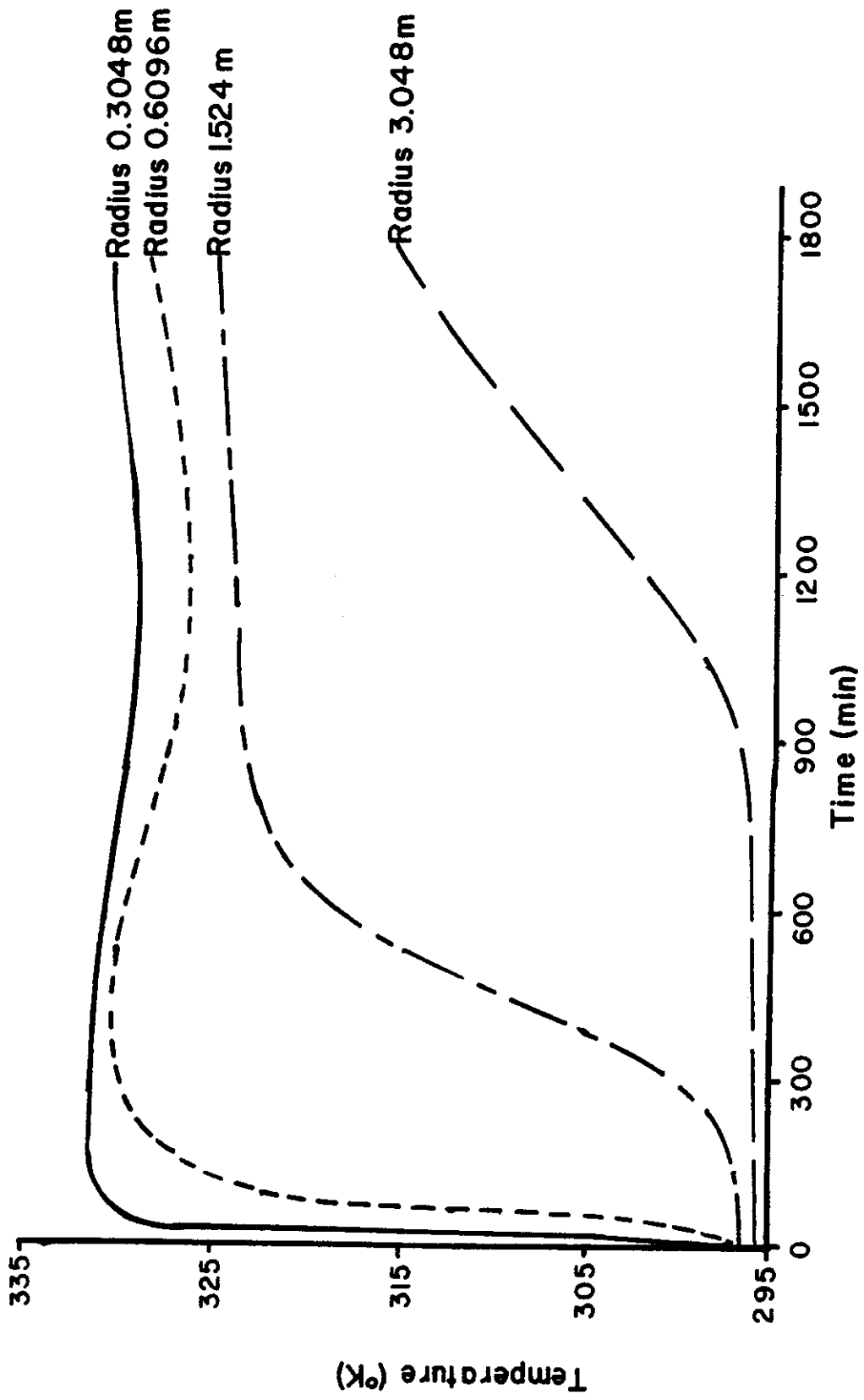

Figure 12. Temperatures measured 0.7620 m above the bottom of the model during the injection cycle of Run 1.

area out the bottom, top, and sides to the volume of storage is smaller as the radius increases in the laboratory model. From Figure 13, the total area for heat transfer from an incremental volume of the laboratory model is:

$$A_t = A_b + A_s \tag{17a}$$

where A_t = total area for heat transfer out top, bottom, and sides (L^2);

A_b = area for heat losses out top and bottom (L^2); and

A_s = area for heat transfer out sides of model (L^2).

Specifically,

$$A_b = 2r\ \Delta\theta\ \Delta r \tag{17b}$$

and

$$A_s = 2\ \Delta r\ h \tag{17c}$$

where r = radial distance from well (L);

$\Delta\theta$ = angle increment (radians);

Δr = radial increment (L); and

h = flow layer thickness (L).

Therefore,

$$A_t = 2r\ \Delta\theta\ \Delta r + 2\ \Delta r\ h \quad . \tag{17d}$$

The volume of storage in the same small radial increment is

$$Vol = r\ \Delta\theta\ \Delta r\ h \tag{18}$$

where Vol = small incremental volume of model (L^3).

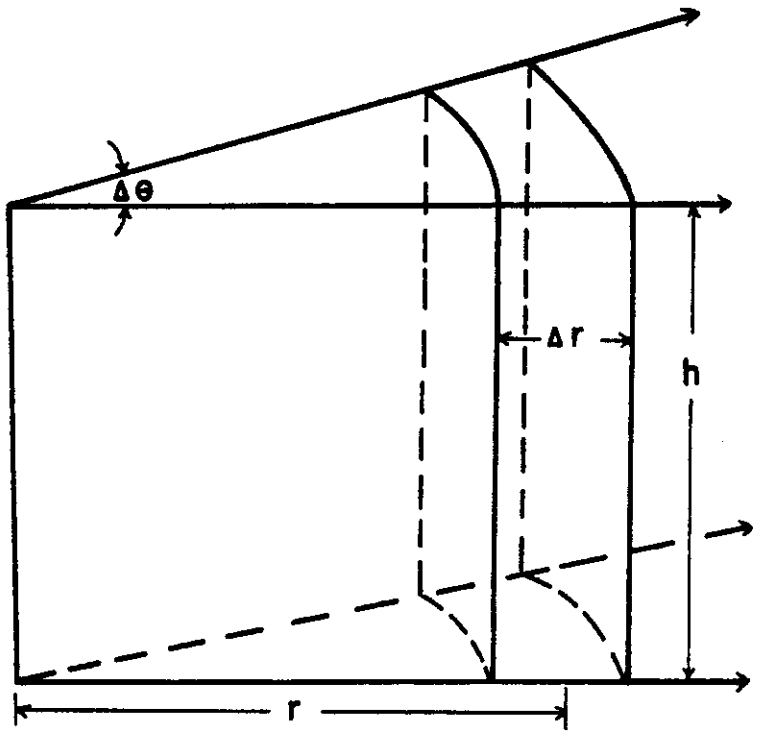

Figure 13. Incremental volume for an incremental radius (Δr) and incremental angle ($\Delta\theta$) in the laboratory model.

The ratio of total area to volume for the radial increment is

$$\frac{2\,\Delta r\,h + 2r\,\Delta\theta\,\Delta r}{r\,\Delta\theta\,\Delta r\,h} = \frac{2}{r\Delta\theta} + \frac{2}{h} \quad . \tag{19}$$

For the laboratory model, $\Delta\theta$ equaled 0.2 equaled 0.2 radians and h was 1.8288 m. For the 0.3048 m and 1.524 m radii, the ratio of the heat transfer area to the storage volume is 33.90 m^{-1} and 7.66 m^{-1} respectively. Thus, the ratio of heat transfer area to volume was decreased by a factor of 4.43 at the larger radii of 1.524 m. The decrease in heat transfer area per unit volume at the larger radii causes a cushioning effect for temperatures in the model against fluctuations in air temperature.

The first term of Equation 19 $(2/(r\,\Delta\theta))$ is the ratio of heat loss area out the sides of the model to storage volume and is a function of radius. The second term, 2/h, is the ratio of heat transfer area out the top and bottom of the model to storage volume and is independent of radius and a constant for a fiven flow layer thickness. For a full circle of 2π radians, no sides exist and the ratio of heat loss area to storage volume is a constant equal to 2/h. The ratio of the heat transfer area to storage volume for the laboratory model of 0.2 radians and a flow thickness of 1.8288 m is plotted in Figure 14 as a function of radius. Also plotted in Figure 14 is the ratio of heat transfer area to storage volume for a laboratory model with a full 2π radians and a flow thickness of 1.8288 m. The percentage of heat lost out the sides of the laboratory model as compared to the volume of storage is much higher than the corresponding percentage for a full circle. It is apparent from Figure 14 that unless the thermal conductivity of the insulation on the laboratory model is zero, then the model will not meet the criteria

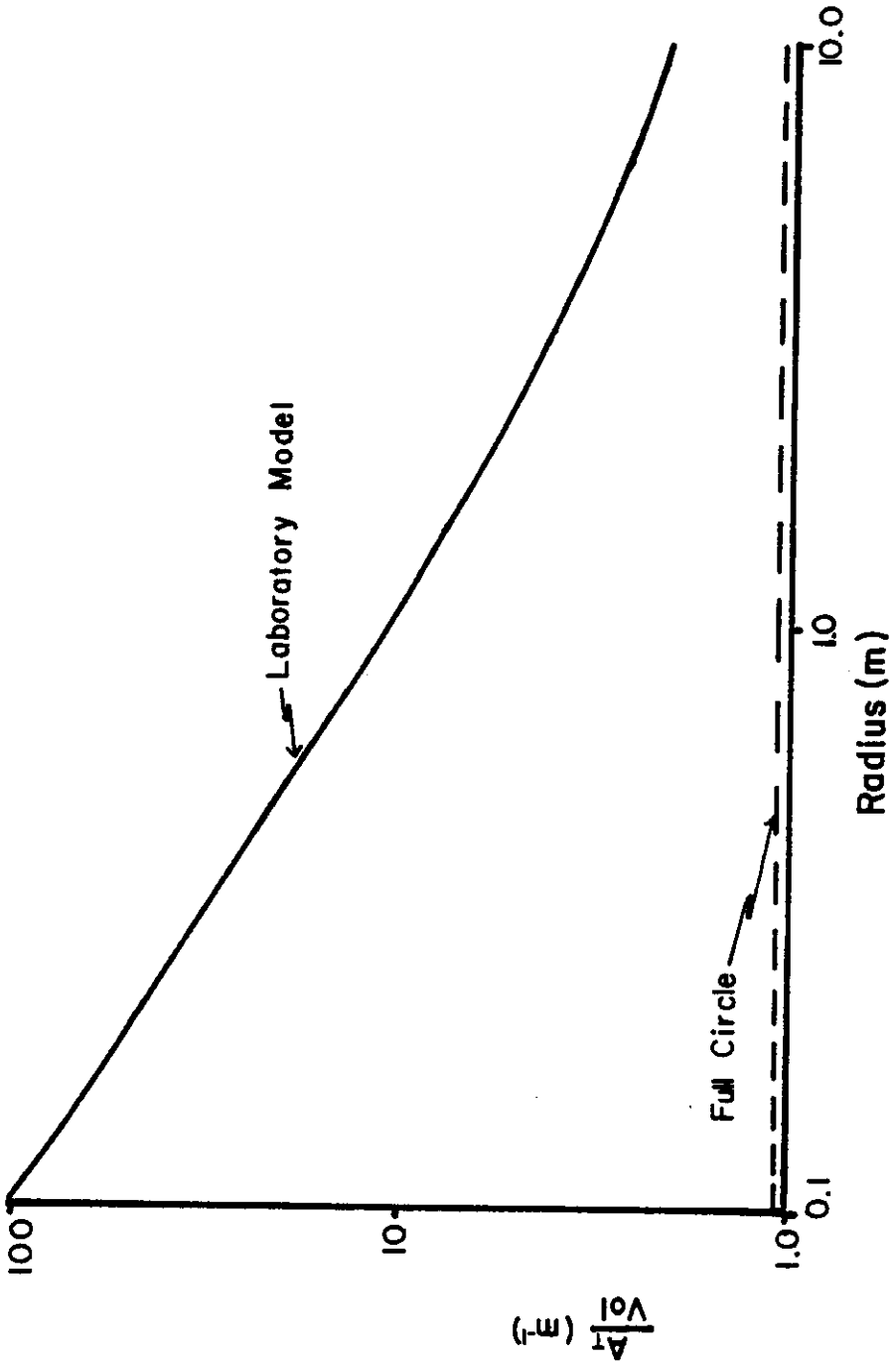

Figure 14. Comparison of the ratio of heat transfer area to storage volume for the laboratory model and a full circle flow layer.

of angular symmetry assumed for field problems of this type. A significant amount of work must be done to reduce the thermal losses out the sides of the model.

The curves in Figure 12 also show that the 0.3048 m, 0.6096 m, and 1.524 m radius had reached a maximum equilibrium temperature. Table 2 lists the maximum equilibrium temperature reached for both Runs 1 and 2 at the 0.7620 m height, and for the 3 radii closest to the well. For both runs, the equilibrium temperature decreased as expected as the radius increased. For all three radii, the equilibrium temperature was greater for Run 2 as compared to Run 1. Since the injection temperature was the same, the increase in temperature at these radii is believed to have resulted from the larger injection rate and the extra thickness of insulation used in Run 2.

Table 2. Maximum equilibrium temperature reached at each radii for Run 1 and 2 at the 0.7620 m height

Radius (m)	Equilibrium Temperature (°K)	
	Run 1	Run 2
0.3048	331.22	332.13
0.6096	330.00	330.60
1.524	326.85	329.81

Figure 15 shows the vertical temperature distributions for each radii at the end of the injection cycle for Run 1. A vertical temperature gradient with the warmer water on top is evident. This occurred because the injected water is less dense than the cold water initially in the model. The hot injected water tended to float out over the cold native water. The temperature at the 3.048 m radius and 0.7620 m height

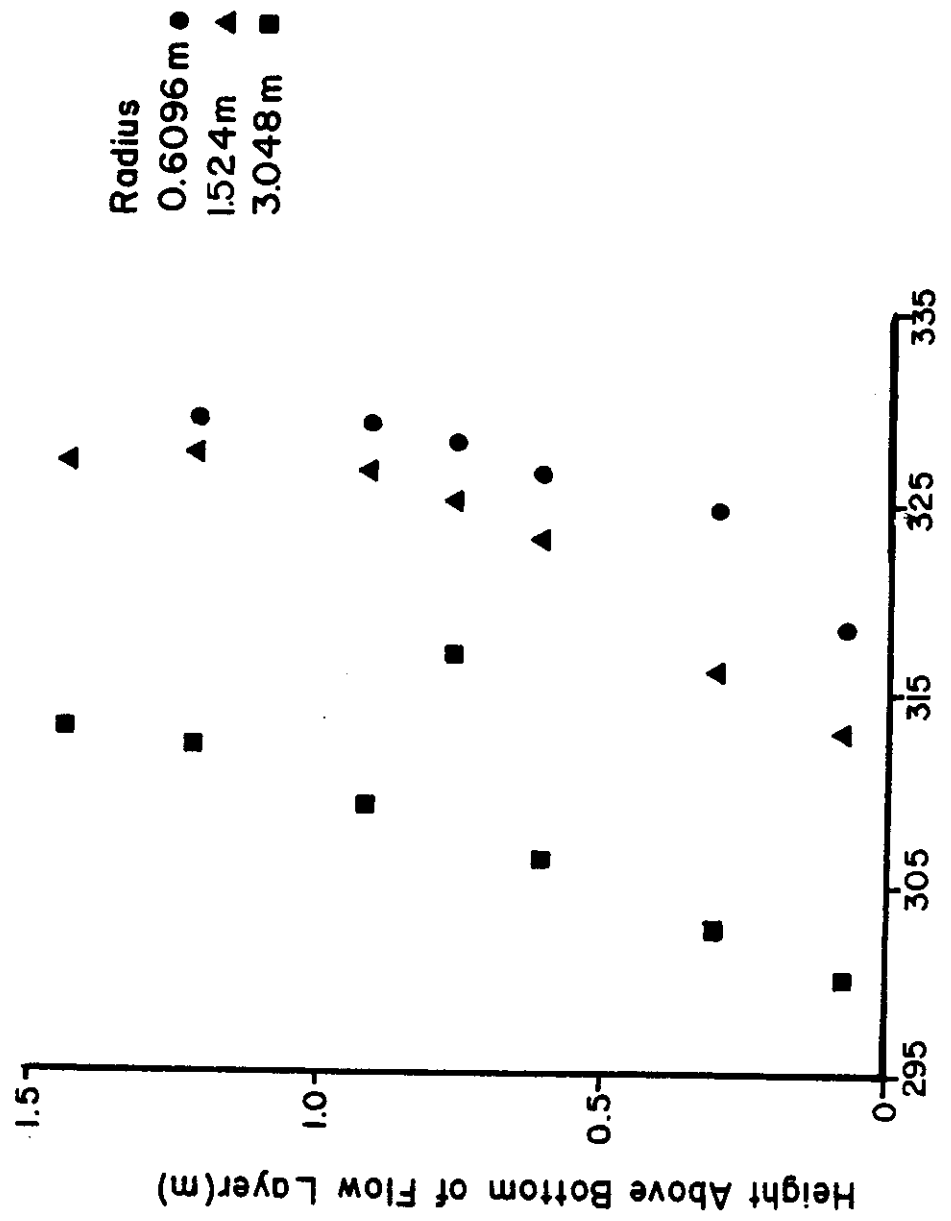

Figure 15. Vertical temperature distribution 1740 minutes after injection began for Run 1.

appears to be in error when compared to other temperatures at the same radius.

Figure 16 is an isothermal map showing the temperature distributions for Run 1 960 minutes after the injection cycle began. The vertical temperature gradient shown in Figure 15 is also apparent in Figure 16. Also, at a radius of 3 to 4 m and a depth of 0.75 m, a temperature "finger" was beginning to develop. A temperature "finger" occurs in a layer or region of a porous media where the resistance to flow is less. When the hot water reaches this region, it moves more rapidly and a temperature "finger" develops. This fingering effect showed up in all runs and was probably caused by poor packing of the porous media in this area of the model.

In Figure 17, temperature is plotted versus time since pumping began for Run 2 at the 0.7620 m height and each of 6 radii. The temperature distributions at the 0.3048 m, 0.6096 m, and 1.524 m radius are similar. Much of the time, the temperature at the 0.6096 m radius is slightly higher than that measured at the 0.3048 m radius. The decrease in temperature while approaching the well results because angular symmetry is not met. Approaching the well, the ratio of the heat transfer area to storage volume increases. Comparing the 0.3048 m and 0.6096 m radii, a higher percentage of stored energy is lost out the sides at the 0.3048 m radius and the temperature is thereby lowered at the smaller radius.

An isothermal map showing the temperature distributions as a function of radial distance from the well and aquifer thickness is shown in Figure 18 480 minutes after the pumping was initiated during Run 1. The vertical thermal gradient exhibited during the injection

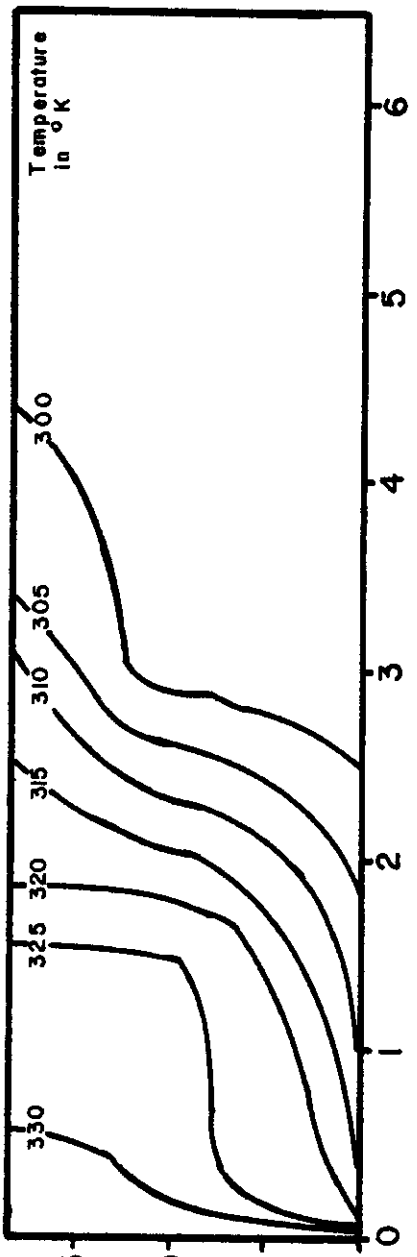

Figure 16. Isothermal map after injecting hot water for 960 minutes in Run 1.

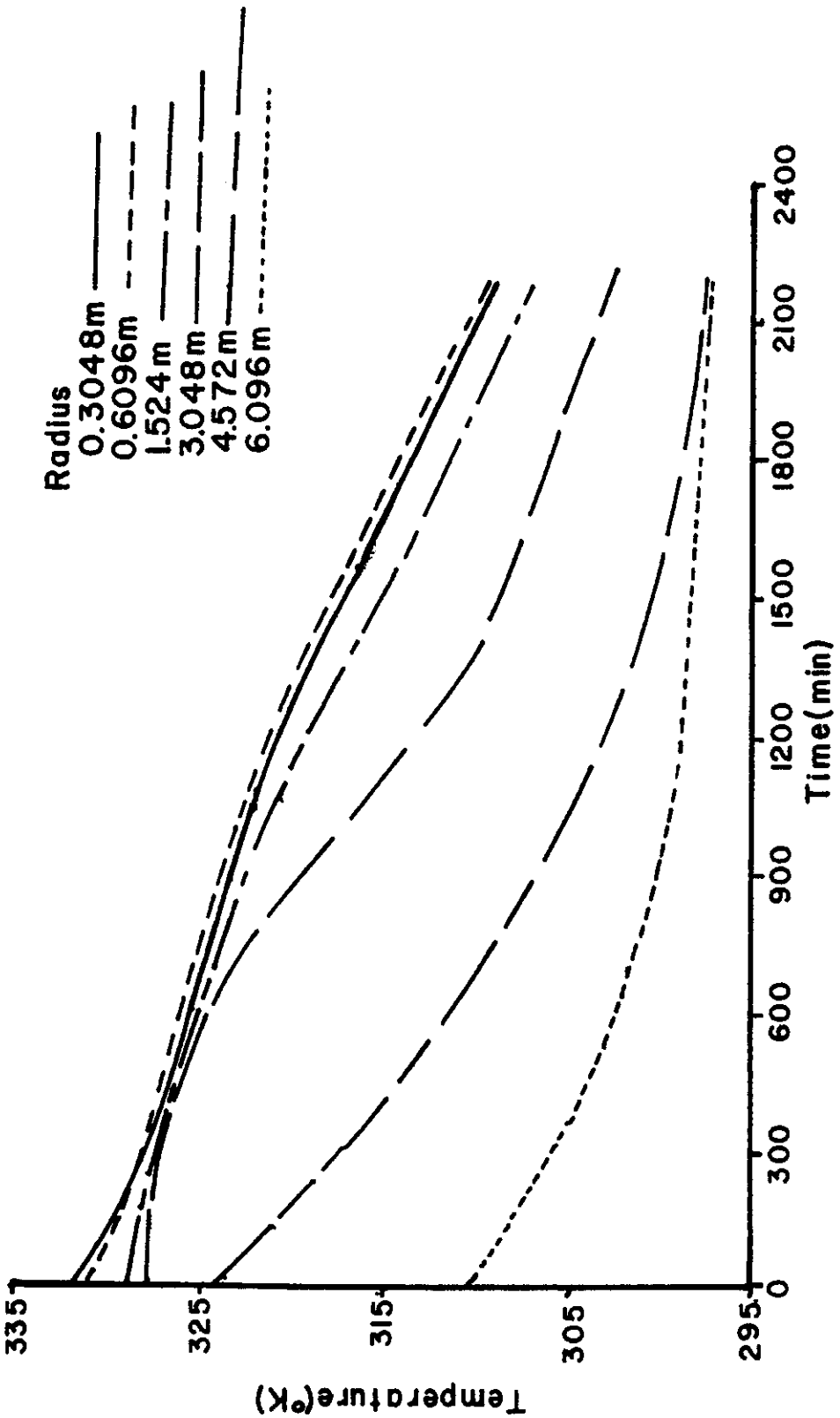

Figure 17. Temperature measured at 0.7620 m height above bottom of flow layer during the pumping cycle of Run 2.

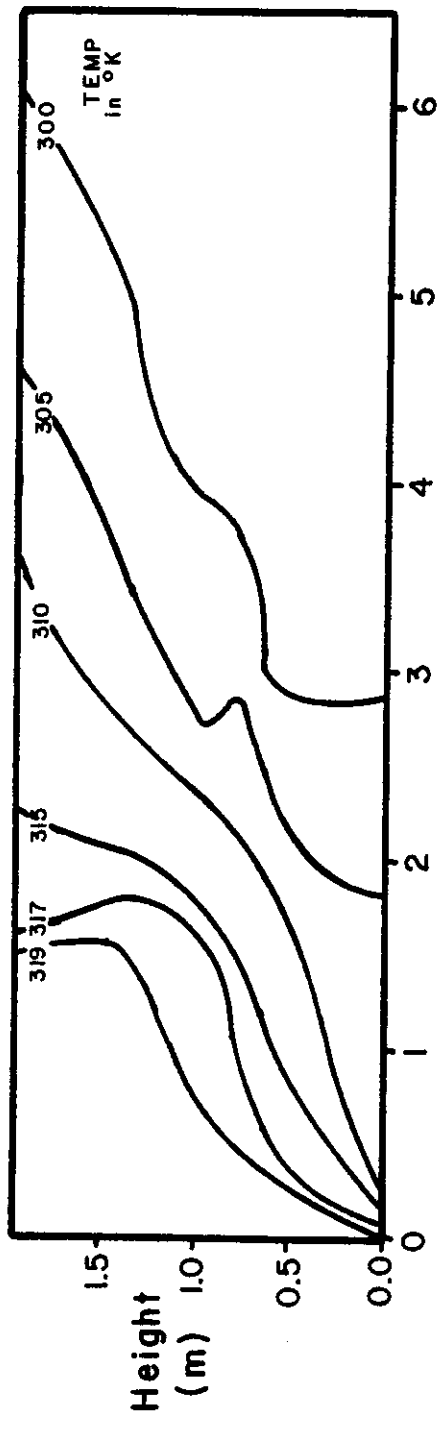

Figure 18. Isothermal map 480 minutes after pumping began in Run 1.

cycle is also noticeable during the pumping cycle. Fingering effects are also indicated in the same location, at a radius of 3 to 4 m and a depth of 0.75 m.

At the end of the pumping cycle for Run 2, temperatures throughout the model were larger than when injection began. This temperature increase indicated that some of the injected energy remained in the model after pumping ceased. Calculations showed that 12 percent of the injected energy for Run 2 remained in the flow layer at the completion of the pumping cycle for Run 2. An isothermal map showing temperature distributions at the end of the pumping cycle for Run 2 (Figure 19) shows that the temperature increase is not restricted to the region near the well bore. In fact, the temperature had increased above the initial aquifer temperature of 296.65°K out to a radius of 4.572 m.

The heat energy in the form of warm water still remaining in the aquifer altered the temperature distributions during Run 3 (the injection cycle immediately following the pumping cycle in Run 2). From the average temperature distribution curves at the 1.524 m radius (Figure 20), the initial average temperature was larger for Run 3 than Run 2 and remained larger for the entire injection cycle. However, an average equilibrium temperature of approximately 327°K was approached during both injection cycles. During Run 3, the equilibirum temperature was reached after about 800 minutes as compared with about 1200 minutes during Run 2. This decrease in time to reach an equilibrium temperature occurred because of the energy remaining in the form of warm water after completion of the pumping cycle for Run 2.

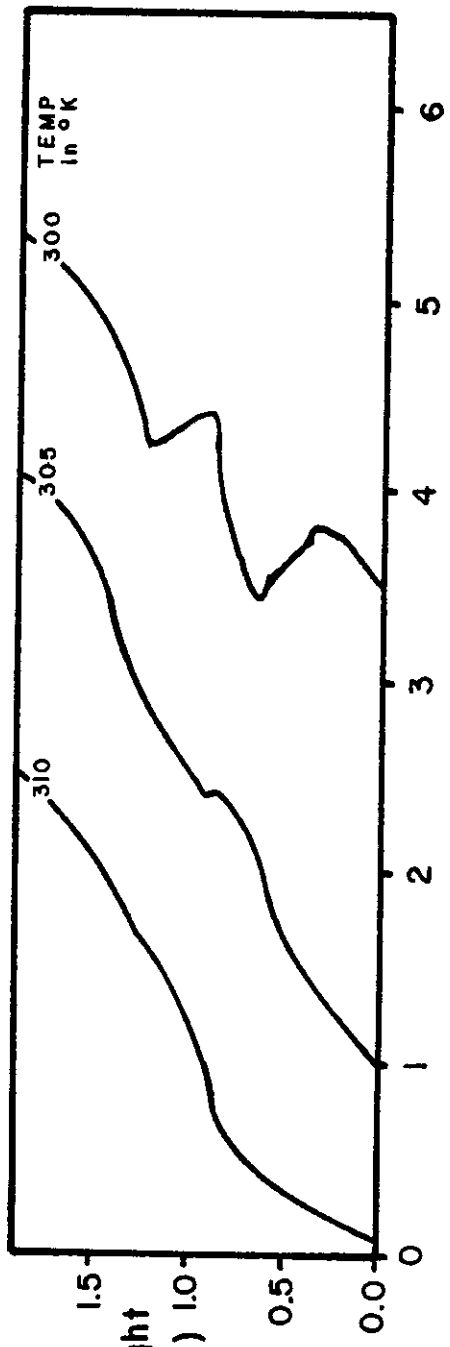

Figure 19. Isothermal map at the end of the pumping cycle for Run 2.

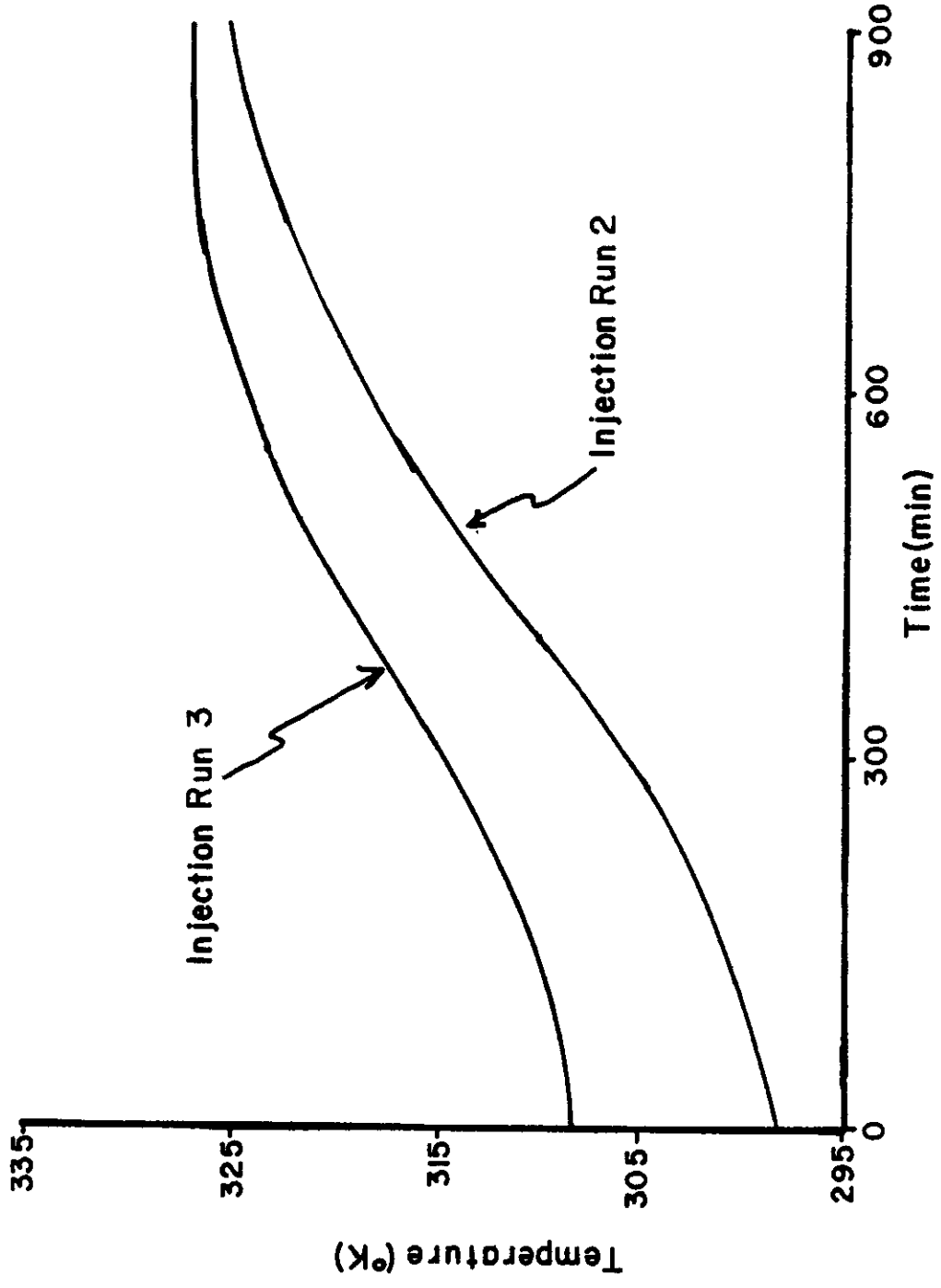

Figure 20. Comparison of average temperature at 1.524 m radius for the injection cycle for Runs 2 and 3.

Energy Recovered

The temperature of the water as it was pumped from the model was measured and the amount of recoverable energy was calculated. The temperature of the water pumped during Run 2 is plotted in Figure 21. After a slight increase in temperature during the first few minutes of the pump-out cycle on Run 2, the temperature decreased smoothly and gradually in almost a linear pattern. The slight initial increase in temperature during pump-out occurred because of a 4 to 5 minute delay between the end of the injection cycle and the beginning of the pumping cycle. Thermal losses occurred in the supply line during this interval and the temperature decreased. As pumping began, water removed from the model, which had not cooled, had to reheat the supply line. The peak temperature during the pump-out for Run 2 was 330.17°K(57.01°C) as compared to the average injection temperature of 332.28°K(59.12°C). For Run 1, the corresponding temperatures were an average injection temperature of 332.65°K(59.49°C) and a maximum pump-out temperature of 325.56°K (53.40°C).

A comparison of temperatures in the aquifer (Figure 17) and temperatures during the pump-out (Figure 21) shows that the formation temperatures are larger than the pump-out temperatures during much of the pump-out cycle. As was discussed earlier, this occurs for the same reason that the temperature at the 0.6096 m radius is larger than the temperature at the 0.3048 m radius. As the well is approached, the ratio of heat transfer area to volume of storage increases. The heat losses per unit volume of storage next to the well bore are extremely large.

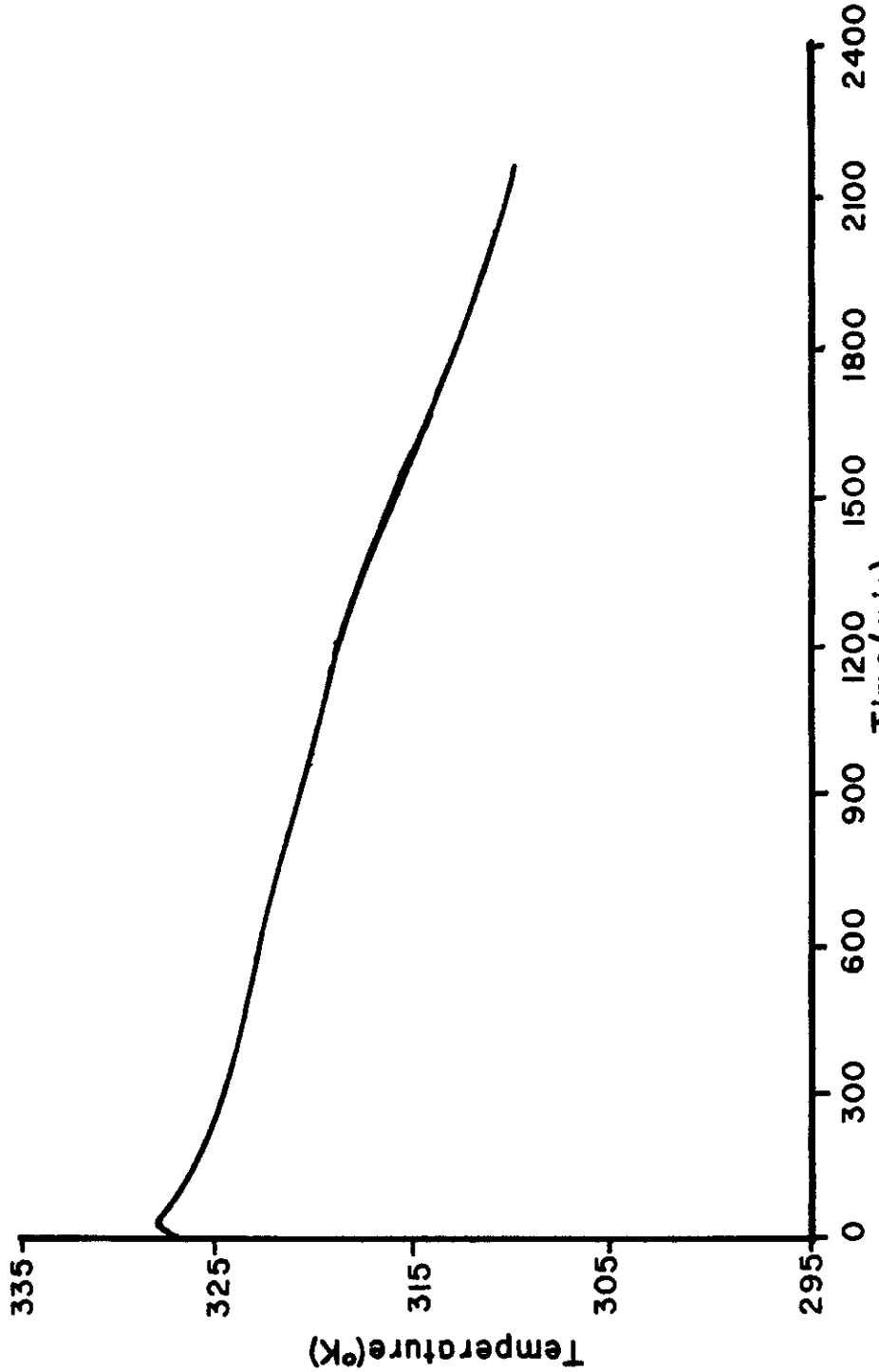

Figure 21. Temperature of water as it is pumped during Run 2.

Table 3 summarizes the information on the amounts of heat injected and recovered during each run. The total energy injected and recovered was calculated using the initial aquifer temperature for a base of reference. For Run 1, the energy recovery efficiency was 46.4 percent, and for Run 2 54.8 percent. More insulation on the sides of the model during Run 2 could have contributed to the increased efficiency of Run 2. Also, a larger injection flowrate and injection time were used in Run 2, which moved the thermal front to a radius of 6.096 m as compared to a radius of 3.048 m for Run 1. Thus, the ratio of surface area to storage volume for Run 2 was much less than for Run 1, and therefore less energy was lost per unit of stored energy.

Table 3 also shows the amounts of energy injected and recovered using 4 different temperatures as a base. The corresponding recovery efficiencies are also given. This type of information will be useful for designing hot water injection pumping systems.

Comparison of Experimental Data to Analytical Models

In comparing the temperature data from the laboratory experiment with the predicted temperatures from the analytical solution of Avdonin (1964), two problems occurred. The first problem was how to characterize the thermal conductivity of the confining layer of the model, which consisted of a 0.00644 m (1/4 in) layer of sheet metal, plus insulation, instead of the shale experienced in nature. The second problem occurred because the laboratory model was a radial sector and had sides. In nature, angular symmetry exists around a well and sides are not present.

Table 3. Quantities of energy injected and recovered during Runs 1 and 2

Injection Cycle	Run 1	Run 2
Average Injection Rate (cc/min)	957.3	1482.0
Flowrate for full circle (m^3/sec)	0.50126×10^{-3}	0.077634×10^{-3}
Average Initial Aquifer Temperature (°K)	295.72	296.64
Average Injection Temperature (°K)	332.65	332.28
Total Energy Injected (J)	2.57×10^{8}	4.78×10^{8}
Energy Injected > 303.16°K(J)	2.05×10^{8}	3.90×10^{8}
Energy Injected > 313.16°K(J)	1.36×10^{8}	2.56×10^{8}
Energy Injected > 323.16°K(J)	6.60×10^{7}	1.22×10^{8}
Time of Cycle (hr)	29.	36.
Volume of Water Injected (m^3)	1.666	3.201
Pumping Cycle		
Average Pumping Rate (cc/min)	1044.5	1245.9
Energy Recovered - Total (J)	1.19×10^{8}	2.62×10^{8}
> 303.16°K(J)	7.26×10^{7}	1.88×10^{8}
> 313.16°K(J)	2.12×10^{7}	7.75×10^{7}
> 323.16°K(J)	1.38×10^{6}	8.58×10^{6}
Recovery Efficiency* - Total (%)	46.4	54.8
> 303.16°K(%)	35.3	48.2
> 313.16°K(%)	15.6	30.3
> 323.16°K(%)	2.9	7.2
Time of Cycle (hr)	24.	36.
Volume of Water Recovered (m^3)	1.504	2.691
Energy in model at end of pumping cycle (J)	1.57×10^{7}	3.14×10^{7}

*All efficiencies are calculated from the energy injected and energy recovered for the given temperature. Total energy is based on initial aquifer temperature.

Thus, in nature heat is only lost out the top and bottom of the aquifer. In the laboratory model, heat was lost out the top, bottom, and sides. The heat lost through the sides is not considered in Avdonin's solution (1964). To account for this problem, the value of the thermal conductivity in the confining layers was assumed to be larger for the calculations using Avdonin's solution (1964). A trial and error procedure was used to select the best values of thermal conductivity to use in Avdonin's solution (1964), and predict the experimental temperature profiles.

For this trial and error procedure, the thermal conductivity of the flow layer was initially assumed to be equal to the stagnant thermal conductivity of 2.65 w/(m°K). Values of the thermal conductivity in the confining layers were varied in Avdonin's solution with little success in predicting experimental values. The experimental heat front appeared to be more spread out and dispersed than the analytical solution was capable of predicting. This indicated that a larger value of thermal conductivity was needed in the confining layers until a good agreement between experimental and predicted temperature profiles was obtained. Using the thermal conductivity value that gave the best agreement, the analytical solution of Avdonin was compared to the experimental data of Run 1 (Figures 22 and 23). A value of 30.0 w/(m°K) for both the thermal conductivity in the flow layer and confining layers gave the best agreement between experimental and predicted temperature profiles.

In formulating Avdonin's solution (1964), a infinite vertical thermal conductivity in the flow layer was assumed. Thus, the temperature obtained using this solution will be an average temperature for the aquifer thickness at a specified radius and time. Figures 22 and 23

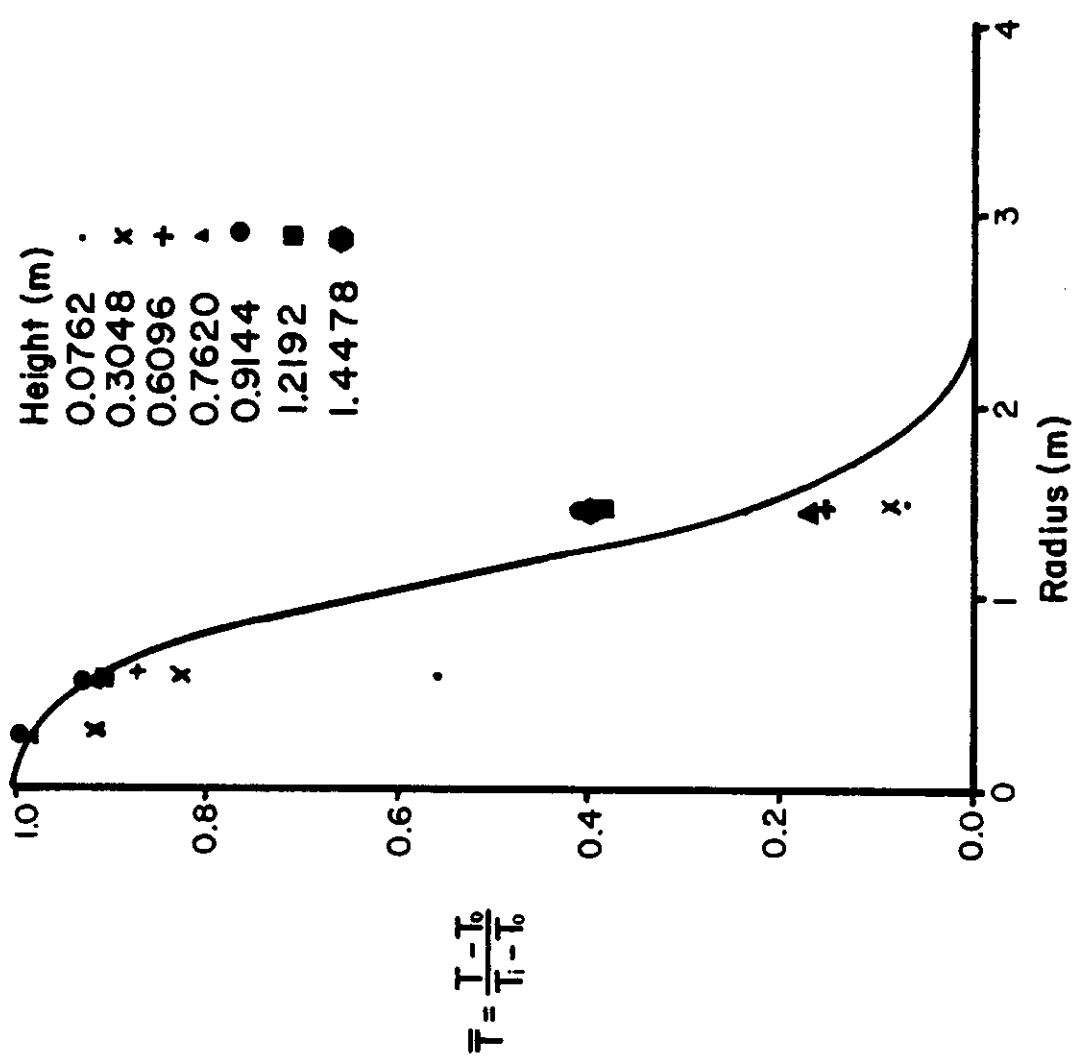

Figure 22. Comparison of Avdonin's solution (1964) to measured temperatures at different depths for Run 1 at t = 300 minutes.

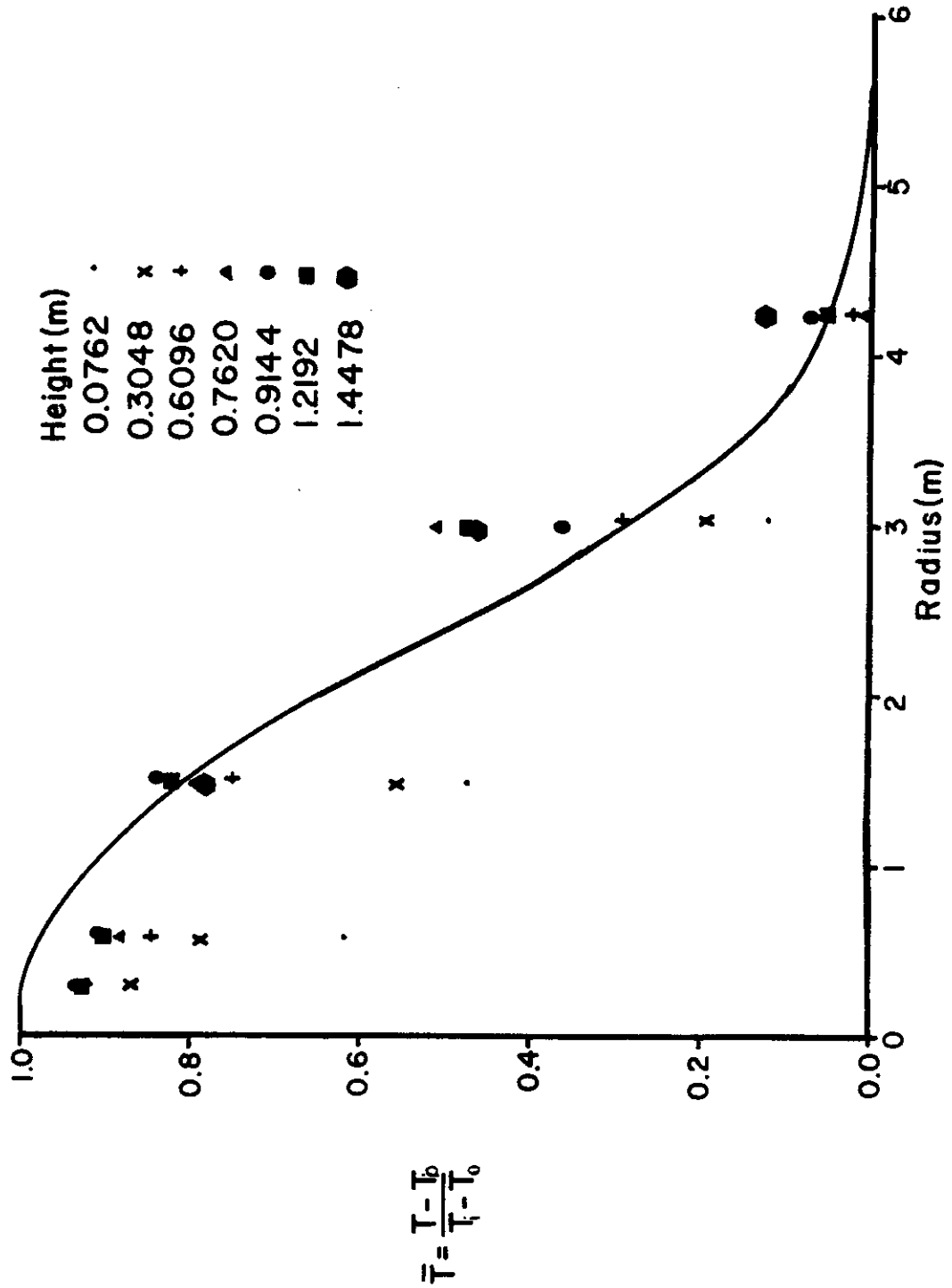

Figure 23. Comparison of Avdonin's solution (1964) to measured temperatures at different depths for Run 1 at t = 1740 minutes.

show that the predicted average temperature is well within the range of measured temperatures.

Using the value for thermal conductivity of 30.0 w/(m°K) determined from Run 1, temperature profiles from Avdonin's solution were compared with the experimental data from Run 2. Five hours into the injection cycle of Run 2, the predicted values closely matched the experimental data as shown in Figure 24. After 36 hours of injection in Run 2, the analytical solution slightly under predicted the temperature profile as shown in Figure 25. The temperature profile moved farther radially in Run 2 than predicted by the analytical solution. Therefore, the use of 30.0 w/(m°K) for the thermal conductivity in the flow layer and confining layers of Avdonin's solution did not predict the temperature profiles as well for Run 2 as for Run 1.

Angular symmetry was assumed in the formulation of Avdonin's solution (1964). However, angular symmetry does not exist in the laboratory model and heat losses are occurring out the sides of the model. It is apparent that heat losses out the sides of the model cannot be completely accounted for by increasing the thermal conductivity in the confining layer. The reasons for this are as follows. By dividing Equation 17b by Equation 17c, the ratio of the heat transfer area out the model sides to the heat transfer area out the top and bottom is

$$\frac{A_s}{A_b} = \frac{2h\ \Delta r}{2r\ \Delta\theta\ \Delta r} = \frac{h}{r\ \Delta\theta} \quad , \tag{20a}$$

where Δr = radial increment (L);

r = radial distance from well (L);

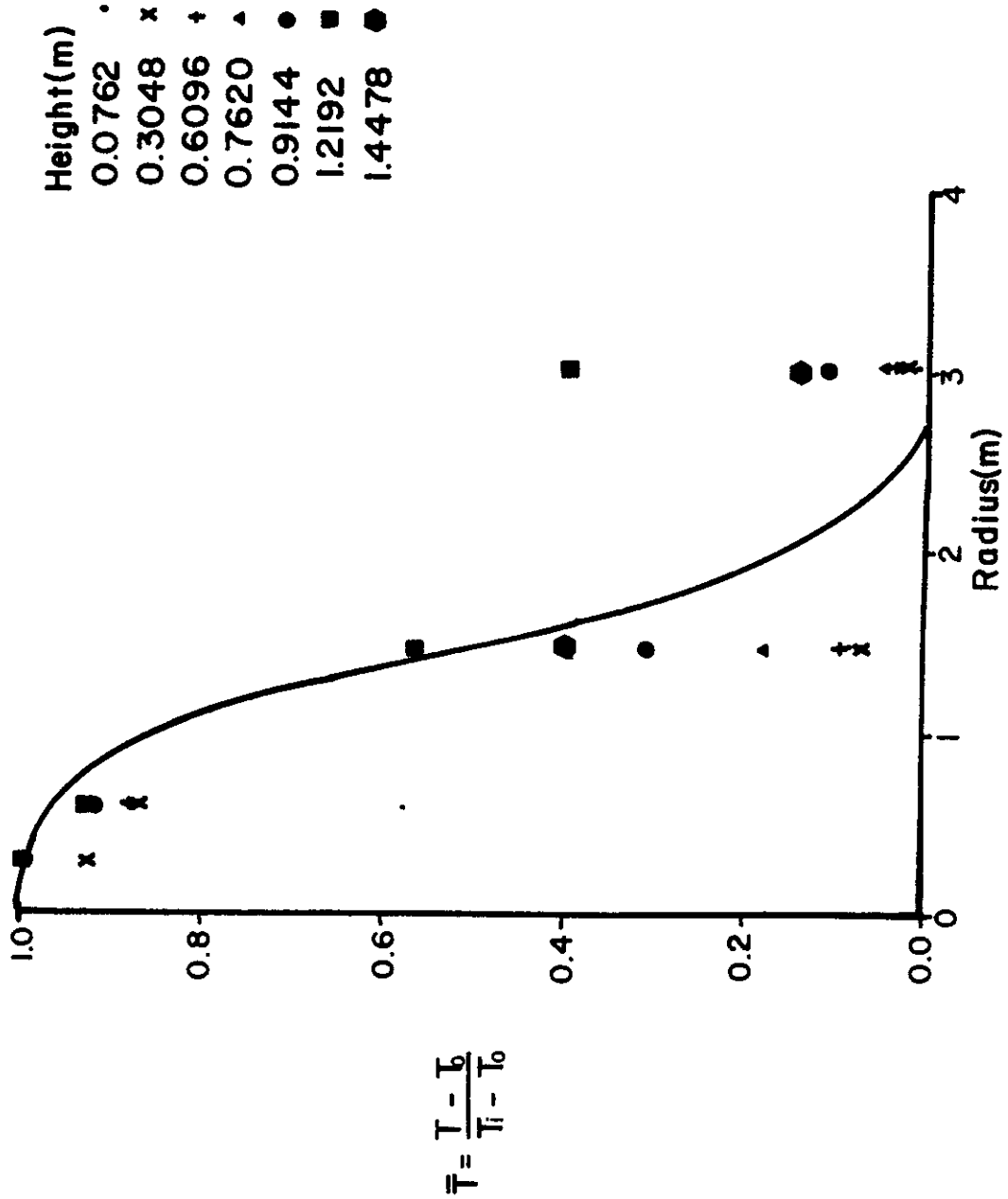

Figure 24. Comparison of Avdonin's solution (1964) to measured temperatures for Run 2 at t = 300 minutes.

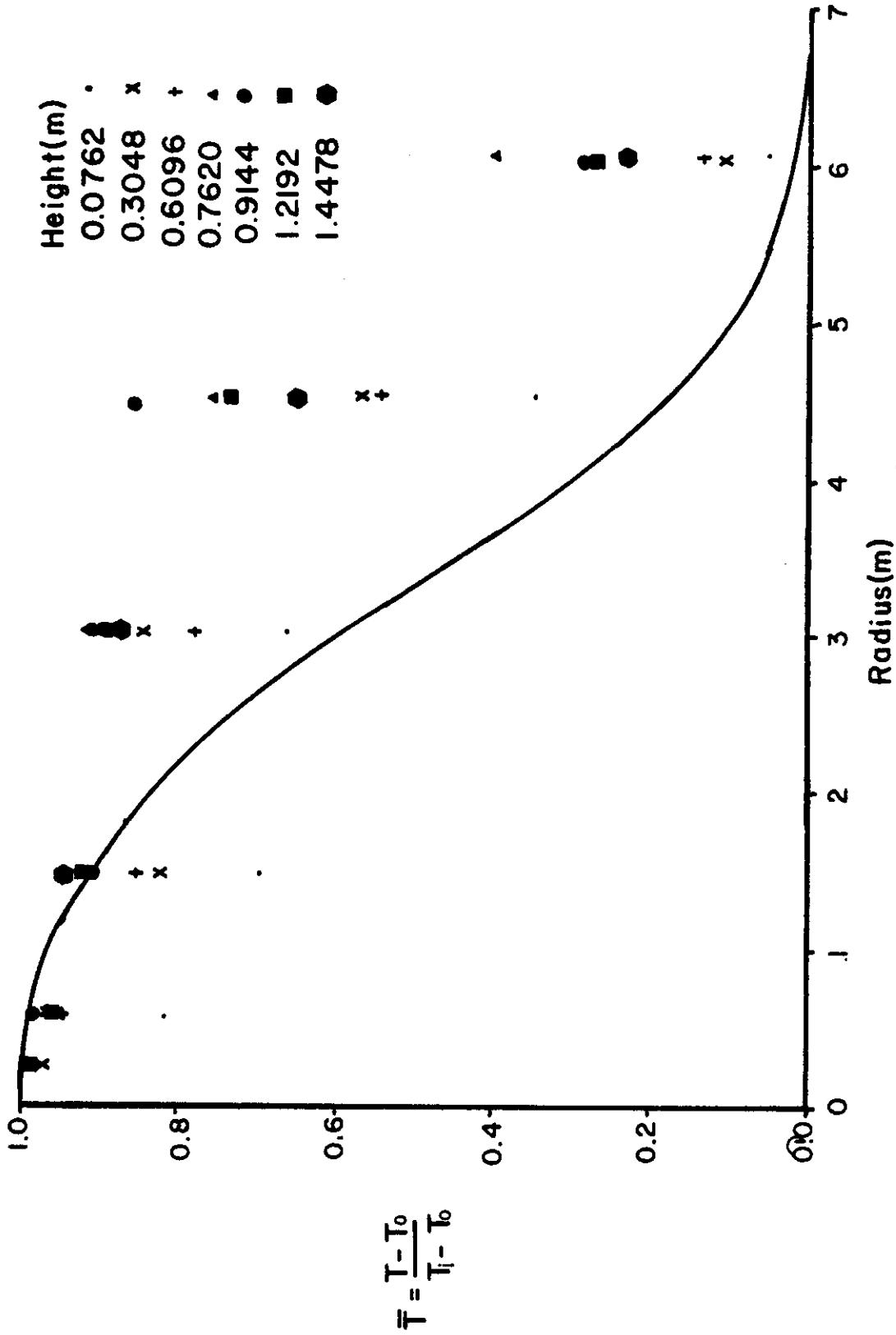

Figure 25. Comparison of Avdonin's solution (1964) to measured temperatures for Run 2 at t = 2160 minutes.

$\Delta\theta$ = angle increment (radian); and

h = flow layer thickness (L).

For a flow layer thickness of 1.8288 m and $\Delta\theta$ of 0.2, this expression becomes

$$\frac{A_s}{A_b} = \frac{9.144}{r} \quad , \tag{20b}$$

with r in meters. Therefore, for radial increments centered at radii of 0.3048 m and 3.048 m, the ratio of heat transfer area out the sides to heat transfer area out the top and bottom is 30.0 and 3.0 respectively. Thus, the ratio of heat loss out the sides to the heat losses out the top and bottom is reduced by a factor of 10 when the radius is increased by a factor of 10. Therefore, as the hot water front moves farther away from the well, the thermal conductivity required in the confining layers of Avdonin's solution must decrease with time to account for the losses out the side of the model.

At the end of the injection cycle for Run 1, the hot water front was at the 3.048m radius and Avdonin's solution accurately predicted the temperature profile. At the end of the injection cycle of Run 2, the hot water front was at the 6.096m radius and Avdonin's solution underpredicted the temperature profiles. For Run 2, less heat was lost out the sides compared to losses out the top and bottom because the heat front had moved farther away from the well. The apparent thermal conductivity in the confining layers should be reduced to accurately predict the temperature at large times for Run 2.

Thermal Efficiency

In Figure 26, the calculated thermal efficiencies for Runs 1 and 2 are plotted along with the analytical results from Rubinshtein (1959) and Lauwerier (1955). In the analytical solutions, a value of 30.0 w/(m°K) was used for both thermal conductivities. Run 1, with its heat front at about 3 m, agrees more closely with the analytical solutions than Run 2. As discussed above, the thermal front in Run 2 moved to a larger radius than Run 1 and heat losses are less per unit volume of stored energy. This made the thermal efficiencies larger for Run 1 than for Run 2.

The thermal efficiency values calculated from the experimental data are erratic. This erratic behavior occured at early times in the injection cycle when the hot water front was very sharp and located close to the well bore. The integration procedure for calculating thermal efficiency was less accurate under these conditions. Two temperature measuring locations ($r = 0.3048$ m and $r = 0.6096$ m) were located close to the well. The next radial measuring location was at $r = 1.524$ m. When the temperature front was located between the 0.6096 m and 1.524 m radius, there was no accurate way to determine the exact location of the temperature profile in this area. This inability to know the exact location of the temperature profile caused erratic values of thermal efficiency to be calculated when the experimental data were used in the integration procedure.

The analytical solutions by Avdonin (1964) for predicting temperature profiles and the one by Rubinshtein (1959) and Lauwerier (1955) for thermal efficiency accurately predicted temperatures and thermal

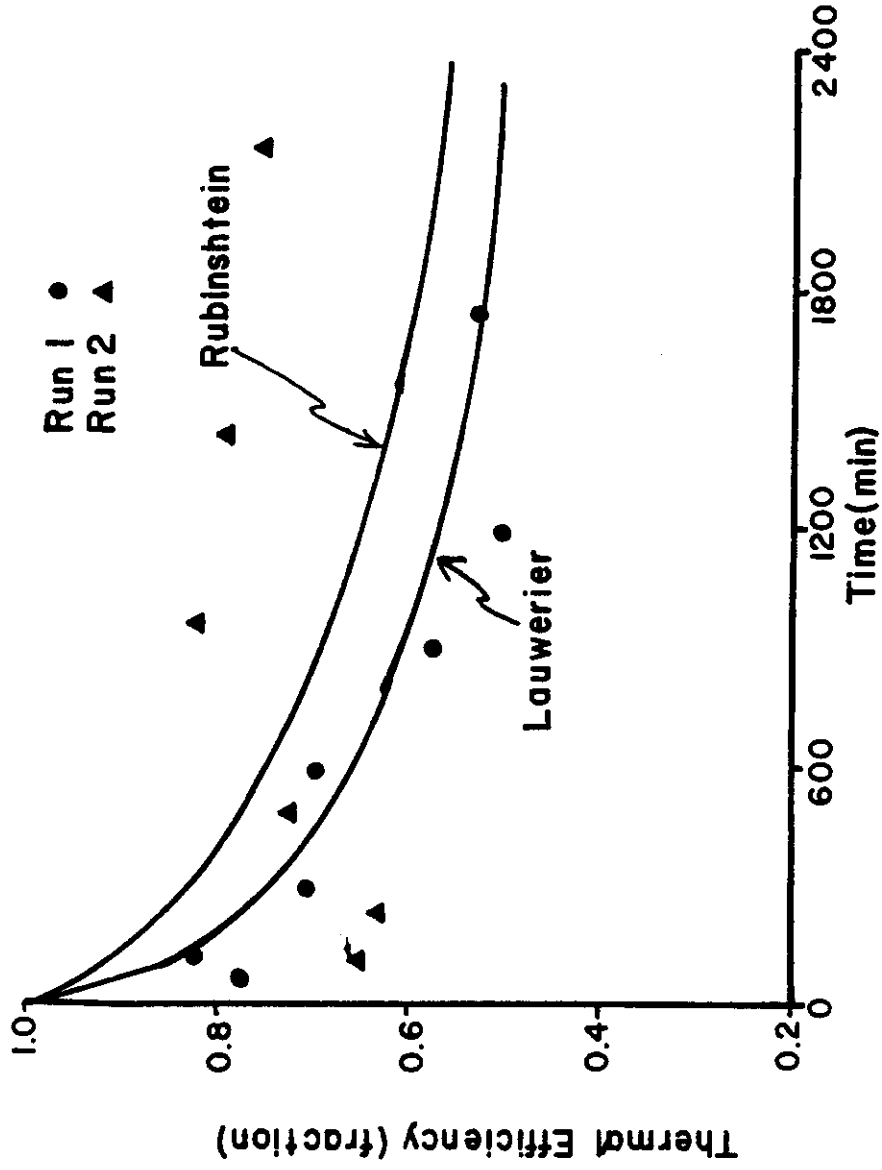

Figure 26. Comparison of thermal efficiencies measured for Runs 1 and 2 with analytical solutions by Rubinshtein (1959) and Lauwerier (1955).

efficiencies for Run 1. These solutions did not give as good of results for Run 2. In nature where there is angular symmetry and no heat losses out the sides, the solutions of Avdonin (1964), Rubinshtein (1959), and Lauwerier (1955) appear to be capable of accurately predicting temperatures and thermal efficiencies resulting from injecting hot water into groundwater aquifers.

Effect of Parameters on Temperature Profiles

From the analytical solution by Avdonin (1964) for the temperature distribution resulting from hot fluid injection and the one by Rubinshtein (1959) for thermal efficiency, the effects of changes in physical properties can be evaluated. Figure 27 shows the effects of varying the thermal conductivity in the flow layer on the radial temperature distribution. As the thermal conductivity in the flow layer was increased, the temperature curve was flattened and the hot water front was less pronounced. Because the larger thermal conductivity allowed more heat transfer radially by conduction, a temperature change resulted at a greater distance from the well. The ratio of heat transfer by conduction to convection was increased.

Figure 28 shows the effect of increasing the thermal conductivity in the confining layers while holding all other properties constant. The hot water front has the same shape for both the large and small values of thermal conductivity in the confining layers. However, the heat front moved farther from the well for the smaller value of thermal conductivity in the confining layers. Because heat is transferred out of the aquifer faster with the larger value of thermal conductivity in the confining

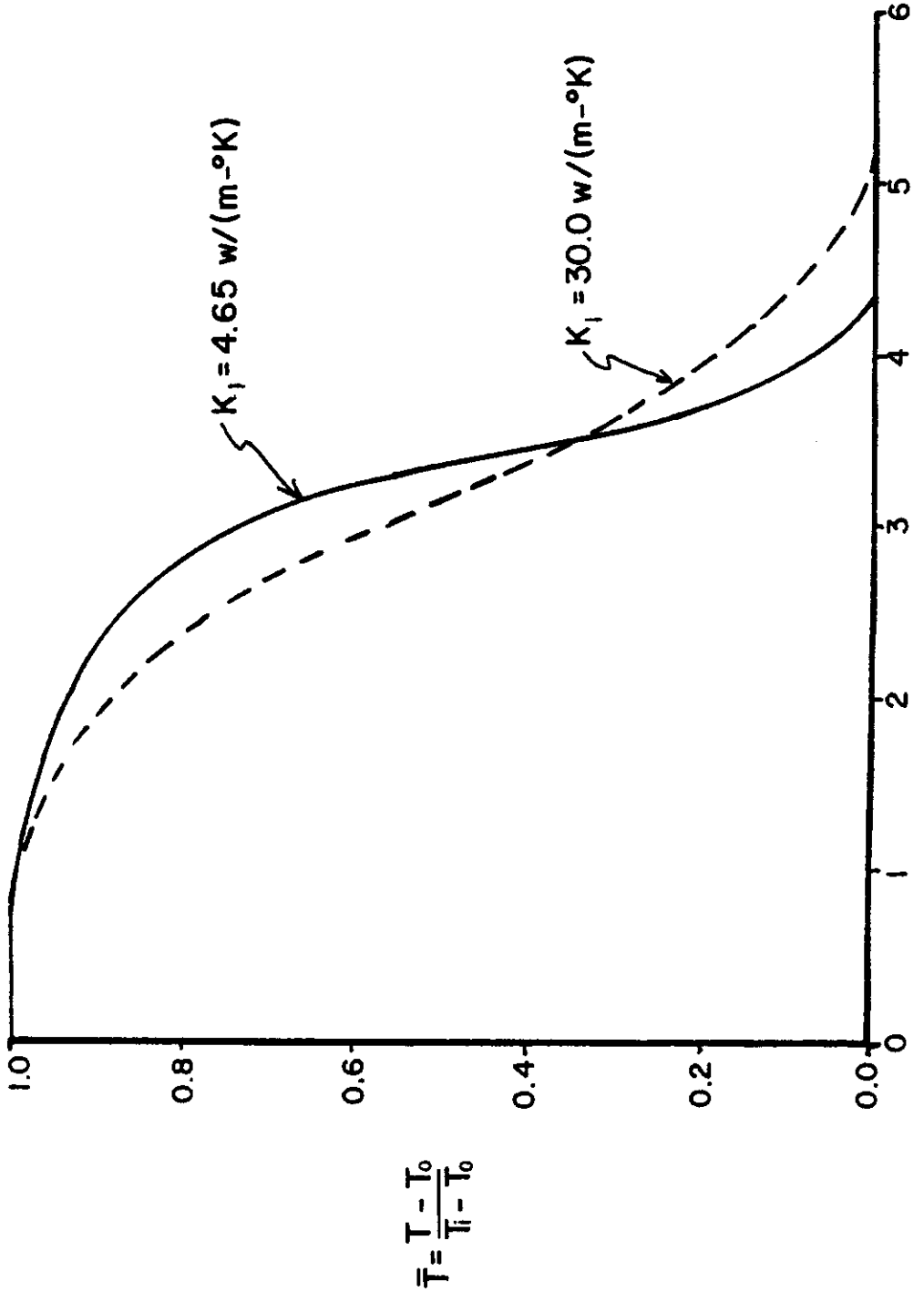

Figure 27. Effect of increasing the thermal conductivity in the flow layer while holding all other parameters constant in Avdonin's (1964) equation (Equation 5).

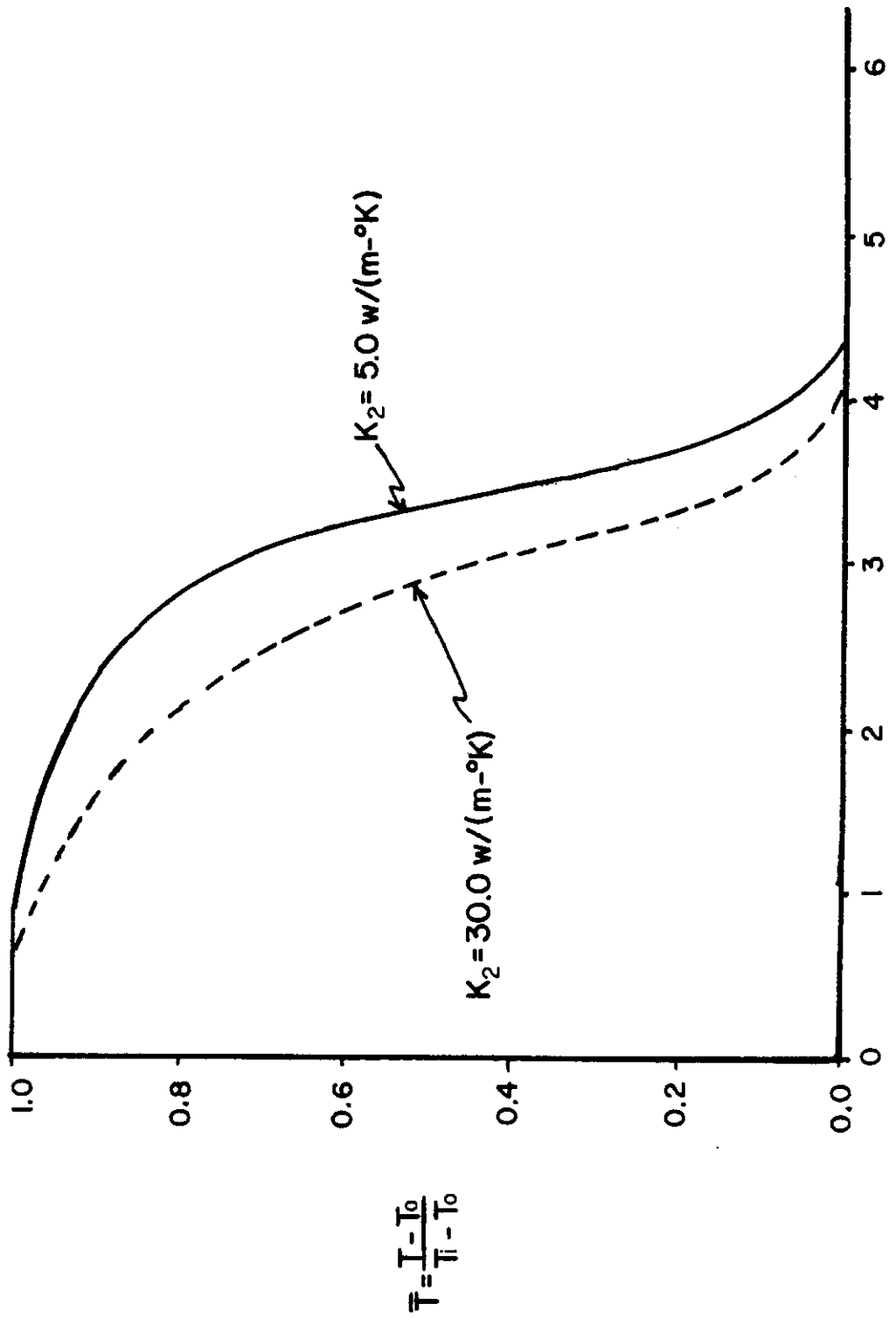

Figure 28. Effect of increasing the thermal conductivity in the confining layers while holding all other parameters constant in Avdonin's (1964) equation (Equation 5).

layers, less heat is stored in the aquifer which prevents the temperature front from moving as far radially.

The effect of increasing the fluid flowrate while holding all other parameters constant is shown in Figure 29. The curves have the same shape, but the temperature profile for the larger flowrate has advanced a greater distance from the well. The flowrate was increased by 54.9 percent and the radius where the dimensionless temperature is 0.5, an indicator of how far the thermal front has advanced, increased from 2.7 m to 3.4 m, a 25.9 percent increase. The percent increase in radius was less than the percent increase in flowrate. Thermal efficiency is independent of flowrate. If the flowrate is increased by 54.9 percent ($Q_2 = 1.549\ Q_1$), the amount of energy stored must increase by 54.9 percent assuming no thermal losses. The volume of energy storage in an aquifer is a function of r^2, not a linear function of r. Therefore, when the volume is increased by 54.9 percent ($V_2 = 1.549\ V_1$), the radius where the thermal front has reached will only increase by the square root of the volume increase ($r_2 = \sqrt{1.549}\ r_1 = 1.245\ r_1$) or 24.5 percent. This increase is in close agreement with the 25.9 percent increase obtained from Figure 29. Therefore, the radius of the thermal front is related to the square root of flowrate and is not a linear function of flowrate.

A family of curves for thermal efficiency from Rubinshtein (1959) is shown in Figure 30. Thermal efficiency is directly dependant on the physical properties of the porous media and confining layers. This dependance is characterized by

$$\alpha = \frac{\lambda a - 1}{\lambda a + 1} \quad , \tag{21}$$

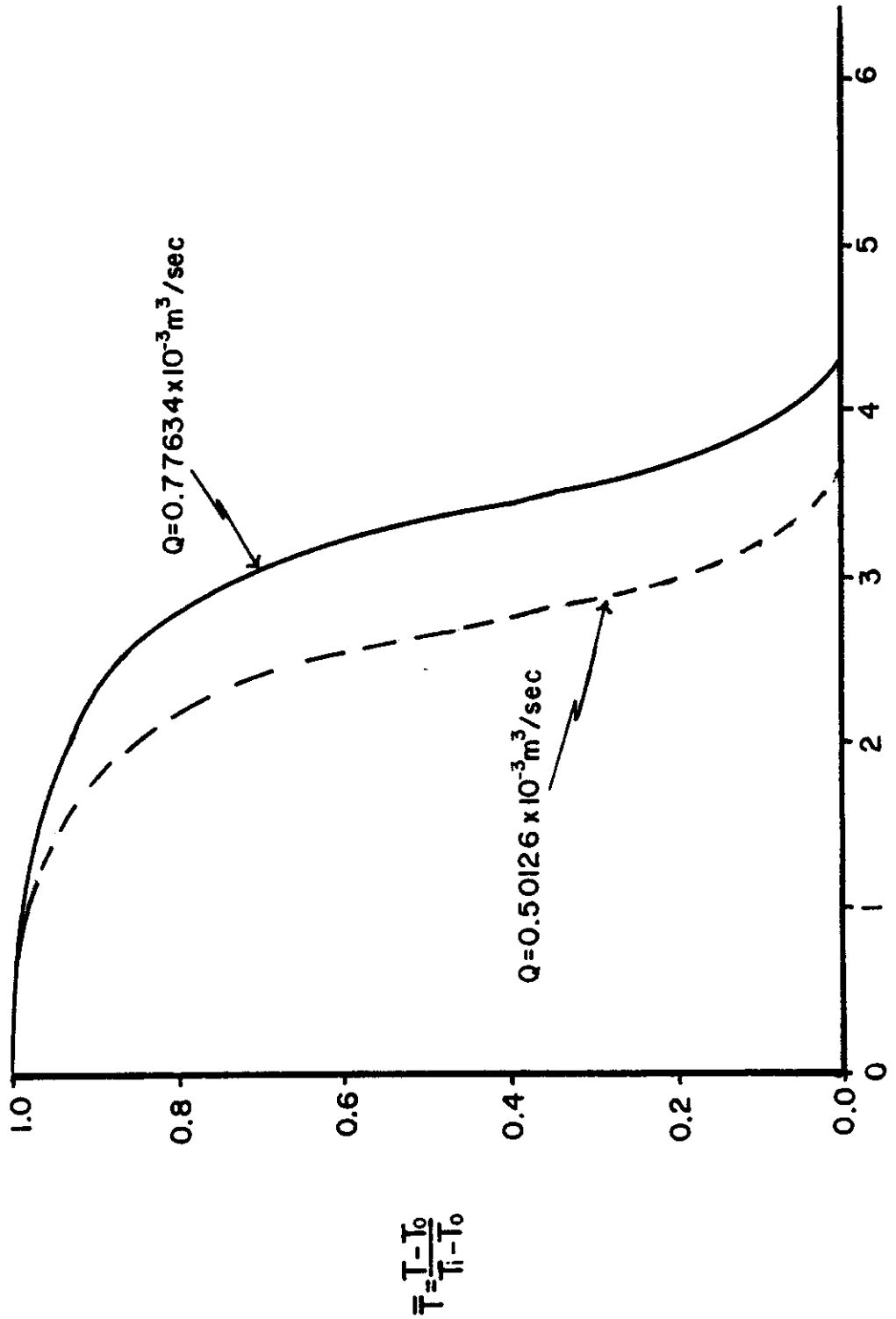

Figure 29. Effect of increasing the flowrate while holding all other parameters constant in Avdonin's (1964) equation (Equation 5).

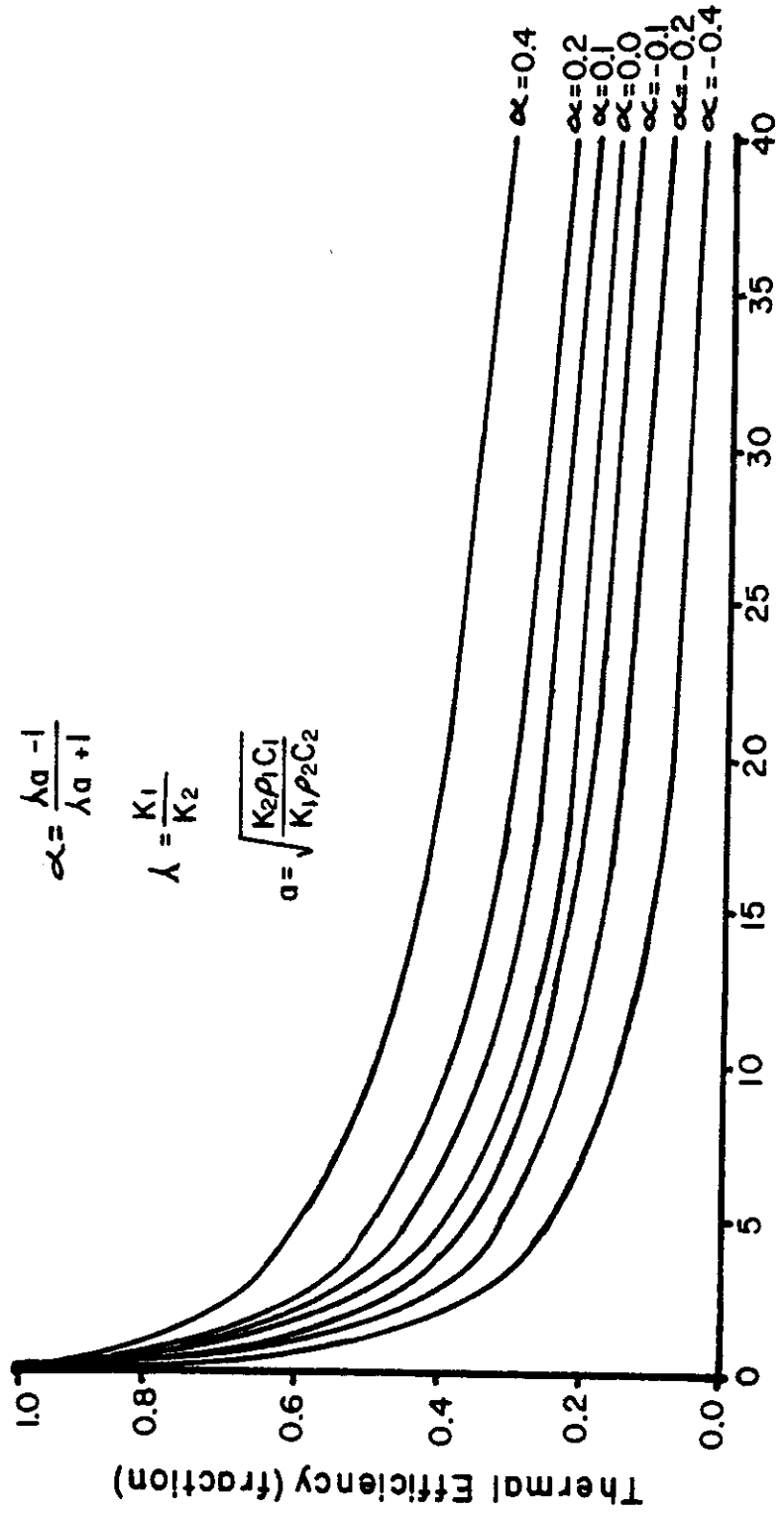

Figure 30. Rubinshtein's (1959) family of curves for thermal efficiency.

where $\lambda = \frac{K_1}{K_2}$; and

$$a = \sqrt{\frac{K_2 \rho_1 C_1}{K_1 \rho_2 C_2}} \quad ; \quad \text{or}$$

$$\lambda a = \sqrt{\frac{K_1 \rho_1 C_1}{K_2 \rho_2 C_2}} \quad .$$

From Figure 30, a definite relationship exists between α and thermal efficiency. For a given dimensionless time, thermal efficiency increases as α increases. Also, a relationship exists between the thermal properties of the system and α as shown in Figure 31. From Figures 30 and 31, it is apparent that as (λa) increases, thermal efficiency increases.

This relationship can be explained by examining the thermal parameters. First, assume that all properties except the thermal conductivity in the flow layer (K_1) are held constant. Also, assume a dimensionless time of 5 and a (λa) of 1, forcing $\alpha = 0$. Going to Figure 30 and reading the $\alpha = 0$ curve at a dimensionless time of 5, the thermal efficiency is 0.4. Increasing the thermal conductivity in the flow layer by a factor of 4 $(K_1 = 4K_1)$ dimensionless time is now 20 (5 x 4) and (λa) is now 2 $(1 \times \sqrt{4})$. For (λa) equal 2 from Figure 31 α is 1/3. By interpolating between α of 0.2 and 0.4 at a dimensionless time of 20 in Figure 30, the thermal efficiency is also 0.4. From this analysis, changing the thermal conductivity in the flow layer does not affect energy storage and thermal efficiency when injecting hot water into a groundwater aquifer.

By holding all thermal properties constant and increasing the thermal conductivity (K_2) in the confining layers, α is decreased and

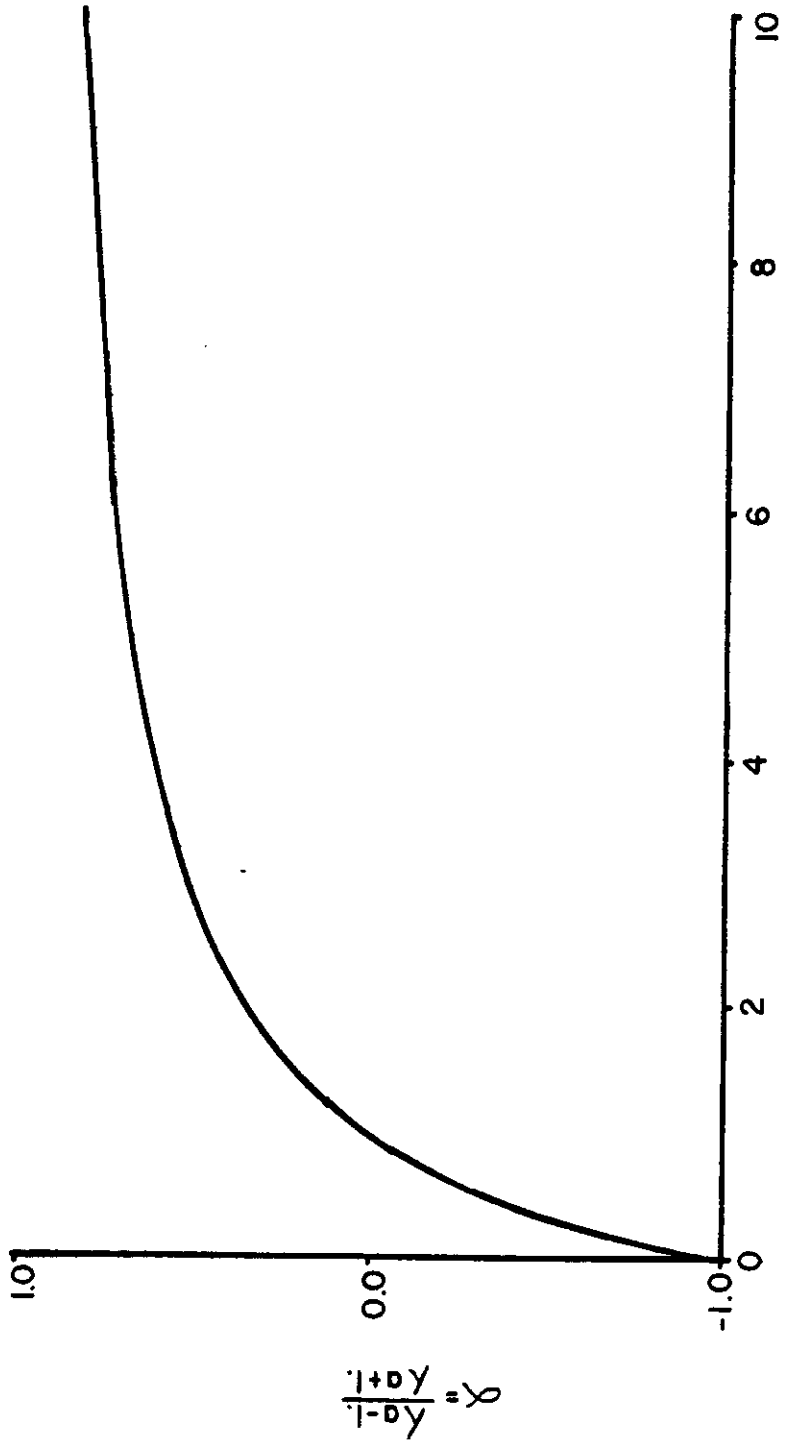

Figure 31. Relationship of α to a thermal properties of the porous media.

thermal efficiency is decreased. This is a result of increased heat transfer out the top and bottom of the aquifer.

Thermal efficiency is very dependant on the thickness of the flow layer (h). This physical parameter enters into the family of curves in Figure 30 via the dimensionless time parameter. By holding all values constant while doubling the flow layer thickness, dimensionless time is decreased by 1/4. For large values of dimensionless time (>15), this change would result in only small changes in thermal efficiency. However for smaller values of dimensionless time, a decrease of 1/4 could result in a very large increase in thermal efficiency.

For most practical injection times and flow thicknesses, dimensionless time will be very small. Assuming a thermal conductivity of 5 w/(m°K) and a specific heat capacity of 2.5×10^6 J(m^3°K) in an 8 m thick flow layer, water could be injected for 90 days with a dimensionless time of only 0.97. Therefore, for most practical purposes, the range in values for dimensionless time will be less than 1.0. The portion of Figure 30 with dimensionless time less than 1.0 has been expanded in Figure 32.

Curves such as Figure 30 and especially Figure 32 can be useful in designing a hot water injection-pumping system. In the design of a hot water injection system, values for thermal conductivity and specific heat capacity can be estimated. For these estimates, a value for α can be calculated and an efficiency curve for operating the system could be established. After determining an injection cycle length and a minimum allowable efficiency, Figure 32 could be used to calculate a critical aquifer thickness. If the aquifer had a thickness greater than the critical thickness, the system would operate at an efficiency greater

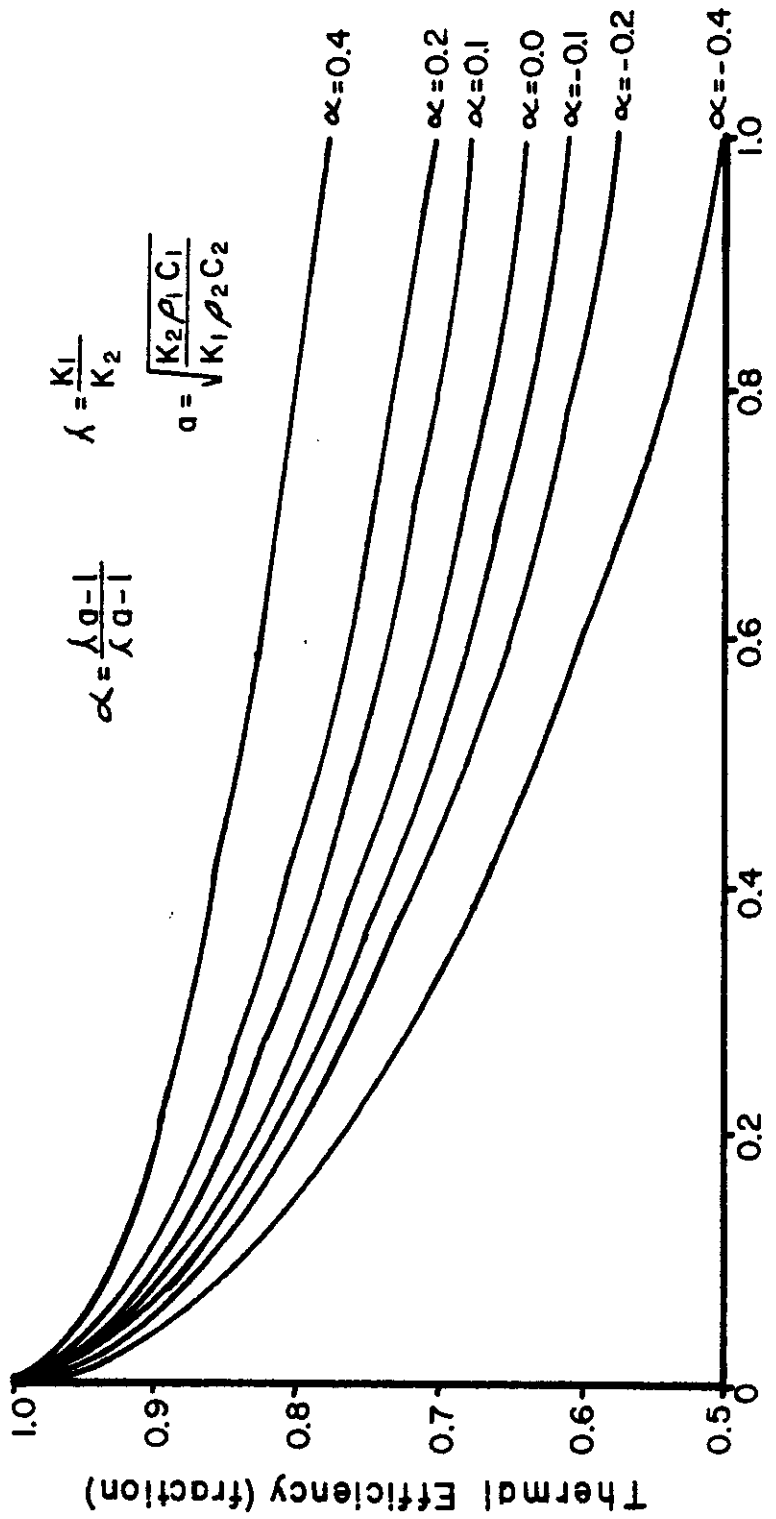

Figure 32. Rubinshtein's (1959) family of curves for thermal efficiency using the range of practical injection times.

than desired. If the aquifer thickness was not as large as the critical thickness, either the time of injection would have to be decreased or a smaller efficiency than desired would be obtained.

The same type of analysis could also yield a critical injection time. After calculating a value for α and determining a minimum allowable efficiency, Figure 32 could be used to find a maximum dimensionless time to get a desired efficiency. By estimating flow layer thickness and thermal properties, the maximum injection time or critical injection time could be calculated. For a given amount of stored energy, the required injection flowrate and injection temperature could be determined.

Thermal efficiency is only indirectly related to flowrate. If the flowrate is doubled, the time for injecting a given amount of energy in the form of hot water is halved. Thus, dimensionless time is also halved and a larger thermal efficiency is obtained.

Using the analytical solution by Avdonin (1964), increasing thermal conductivity in the flow layer showed that the temperature profile became less pronounced. Thermal efficiency did not change with changes in thermal conductivity of the flow layer. If the thermal conductivity in the confining layers is increased, the heat front does not move as far from the well, more heat is lost through the top and bottom of the aquifer, and thermal efficiency decreases. Thermal efficiency is dependant on the porous media but is the most sensitive to changes in flow layer thickness. Thermal efficiency is only indirectly related to injection flowrate.

CHAPTER VII

SUMMARY AND CONCLUSIONS

The objectives of this study were to construct a laboratory model to simulate hot fluid injection into a confined aquifer, collect temperature and fluid pressure data from this laboratory model, and use them to verify existing analytical solutions. Also, the analytical solutions were used to evaluate the effects of various system parameters (thermal conductivities, flow layer thickness, and injection rate) on efficiency of energy storage and total energy recovery efficiency.

A laboratory model was constructed that simulated hot water injection into a confined aquifer. Temperature and pressure data were taken to monitor the hot water front as it moved through the model which was a 1.8288 m deep, 0.2 radian sector tank with a radial extent of 7.01 m. Temperatures were measured using thermistors at 6 different radial distances from the well and 7 vertical heights above the bottom of the flow layer. Piezometric water levels were measured at 5 radial distances from the well and 3 heights above the bottom of the flow layer. All data were manually read and recorded. Water was supplied to the model at a constant temperature and flow rate. The flow layer was composed of a Texblast fine grained blasting sand and all physical properties of the porous media were measured using standard laboratory procedures.

One run was made where no heat transfer took place. Using water level data from this Run and a steady state well formula, the hydraulic conductivity was measured. The hydraulic conductivity measured during the first heat transfer, Run 1, was slightly higher than originally

measured because as the aquifer temperature increases, the hydraulic conductivity increases. For both Runs 1 and 2, the temperature of the laboratory model increased, the hydraulic conductivity increased, and the water levels decreased. The hydraulic conductivity measured during Run 2 was less than that measured in Run 1 because there was more entrapped air in the flow layer during Run 2.

Three runs were made where heat transfer took place. The first run, with an injection cycle of 29 hours, was conducted at an average sector flow rate of 957.34 cc/min and an average injection temperature of 333.65°K. The injection cycle was followed by a 24 hour pumping cycle. Run 2 had an injection rate of 1482 cc/min at an average injection temperature of 332.28°K for 36 hours, which was followed by a 36 hour pumping cycle. Run 3 was an injection cycle at the same injection rate as Run 2 and immediately followed the pumping cycle of Run 2.

Temperature for Runs 1 and 2 showed that the 0.3048 m, 0.6096 m, and 1.524 m radii reached thermal equilibrium during the injection cycle. The equilibrium temperature decreased with increasing radii. For these radii, the equilibrium temperature increased from Run 1 to Run 2 because a higher flow rate was used for Run 2 and there was increased insulation on the model. A vertical thermal gradient existed at each radii with the warm water on top. The less dense warm water floated over the more dense cooler water initially in the model.

Temperature distributions at the 0.3048 m and 0.6096 m radii showed the effects of changing air temperature. There were more heat losses out the sides of the model than out the top and bottom. The condition of angular symmetry required in the analytical solutions was not met.

The thermal energy recovered was measured, and the thermal efficiency calculated. There was an increase in thermal efficiency from Run 1 to Run 2. Energy in the form of warm water remained in the flow layer at the end of the pumping cycle on Run 2 and the temperature curves for Run 3 were affected by this remaining energy.

Angular symmetry, an assumption in all analytical solutions, was not met in the laboratory model. For this reason, the analytical solution did not accurately predict formation temperatures at all times. Thermal efficiency curves showed the same results.

Using analytical solutions, the effects of various system parameters were easily seen. Increasing thermal conductivity in the flow layer caused the hot water front to flatten out and reach farther into the flow layer. Increasing the thermal conductivity in the confining layers resulted in more heat lost out the top and bottom of the aquifer, and the temperature for a given radius and time was decreased. Increasing the flow rate moves the heat front farther into the flow layer. In general for the short times studied (less than 36 hours), the temperature distribution tends to be insensitive to changes in thermal conductivity in the flow layer and confining layers. Thermal efficiency was most affected by a change in flow layer thickness.

As a result of this research, the following specific conclusions were drawn:

1. Because the assumption of angular symmetry was not met, the laboratory model did not simulate the injection and pumping of hot fluid into a confined aquifer as described by the analytical solutions.

2. When injecting hot water into a confined aquifer, the hydraulic conductivity will increase with an increase in formation temperature.
3. During a series of injection-pumping cycles, the energy remaining in the form of warm water at the end of a pumping cycle will alter the temperature distribution curves on subsequent injection cycles.
4. During hot fluid injection, a vertical temperature gradient exists with the warmer water on top.
5. Temperature distributions from analytical solutions modeling hot fluid injection are relatively insensitive to changes in thermal conductivity in the flow layer and confining layers.
6. The physical property of a system that most affects thermal efficiency during hot water injection is flow layer thickness.

Research concerning the injection of hot fluids into confined aquifers should be improved as follows:

1. A numerical model should be developed that models the laboratory model and the data obtained from the laboratory model could be used to verify the numerical model.
2. Further work needs to be done to more accurately determine the effects of injection rate and injection temperature on thermal efficiency.
3. Laboratory data should be collected to determine how temperature distributions will change when a cooler fluid is injected into a confined aquifer.

4. A method of preventing heat transfer out the sides of the laboratory model is required to meet the assumptions in the analytical solutions.

LIST OF REFERENCES

1. Avdonin, N. A. 1964. Some formulas for calculating the temperature field of a stratum subject to thermal injection. Neft'i Gaz. 7(3):37.

2. Baker, P. E. 1967. Heat wave propagation and losses in the thermal oil recovery process. Proceedings 7th World Petroleum Congress. 4:459-470.

3. Baker, P. E. 1969. An experimental study of heat flow in steam flooding. Society of Petroleum Engineers Journal. 9(1):89-99.

4. Brady, Nyle C. 1974. The Nature and Properties of Soils. MacMillian Publishing Co., Inc. New York, New York.

5. Breston, J. N. and B. R. Pearman. 1953. Hot water injection treatment of wells to increase water intake rates. Producers Monthly. 18(1):15-23.

6. Chappelear, J. E. and C. W. Volek. 1969. The injection of a hot liquid into a porous media. Society of Petroleum Engineers Journal 9(1):100-114.

7. Davidson, L. B., F. G. Miller, and T. D. Mueller. 1967. A mathematical model of reservoir response during cyclic injection of steam. Society of Petroleum Engineers Journal. 7(2): 174-187.

8. Davison, R. R., W. B. Harris, and J. H. Martin. 1975. Storing sunlight underground. Chem. Tech. 5:736-741.

9. Duffie, John A. and William A. Beckman. 1976. Solar heating and cooling. Science. 191:143-145.

10. Ebeling, L. L. and D. L. Reddell. 1976. Energy (hot water) storage in groundwater aquifers. American Society of Agricultural Engineers, Technical Paper No. 76-2540.

11. Flock, D. L., D. Quon, M. A. Leal and A. R. Thachuk. 1976. Modelling of a thermally stimulated oil reservoir - an evaluation of theoretical and numerical methods. Journal of Canadian Pet. Tech. 6:136-143.

12. Fournier, K. P. 1965. A numerical method for computing recovery of oil by hot water injection in a radial system. Society of Petroleum Engineers Journal. 5(2):131-140.

13. Gottfried, B. S. 1965. A mathematical model of thermal oil recovery in linear systems. Society of Petroleum Engineers Journal. 5(3):196-210.

14. Green, D. H., R. H. Perry, and R. E. Babcock. 1964. Longitudinal dispersion of thermal energy through a porous media with a flowing fluid. A. I. Ch. E. Journal. 10(5):645-651.

15. Gringarten, A. C. and J. D. Sauty. 1975. A theoretical study of heat extraction from aquifers with uniform regional flow. Journal of Geophysical Research. 80(35):4956-4962.

16. Johnson Division UOP Inc. 1975. Ground Water and Wells. Johnson Division, UOP Inc. Saint Paul, Minnesota.

17. Kenward, Michael. 1976. Potential energy, an analysis of world energy technology. Cambridge University Press. London, England.

18. Landrum, Bobby L., James E. Smith, and Paul B. Crawford. 1960. Calculation of crude oil recoveries by steam injection. Trans. AIME. 219:251-256.

19. Lauwerier, H. A. 1955. The transport of heat in an oil layer caused by injection of a hot fluid. Applied Scientific Research, Sect. A. 5:145-150.

20. Malofeev, G. E. 1960. Calculation of the temperature distribution in a formation when pumping hot fluid in a well. Neft'i Gaz. 3(7):59.

21. Malofeev, G. E. 1960. Simulation of the formation heating process during the injection of hot fluid. Neft'i Gaz. 2(9):49.

22. Martin, J. H., W. B. Harris, and R. R. Davison. 1974. Economic feasibility of the "Solaterre" system. Department of Chemical Engineering, Texas A&M University.

23. Marx, J. E. and R. H. Langheim. 1959. Reservoir heating by hot fluid injection. Trans. AIME. 216:312-315.

24. Meinel, Aden. B. and Marjorie P. Meinel. 1976. Applied solar energy. Addison - Wesley Publishing Company. Reading, Mass.

25. Meyer, C. V. and D. K. Todd. 1973. Conserving energy with heat storage wells. Environmental Science and Technology. 7(6):512-518.

26. Preston, Floyd W. and Richard D. Hazen. 1954. Further studies on heat transfer in unconsolidated sands during water injection. Producers Monthly. 19(2):24-32.

27. Rabbimov, R. T., R. A. Zhakhidov, and G. Ya. Umarov. 1974a. Temperature distribution in accumulation of solar energy in aquifers. Geliotekhnika. 10(2):15-19.

28. Rabbimov, R. T., R. A. Zhakhidov, and G. Ya. Umarov. 1974b. Experimental study of aquifer heating in solar energy accumulation. Geliotekhnika. 10(2):20-27.

29. Ramey, H. J. 1959. Transient heat conduction during radial movement of a cylindrical heat source-applications to the thermal recovery process. Trans. AIME. 216:364-368.

30. Ramey, H. J. 1964. How to calculate heat transmission in hot fluid injection. Petroleum Engineer 4(4):110-120.

31. Ramey, H. J. 1967. A current review of oil recovery by steam injection. Proceedings 7th World Petroleum Congress. 4:471-476.

32. Reed, David B. 1977. Long term storage of solar energy by injecting hot water into groundwater aquifers. Report to the Texas A&M Undergraduate Fellows Program. College Station, Texas.

33. Rubinshtein, L. I. 1959. The total heat losses in injection of a hot liquid into a stratum. Meft'i Gaz. 2(9):41.

34. Schumann, T. E. W. 1929. Heat transfer: a liquid flowing through a porous prism. J. Franklin Institute. 208:405-416.

35. Spillette, Arthur G. 1965. Heat transfer during hot fluid injection into an oil reservoir. Journal of Canadian Pet. Tech. 4:213-218.

36. Streeter, Victor L. and E. Benjamin Wylie. 1975. Fluid mechanics. McGraw Hill, Inc. New York.

37. Sweat, V. E. 1976. A miniature thermal conductivity probe for foods. American Society of Mechanical Engineers, Technical Paper 76-HT60.

38. Thomas, G. W. 1964. A simplified model of conduction heating in systems of limited permeability. Society of Petroleum Engineers Journal. 4(4):335-344.

39. Thomas, G. W. 1967. Approximate methods for calculating the temperature distribution during hot fluid injection. Journal of Canadian Pet. Tech. 6:123-129.

40. Todd, David Keith. 1964. Groundwater. p13-1 to 13-55. In: Ven te Chow. (ed.) Handbook of Applied Hydrology. McGraw-Hill, Inc. New York, New York.

41. Weinstein, H. G. 1972. A semi-analytic method for thermal coupling of reservoir and overburden. Society of Petroleum Engineers Journal. 12(4):439-447.

42. William, B. T., V. V. Valleroy, G. W. Runberg, A. J. Cornelius, and L. W. Powers. 1961. Laboratory studies of oil recovery by steam injection. Trans. AIME. 222:681-690.

APPENDIX A

DERIVATION OF HEAT FLOW EQUATION

APPENDIX A

DERIVATION OF HEAT FLOW EQUATION

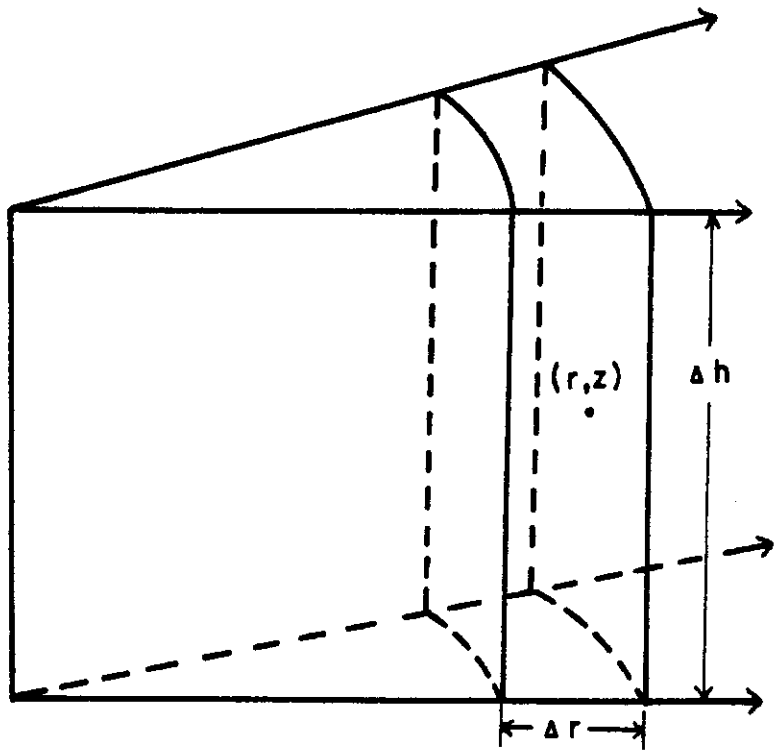

Figure A-1. Cylindrical element of a well sector used to develop heat flow equation.

$$\text{Heat in - Heat out = change in heat storage} \tag{A1}$$

or

$$J_{r-\frac{\Delta r}{2}} A_{r-\frac{\Delta r}{2}} + J_{z-\frac{\Delta z}{2}} A_{z-\frac{\Delta z}{2}} - J_{r+\frac{\Delta r}{2}} A_{r+\frac{\Delta r}{2}} -$$

$$J_{z+\frac{\Delta z}{2}} + A_{z+\frac{\Delta z}{2}} = \frac{\partial}{\partial t} (\text{heat in volume}) \tag{A2}$$

where J = heat flux at respective faces

A = area of face.

By a Taylor Series Expansion

$$J_{r-\frac{\Delta r}{2}} = J_r - \frac{\Delta r}{2}\frac{\partial J_r}{\partial r} + \left(\frac{\Delta r}{2}\right)^2 \frac{\partial^2 J_r}{\partial r^2}\frac{1}{2!} - \cdots \quad \text{(A3a)}$$

$$J_{r+\frac{\Delta r}{2}} = J_r + \frac{\Delta r}{2}\frac{\partial J_r}{\partial r} + \left(\frac{\Delta r}{2}\right)^2 \frac{\partial^2 J_r}{\partial r^2}\frac{1}{2!} + \cdots \quad \text{(A3b)}$$

$$J_{z-\frac{\Delta z}{2}} = J_z - \frac{\Delta z}{2}\frac{\partial J_z}{\partial z} + \left(\frac{\Delta z}{2}\right)^2 \frac{\partial^2 J_z}{\partial z^2}\frac{1}{2!} + \cdots \quad \text{(A3c)}$$

$$J_{z+\frac{z}{2}} = J_z + \frac{\Delta z}{2}\frac{\partial J_z}{\partial z} + \left(\frac{\Delta z}{2}\right)^2 \frac{\partial^2 J}{\partial z^2}\frac{1}{2!} + \cdots \quad \text{(A3d)}$$

Also

$$A_{r-\frac{\Delta r}{2}} = \left(r-\frac{\Delta r}{2}\right)\Delta\theta\Delta z \quad \text{(A4a)}$$

$$A_{r+\frac{\Delta r}{2}} = \left(r+\frac{\Delta r}{2}\right)\Delta\theta\Delta z \quad \text{(A4b)}$$

$$A_{z-\frac{\Delta z}{2}} = r\Delta\theta\Delta r \quad \text{(A4c)}$$

$$A_{z+\frac{\Delta z}{2}} = r\Delta\theta\Delta z \quad \text{(A4d)}$$

Neglecting all second order terms and higher, equation A2 becomes:

$$\left[J_r - \frac{\Delta r}{2} \frac{\partial J_{r|z}}{\partial 2r} \right] \left[(r-\frac{\Delta r}{2}) \Delta\theta \Delta z \right] +$$

$$\left[J_z - \frac{\Delta z}{2} \frac{\partial J_{r|z}}{\partial z} \right] \left[r \Delta\theta \Delta r \right] -$$

$$\left[J_r + \frac{\Delta r}{2} \frac{\partial J_r}{\partial r} \right] \left[(r+\frac{\Delta r}{2}) \Delta\theta \Delta z \right] -$$

$$\left[J_z + \frac{\Delta z}{2} \frac{\partial J_{r|z}}{\partial z} \right] \left[r \Delta\theta \Delta r \right] =$$

$$\frac{\partial}{\partial t} \text{ (heat in volume element)} \tag{A5}$$

Multiplying these terms out and rearranging yields:

$$\Delta\theta \Delta z \left[-r \Delta r \frac{\partial J_r}{\partial r} - \Delta r J_r \right] - r \Delta\theta \Delta r \Delta z \frac{\partial J}{\partial z} =$$

$$\frac{\partial}{\partial t} (\rho_f C_f r \Delta\theta \Delta r \Delta z T) \tag{A6}$$

$$J_r = -K \frac{\partial T}{\partial r} + \rho_f C_f V T \tag{A7}$$

However $V = \frac{Q}{2\pi rh}$ (A8)

where h = aquifer thickness (L), and

Q = injection rate (L^3/T).

Since mass flow is in only radially (one-dimensional),

$$J_z = -K \frac{\partial T}{\partial z} \tag{A9}$$

Equation A6 becomes

$$\Delta\theta\ \Delta z \left[- r\ \Delta r \frac{\partial}{\partial r} \left(-K\frac{\partial T}{\partial r} + \frac{\rho_f C_f Q T}{2\pi rh} \right) - \Delta r \left(-K\frac{\partial T}{\partial r} + \frac{\rho_f C_f Q T}{2\pi hr} \right) \right] - r\ \Delta\theta\ \Delta r\ \Delta z \frac{\partial}{\partial z} \left(-K \frac{\partial T}{\partial z} \right) =$$

$$\frac{\partial}{\partial t} \left(\rho_f C_f\ r\ \Delta\theta\ \Delta r\ \Delta z\ T \right) \tag{A10}$$

By product rule differentiation, Equation A10 becomes

$$\Delta\theta\ \Delta z\ \Delta r \left[+ r \frac{\partial}{\partial r} K_r \frac{\partial T}{\partial r} - r \frac{\partial}{\partial r} \left(\frac{\rho_f C_f Q T}{2\pi rh} \right) \right] +$$

$$\Delta\theta\ \Delta z\ \Delta r\ K_r \frac{\partial T}{\partial r} - \Delta r\ \Delta\theta\ \Delta z \frac{\rho_f C_f Q T}{2\pi hr} +$$

$$+ r\,\Delta\theta\,\Delta r\,\Delta z\,\frac{\partial}{\partial z}\left(K_z\,\frac{\partial T}{\partial z}\right) = \frac{\partial}{\partial t}\left(\rho_f C_f\, r\,\Delta\theta\,\Delta r\,\Delta z\, T\right) \qquad (A11)$$

Assuming that fluids and media properties are constant with time and space, A11 becomes

$$r\,K_r\,\frac{\partial^2 T}{\partial r^2} - r\,\frac{\rho_f C_f Q}{2\pi h}\,\frac{\partial}{\partial r}\left(\frac{T}{r}\right) + K_r\,\frac{\partial T}{\partial r} - \frac{\rho_f C_f Q T}{2\pi h r} +$$

$$r\,K_z\,\frac{\partial^2 T}{\partial z^2} = \rho_a C_a r\,\frac{\partial T}{\partial t} \qquad (A12)$$

Product nine differentiation again yields

$$r\,K_r\,\frac{\partial^2 T}{\partial r^2} + \frac{\rho_f C_f Q T}{2\pi h r} - \frac{\rho_f C_f Q}{2\pi h}\,\frac{\partial T}{\partial r} + K_r\,\frac{\partial T}{\partial r} - \frac{\rho_f C_f Q T}{2\pi h r} +$$

$$r\,K_z\,\frac{\partial^2 T}{\partial z^2} = \rho_a C_a r\,\frac{\partial T}{\partial t} \qquad (A13)$$

or

$$K_r\,\frac{\partial^2 T}{\partial r} + K_z\,\frac{\partial^2 T}{\partial z^2} + \frac{1}{r}\left(-\frac{\rho_f C_f Q}{2\pi h} + K_r\right)\frac{\partial T}{\partial r} =$$

$$\rho_a C_a\,\frac{\partial T}{\partial t} \qquad (A14)$$

This is the equation presented by Baker (1967). In the caprock and bedrock, there is no convective heat transfer because the fluid velocity in this region is assumed zero. The governing equation for these

regions is

$$K_r \frac{\partial^2 T}{\partial r^2} + \frac{1}{r} K \frac{\partial T}{\partial r} + K_z \frac{\partial^2 T}{\partial z^2} = \rho_a C_a \frac{\partial T}{\partial t} \qquad (A15)$$

Avdonin (1964) assumed infinite vertical thermal conductivity in the flow area. In the underlying and overlying strata, horizontal thermal conductivity is neglected. Vertically, heat transfer is only by conduction in this region. For the aquifer, Equation A1 becomes

$$J_{r-\frac{\Delta r}{2}} A_{r-\frac{\Delta r}{2}} - J_{r+\frac{\Delta r}{2}} A_{r+\frac{\Delta r}{2}} - J_{z-\frac{\Delta z}{2}} A_{z-\frac{\Delta z}{2}} -$$

$$J_{z+\frac{\Delta z}{2}} A_{z+\frac{\Delta z}{2}} = \frac{\partial}{\partial t} (\text{heat in volume}). \qquad (A16)$$

Expanding the first two terms as done previously and simplifying yields

$$\left[K_r \frac{\partial^2 T}{\partial r^2} + \frac{1}{r} \left(K_r - \frac{\rho_f C_f Q}{2\pi h} \right) \frac{\partial T}{\partial r} \right] r \, \Delta\theta \, \Delta r \, h =$$

$$= J_{r-\frac{\Delta r}{2}} A_{r-\frac{\Delta r}{2}} - J_{r+\frac{\Delta r}{2}} A_{r+\frac{\Delta r}{2}} \qquad (A17)$$

By the Taylor Series expansion from Equation A3c and A3d,

$$+ J_{z-\frac{\Delta z}{2}} A_{z-\frac{\Delta z}{2}} + J_{z+\frac{\Delta z}{2}} A_{z+\frac{\Delta z}{2}} =$$

$$\left(J_z - \frac{\Delta z}{2} \frac{\partial J_z}{\partial z} \right) \left(r \, \Delta\theta \, \Delta r \right) +$$

$$+ \left[J_z + \frac{\Delta z}{2} \frac{\partial J_2}{\partial z}\right] \left[r \, \Delta\theta \, \Delta r\right] =$$

$$2 \, r \, \Delta\theta \, \Delta r \, J_z \, . \qquad \text{(A18)}$$

but

$$J_z = -K_z \frac{\partial T}{\partial z} \qquad \text{(A19)}$$

where K_z = vertical thermal conductivity in the confining layers.

Substituting A17 and A19 into A16 yields

$$r \, \Delta\theta \, \Delta r \, h \left[K_r \frac{\partial^2 T}{\partial r^2} + \frac{1}{r} \left(K_r - \frac{\rho_f C_f Q}{2\pi h}\right) \frac{\partial T}{\partial r}\right] +$$

$$2 \, r \, \Delta\theta \, \Delta r \, K_z \frac{\partial T}{\partial Z} = r \, \Delta\theta \, \Delta r \, h \, \rho_a C_a \frac{\partial T}{\partial t} \qquad \text{(A20)}$$

or

$$K_r \frac{\partial^2 T}{\partial r^2} + \frac{1}{r} \left(K_1 - \frac{\rho_f C_f Q}{2\pi h}\right) \frac{\partial T}{\partial r} + \frac{2K_z}{h} \frac{\partial T}{\partial z} =$$

$$\rho_a C_a \frac{\partial T}{\partial t} \qquad \text{(A21)}$$

or

$$\frac{\partial^2 T}{\partial r^2} + \frac{1}{r} \left(1 - \frac{\rho_f C_f Q}{2\pi h K_r}\right) \frac{T}{r} + \frac{2K_z}{h K_r} \frac{T}{t} =$$

$$\rho_a C_a \frac{T}{t} \qquad \text{(A22)}$$

To non-dimensionalize the problem, let

$$\bar{r} = \frac{2r}{h}$$

$$\bar{T} = \frac{T - T_o}{T_i - T_o}$$

$$\nu = \frac{\rho_f C_f Q}{4\pi h K_r}$$

$$\alpha = \frac{K_z}{K_r}$$

$$\bar{t} = \frac{4 K_r t}{h^2 \rho_a C_a}$$

$$\bar{z} = \frac{2z}{h}$$

$$\frac{\partial T}{\partial r} = \frac{\partial T}{\partial \bar{T}} \frac{\partial \bar{T}}{\partial \bar{r}} \frac{\partial \bar{r}}{\partial r} = \frac{2}{h} \frac{\partial \bar{T}}{\partial \bar{r}} \frac{\partial^2 T}{\partial r^2} = \frac{4}{h^2} \frac{\partial^2 \bar{T}}{\partial \bar{r}^2}$$

Equation A22 becomes

$$\frac{\partial^2 \bar{T}}{\partial \bar{r}^2} + \left(\frac{1-2\nu}{\bar{r}}\right) \frac{\partial \bar{T}}{\partial \bar{r}} + \alpha \frac{\partial \bar{T}}{\partial \bar{z}} = \frac{\partial \bar{T}}{\partial \bar{r}} \qquad \text{(A23)}$$

This is Avdonins (1964) equation for the aquifer. In the confining strata considering only vertical conduction, the equation is

$$\frac{\partial^2 \bar{T}}{\partial \bar{z}^2} = \frac{1}{a_1^2} \frac{\partial \bar{T}}{\partial \bar{t}} \qquad \text{(A24)}$$

where $a^2 = \frac{K_z}{\rho_r C_r}$.

APPENDIX B

MEASURED TEMPERATURES

RUN 1 INJECTION 1 RADIUS=0.3048M
FLOWRATE=957.3 CM**3/MIN FOR 0.2 RADIANS
FLOWRATE=0.50126X10**-3/SEC FOR FULL CIRCLE

TEMPERATURE IN DEGREES KELVIN

HEIGHT ABOVE BOTTOM OF FLOW LAYER IN METERS

TIME	0.3048	0.6096	0.7520	0.9144	1.2192	AVG
0.0	295.75	296.46	296.80	296.79	296.66	296.44
10.0	296.36	303.06	303.77	306.45	316.99	305.59
20.0	306.32	317.60	318.48	321.50	327.80	318.17
30.0	311.90	324.59	325.23	326.87	329.96	323.27
40.0	316.93	327.59	328.12	328.90	330.68	326.01
50.0	320.18	329.02	329.39	329.77	330.99	327.49
60.0	322.48	329.85	330.07	330.28	331.17	328.45
120.0	326.67	330.95	331.03	330.95	331.36	329.99
180.0	328.14	331.31	331.28	331.39	331.54	330.59
240.0	329.00	331.36	331.35	331.46	331.67	330.86
300.0	329.50	331.78	331.81	332.06	332.35	331.41
360.0	329.76	331.26	331.03	331.26	331.42	330.90
420.0	329.82	331.47	331.22	331.46	331.60	331.06
480.0	329.76	331.26	331.09	331.19	331.29	330.86
540.0	329.56	331.26	331.09	331.19	331.29	330.81
600.0	329.44	331.06	331.03	331.06	331.17	330.68
660.0	328.20	330.35	330.45	330.60	330.50	329.91
720.0	327.13	329.90	330.07	330.28	330.38	329.42
840.0	326.11	329.46	329.51	329.84	330.20	328.88
960.0	325.72	329.36	329.51	329.71	330.38	328.79
1080.0	325.45	329.26	329.32	329.52	330.50	328.67
1200.0	325.34	329.02	328.96	329.15	329.84	328.32
1320.0	326.05	329.61	329.57	329.77	330.38	328.94
1440.0	326.50	329.80	329.82	329.90	330.44	329.16
1560.0	327.13	330.30	330.32	330.50	330.93	329.70
1740.0	327.66	330.65	330.64	330.80	330.26	329.83

RUN 1 INJECTION 1 RADIUS=0.6096M
FLOWRATE=957.3 CM**3/MIN FOR 0.2 RADIANS
FLOWRATE=0.50126X10**-3/SEC FOR FULL CIRCLE

TEMPERATURE IN DEGREES KELVIN

HEIGHT ABOVE BOTTOM OF FLOW LAYER IN METERS

TIME	0.0762	0.3048	0.6096	0.7520	0.9144	1.2192	AVG
0.0	296.35	296.51	295.87	296.41	296.44	296.33	296.32
12.0	296.39	296.56	295.89	296.39	296.47	296.44	296.37
20.0	296.44	296.73	295.96	296.45	296.61	297.07	296.59
30.0	296.52	297.66	296.44	296.96	297.44	299.09	297.53
40.0	296.79	299.59	298.08	298.90	299.56	302.31	299.55
50.0	297.28	302.06	300.85	302.75	303.00	306.10	302.46
60.0	297.98	305.26	305.14	308.34	307.86	310.40	306.35
80.0	299.57	310.88	312.29	316.78	315.40	316.39	312.49
100.0	301.50	315.93	317.65	321.87	320.77	320.67	317.13
120.0	303.52	319.28	321.09	324.70	324.08	323.49	320.17
180.0	308.81	323.19	325.70	328.12	328.28	327.46	324.36
240.0	313.27	325.34	327.41	329.34	329.68	329.02	326.33
300.0	316.37	326.29	327.94	329.63	330.04	329.58	327.19
360.0	318.22	327.16	328.36	329.99	330.45	329.97	327.85
420.0	319.47	327.26	328.41	329.93	330.45	330.01	328.03
480.0	320.02	327.42	328.36	329.87	330.40	330.01	328.10
540.0	320.02	327.21	328.20	329.69	330.19	329.88	327.94
600.0	320.40	327.11	328.04	329.57	330.14	329.80	327.90
660.0	320.02	325.99	327.41	329.10	329.68	328.51	327.08
720.0	319.15	324.95	326.80	328.47	328.97	327.96	326.34
840.0	317.70	323.57	325.65	327.39	327.98	327.83	325.37
960.0	316.82	322.78	324.87	326.78	327.50	327.92	324.84
1080.0	316.25	322.33	324.43	326.40	327.26	327.88	324.51
1200.0	316.05	322.10	324.15	326.12	327.02	327.67	324.27
1320.0	316.66	322.73	324.77	326.67	327.59	328.17	324.85
1440.0	317.03	323.10	325.16	327.05	327.89	328.38	325.18

RUN 1 INJECTION 1 RADIUS=0.6096M
FLOWRATE=957.3 CM**3/MIN FOR 0.2 RADIANS
FLOWRATE=0.50126X10**-3/SEC FOR FULL CIRCLE

TEMPERATURE IN DEGREES KELVIN

HEIGHT ABOVE BOTTOM OF FLOW LAYER IN METERS

TIME	0.0762	0.3048	0.6096	0.7520	0.9144	1.2192	AVG
1560.0	317.70	323.89	325.74	327.56	328.28	328.67	325.71
1740.0	318.62	324.90	326.65	328.41	329.02	328.89	326.46

RUN 1 INJECTION 1 RADIUS=1.524M
FLOWRATE=957.3 CM**3/MIN FOR 0.2 RADIANS
FLOWRATE=0.50126X10**-3/SEC FOR FULL CIRCLE

TEMPERATURE IN DEGREES KELVIN

HEIGHT ABOVE BOTTOM OF FLOW LAYER IN METERS

TIME	0.0762	0.3048	0.6096	0.7520	0.9144	1.2192	1.4478	AVG
0.0	296.38	296.16	296.51	296.87	296.62	296.48	296.59	296.50
60.0	296.54	296.25	296.59	296.94	296.61	297.18	297.06	296.78
120.0	296.71	296.42	296.68	297.07	296.94	299.80	299.45	297.92
180.0	297.06	296.85	296.87	297.41	297.85	303.27	302.82	299.60
240.0	297.61	297.61	297.42	298.29	299.55	306.94	306.34	301.62
300.0	298.39	298.90	298.98	313.48	302.18	310.61	310.00	305.22
360.0	299.34	300.72	301.80	303.59	305.54	313.77	313.14	306.86
420.0	300.56	303.06	305.65	307.70	309.56	316.52	315.81	309.81
480.0	301.83	305.56	309.70	311.86	313.58	318.84	318.05	312.63
540.0	303.00	308.02	313.24	315.46	317.02	320.73	319.85	315.07
600.0	304.42	310.17	316.11	318.23	319.70	322.24	321.22	317.07
660.0	305.47	311.60	318.19	320.30	316.85	323.58	322.48	318.01
720.0	306.36	312.70	319.59	321.60	323.13	324.12	323.17	319.60
780.0	307.15	313.66	320.57	322.52	323.91	324.42	323.60	320.28
840.0	307.84	314.42	321.36	323.02	324.26	324.77	323.98	320.80
900.0	308.37	315.08	321.86	323.32	324.56	325.13	324.51	321.27
960.0	308.82	315.66	322.13	323.53	324.87	325.49	324.90	321.65
1020.0	309.27	315.46	322.32	323.68	325.12	325.80	325.24	321.86
1080.0	309.60	316.36	322.41	323.78	325.33	326.06	325.54	322.20
1140.0	309.93	316.49	322.50	323.89	325.53	326.27	325.79	322.40
1200.0	310.13	316.46	322.36	323.73	325.43	326.17	325.74	322.33
1320.0	311.06	316.86	322.83	324.20	326.00	326.75	326.40	322.91
1440.0	311.67	317.07	323.06	324.52	326.21	327.02	326.71	323.20
1560.0	312.35	317.31	323.34	324.78	326.59	327.29	327.13	323.55
1740.0	313.16	316.39	323.49	325.16	326.85	327.56	327.44	323.67

RUN 1 INJECTION 1 RADIUS=3.048M
FLOWRATE=957.3 CM**3/MIN FOR 0.2 RADIANS
FLOWRATE=0.50126X10**-3/SEC FOR FULL CIRCLE

TEMPERATURE IN DEGREES KELVIN

HEIGHT ABOVE BOTTOM OF FLOW LAYER IN METERS

TIME	0.0762	0.3048	0.6096	0.7520	0.9144	1.2192	1.4478	AVG
0.0	295.72	295.72	295.72	295.72	295.83	296.21	296.44	296.00
241.0	295.72	295.72	295.72	295.72	295.91	296.25	296.67	296.07
367.0	295.76	295.72	295.72	295.74	295.96	296.34	297.12	296.21
483.0	295.86	295.72	295.72	295.83	296.03	296.50	297.93	296.46
597.0	295.94	295.77	295.72	295.95	296.10	296.76	299.02	296.81
717.0	296.00	295.89	295.72	296.14	296.21	297.20	300.43	297.29
839.0	296.06	296.00	295.72	296.57	296.36	297.82	301.93	297.85
900.0	296.10	296.10	295.72	297.00	296.49	298.22	302.72	298.18
960.0	296.16	296.17	295.72	297.52	296.66	298.64	303.37	298.50
1020.0	296.23	296.32	295.72	298.27	296.93	299.18	304.14	298.91
1075.0	296.32	296.47	295.72	299.25	297.28	299.73	304.79	299.32
1135.0	296.46	296.71	295.90	300.45	297.76	300.43	305.50	299.85
1195.0	296.63	297.01	296.42	301.82	298.36	301.24	306.19	300.47
1265.0	296.90	297.47	297.28	303.57	299.28	302.35	307.03	301.34
1315.0	297.15	297.91	298.17	305.03	300.06	303.32	307.69	302.09
1380.0	297.45	298.42	299.17	306.65	301.20	304.48	308.43	302.98
1440.0	297.82	299.06	300.28	308.23	302.43	305.75	309.19	303.94
1500.0	298.21	299.71	301.44	309.70	303.71	307.04	309.97	304.92
1560.0	298.69	300.48	302.88	311.17	305.17	308.47	310.83	306.03
1620.0	299.14	301.25	304.01	312.40	306.52	309.75	311.61	307.01
1680.0	299.53	302.08	305.31	313.65	307.93	311.06	312.45	308.06
1740.0	300.21	302.92	306.55	314.72	309.33	312.31	313.29	309.09

RUN 1 INJECTION 1 RADIUS=4.572M
FLOWRATE=957.3 CM**3/MIN FOR 0.2 RADIANS
FLOWRATE=0.50126X10**-3/SEC FOR FULL CIRCLE

TEMPERATURE IN DEGREES KELVIN

HEIGHT ABOVE BOTTOM OF FLOW LAYER IN METERS

TIME	0.0762	0.3048	0.6096	0.7520	0.9144	1.2192	1.4478	AVG
0.0	295.72	295.72	295.72	295.72	297.35	295.72	296.08	296.01
64.0	295.72	295.72	295.72	295.72	297.36	295.72	295.90	295.97
102.0	295.72	295.72	295.72	295.72	297.37	295.72	296.10	296.02
181.0	295.72	295.72	295.72	295.72	297.38	295.72	296.14	296.03
241.0	295.72	295.72	295.72	295.72	297.39	295.72	296.18	296.04
301.0	295.72	295.72	295.72	295.72	297.38	295.72	296.20	296.05
367.0	295.72	295.72	295.72	295.72	297.42	295.72	296.27	296.07
417.0	295.72	295.72	295.72	295.72	297.44	295.72	296.32	296.08
483.0	295.72	295.72	295.72	295.72	297.45	295.72	296.38	296.10
536.0	295.72	295.72	295.72	295.72	297.46	295.75	296.43	296.12
596.0	295.72	295.72	295.72	295.72	297.49	295.80	296.52	296.15
656.0	295.72	295.72	295.72	295.72	297.92	295.86	296.61	296.24
717.0	295.72	295.72	295.72	295.72	297.55	295.91	296.71	296.23
777.0	295.72	295.72	295.72	295.72	297.57	295.97	296.83	296.27
839.0	295.72	295.72	295.72	295.72	297.59	296.03	296.96	296.31
900.0	295.72	295.72	295.72	295.72	297.62	296.10	297.12	296.37
960.0	295.72	295.72	295.72	295.72	297.65	296.17	297.26	296.42
1020.0	295.72	295.72	295.72	295.72	297.69	296.25	297.43	296.48
1090.0	295.72	295.72	295.72	295.72	297.74	296.37	297.65	296.56
1165.0	295.72	295.72	295.72	295.80	297.77	296.48	297.90	296.65
1195.0	295.72	295.72	295.72	295.79	297.80	296.54	298.00	296.69
1255.0	295.72	295.72	295.72	295.81	297.84	297.60	298.21	296.93
1345.0	295.72	295.72	295.72	295.90	297.93	296.85	298.53	296.90
1380.0	295.72	295.72	295.72	295.91	297.95	296.93	298.66	296.95
1440.0	295.72	295.77	295.72	295.98	298.02	297.08	298.90	297.06
1500.0	295.72	313.91	295.72	296.04	298.08	297.23	299.13	300.18

RUN 1 INJECTION 1 RADIUS=4.572M
FLOWRATE=957.3 CM**3/MIN FOR 0.2 RADIANS
FLOWRATE=0.50126X10**-3/SEC FOR FULL CIRCLE

TEMPERATURE IN DEGREES KELVIN

HEIGHT ABOVE BOTTOM OF FLOW LAYER IN METERS

TIME	0.0762	0.3048	0.6096	0.7520	0.9144	1.2192	1.4478	AVG
1560.0	295.72	295.82	295.72	296.11	298.17	297.41	299.41	297.28
1620.0	295.72	295.84	295.72	296.18	298.26	297.60	299.67	297.40
1680.0	295.72	295.87	295.72	296.26	298.37	297.80	299.97	297.53
1740.0	295.72	295.90	295.72	296.30	298.48	298.03	300.28	297.67

RUN 1 INJECTION 1 RADIUS=6.096M
FLOWRATE=957.3 CM**3/MIN FOR 0.2 RADIANS
FLOWRATE=0.50126X10**-3/SEC FOR FULL CIRCLE

TEMPERATURE IN DEGREES KELVIN

HEIGHT ABOVE BOTTOM OF FLOW LAYER IN METERS

TIME	0.0762	0.3048	0.6096	0.7520	0.9144	1.2192	1.4478	AVG
0.0	295.72	295.72	295.72	297.31	295.42	295.72	295.72	295.81
64.0	295.72	295.72	295.72	296.93	295.72	295.72	295.72	295.82
102.0	295.72	295.72	295.72	297.35	295.72	295.72	295.78	295.87
181.0	295.72	295.72	295.72	297.39	295.72	295.72	295.82	295.88
241.0	295.72	295.72	295.72	297.41	295.72	295.72	295.84	295.89
301.0	295.72	295.72	295.72	297.41	295.72	295.72	295.82	295.89
367.0	295.72	295.72	295.72	297.44	295.72	295.72	295.87	295.90
417.0	295.72	295.72	295.72	297.47	295.72	295.72	295.89	295.91
483.0	295.72	295.72	295.72	297.48	295.72	295.72	295.96	295.93
536.0	295.72	295.72	295.72	297.50	295.72	295.72	295.93	295.92
596.0	295.72	295.72	295.72	297.54	295.72	295.74	296.00	295.94
656.0	295.72	295.73	295.72	297.56	295.72	295.78	296.04	295.96
717.0	295.72	295.74	295.72	297.59	295.72	295.83	296.11	295.99
777.0	295.72	295.76	295.72	297.62	295.72	295.89	296.16	296.02
839.0	295.72	295.79	295.72	297.64	295.72	295.94	296.20	296.05
900.0	295.72	295.79	295.72	297.68	295.72	296.01	296.26	296.08
960.0	295.72	295.81	295.72	297.71	295.72	296.07	296.33	296.11
1020.0	295.72	295.83	295.72	297.75	295.72	296.14	296.38	296.14
1090.0	295.72	295.87	295.74	297.79	295.72	296.22	296.49	296.20
1165.0	295.72	295.88	295.77	297.84	295.72	296.32	296.61	296.25
1195.0	295.72	295.89	295.80	297.85	295.72	296.37	296.64	296.27
1255.0	295.72	295.90	295.85	297.88	295.72	296.41	296.72	296.31
1320.0	295.72	295.94	295.85	297.95	295.75	296.55	296.82	296.38
1380.0	295.72	295.94	295.88	298.00	295.79	296.65	296.92	296.43
1440.0	295.72	295.98	295.93	298.05	295.86	296.75	297.05	296.51
1500.0	295.72	295.98	295.96	298.09	295.92	296.87	297.15	296.56

RUN 1 INJECTION 1 RADIUS=6.096M
FLOWRATE=957.3 CM**3/MIN FOR 0.2 RADIANS
FLOWRATE=0.50126X10**-3/SEC FOR FULL CIRCLE

TEMPERATURE IN DEGREES KELVIN

HEIGHT ABOVE BOTTOM OF FLOW LAYER IN METERS

TIME	0.0762	0.3048	0.6096	0.7520	0.9144	1.2192	1.4478	AVG
1560.0	295.72	295.99	296.01	298.17	296.00	296.99	297.31	296.65
1620.0	295.72	296.01	296.04	298.23	296.07	297.12	297.46	296.73
1680.0	295.72	296.02	296.09	298.31	296.17	297.28	297.62	296.82
1740.0	295.72	296.07	296.15	298.39	296.26	297.45	297.78	296.93

RUN 1 PUMPING RADIUS=0.3048M
FLOWRATE=957.3 CM**3/MIN FOR 0.2 RADIANS
FLOWRATE=0.50126X10**-3/SEC FOR FULL CIRCLE

TEMPERATURE IN DEGREES KELVIN

HEIGHT ABOVE BOTTOM OF FLOW LAYER IN METERS

TIME	0.3048	0.6096	0.7520	0.9144	1.2192	AVG
0.0	327.12	329.65	329.63	329.70	329.42	328.97
20.0	323.54	328.49	328.90	329.21	328.32	327.40
40.0	321.34	326.58	327.47	328.11	327.86	325.99
80.0	318.94	323.66	325.45	326.64	327.24	324.16
115.0	317.71	322.11	324.33	325.79	326.69	323.12
175.0	316.19	320.21	322.70	324.58	325.60	321.68
235.0	315.05	318.90	321.50	323.49	324.34	320.48
295.0	314.07	317.77	320.44	322.47	323.02	319.37
355.0	313.26	316.76	319.46	321.50	321.80	318.37
415.0	312.41	315.72	318.36	320.47	320.49	317.31
475.0	311.60	314.63	317.34	319.35	319.19	316.24
535.0	310.83	313.62	316.23	318.23	317.82	315.16
595.0	310.14	312.68	315.23	317.13	316.55	314.17
655.0	309.42	311.75	314.12	316.04	315.30	313.16
730.0	308.56	310.45	312.74	314.51	313.72	311.84
850.0	307.24	308.59	310.68	312.23	311.40	309.90
970.0	306.05	306.87	308.67	310.03	309.34	308.10
1090.0	304.97	305.42	307.02	308.20	307.74	306.61
1210.0	305.09	304.14	305.51	306.54	306.40	305.56
1330.0	302.95	302.91	304.18	305.08	305.28	304.08
1450.0	302.01	301.90	303.04	303.82	304.29	303.03

RUN 1 PUMPING RADIUS=0.6096M
FLOWRATE=957.3 CM**3/MIN FOR 0.2 RADIANS
FLOWRATE=0.50126X10**-3/SEC FOR FULL CIRCLE

TEMPERATURE IN DEGREES KELVIN

HEIGHT ABOVE BOTTOM OF FLOW LAYER IN METERS

TIME	0.0762	0.3048	0.6096	0.7520	0.9144	1.2192	AVG
0.0	318.53	324.41	326.54	328.29	328.92	328.72	326.25
55.0	316.78	320.66	324.20	326.34	327.64	327.54	324.14
115.0	315.22	318.75	322.58	324.85	326.59	326.65	322.74
175.0	314.11	328.49	320.83	323.62	325.66	325.69	323.98
235.0	313.03	316.37	319.66	322.49	324.71	324.53	320.43
295.0	312.09	315.32	318.58	321.39	323.69	323.30	319.35
355.0	311.23	314.46	317.57	320.47	322.70	322.15	318.37
415.0	310.30	313.43	316.53	319.40	321.66	320.87	317.29
475.0	309.40	312.44	315.53	318.33	320.53	319.61	316.21
535.0	308.58	311.47	314.36	317.18	319.33	318.34	315.10
595.0	307.95	310.59	313.32	316.04	318.17	317.09	314.06
670.0	307.02	309.43	311.87	314.58	316.65	315.54	312.70
730.0	306.29	308.54	310.88	313.28	315.33	314.23	311.60
790.0	305.63	307.69	309.83	312.11	314.09	313.02	310.56
850.0	305.08	306.82	308.70	310.98	312.78	311.80	309.50
910.0	304.54	306.07	307.72	309.84	311.61	310.71	308.55
970.0	304.08	305.30	306.80	308.69	310.36	309.64	307.60
1030.0	303.70	304.66	306.05	307.87	309.42	308.86	306.87
1090.0	303.27	303.99	305.16	306.83	308.30	308.00	306.03
1150.0	302.92	303.39	304.39	305.97	307.36	307.24	305.31
1210.0	302.51	302.84	303.72	305.13	306.41	306.50	304.61
1270.0	302.15	302.35	302.95	304.33	305.59	305.85	303.97
1330.0	301.80	301.89	302.34	303.70	304.79	305.23	303.38
1390.0	301.44	301.45	301.77	303.04	304.10	304.69	302.84
1450.0	301.13	301.08	301.29	302.49	303.48	304.19	302.37

RUN 1 PUMPING RADIUS=1.524M
FLOWRATE=957.3 CM**3/MIN FOR 0.2 RADIANS
FLOWRATE=0.50126X10**-3/SEC FOR FULL CIRCLE

TEMPERATURE IN DEGREES KELVIN

HEIGHT ABOVE BOTTOM OF FLOW LAYER IN METERS

TIME	0.0762	0.3048	0.6096	0.7520	0.9144	1.2192	1.4478	AVG
0.0	313.09	316.18	323.73	325.10	326.55	327.56	327.39	323.60
20.0	312.73	313.69	323.49	324.94	326.69	327.40	327.23	323.07
40.0	312.35	311.84	323.25	324.62	326.43	327.13	326.97	322.53
80.0	311.79	312.09	322.59	324.04	325.90	326.70	326.51	322.14
115.0	311.24	311.82	322.00	323.48	325.43	326.27	326.05	321.68
175.0	310.53	310.02	320.92	322.47	324.51	325.49	325.10	320.62
235.0	309.77	309.17	319.76	321.32	323.47	324.52	323.98	319.60
295.0	309.08	311.29	318.51	320.08	322.28	323.34	322.71	318.98
355.0	308.22	310.25	317.28	318.90	321.12	322.29	321.53	317.87
415.0	307.44	308.68	315.92	317.58	319.78	321.09	320.31	316.59
475.0	306.73	307.06	314.49	316.09	318.31	319.77	318.97	315.22
535.0	305.79	306.01	312.98	314.60	316.75	318.38	317.65	313.89
595.0	304.93	305.04	311.59	313.22	315.28	317.10	316.44	312.67
655.0	304.20	304.79	310.26	311.86	313.32	315.80	315.24	311.53
730.0	303.20	304.15	308.65	310.24	312.07	314.22	313.79	310.22
850.0	301.95	302.59	306.37	307.91	309.48	311.85	311.60	308.11
970.0	301.08	301.35	304.53	306.00	307.27	309.85	309.70	306.36
1090.0	300.65	300.42	303.14	304.52	305.65	308.16	308.19	305.01
1210.0	300.12	299.67	301.99	303.29	304.22	306.61	306.85	303.82
1330.0	299.81	299.19	301.28	302.53	303.35	305.65	305.72	303.01
1450.0	299.34	298.55	300.38	301.52	302.18	304.31	304.76	302.06

RUN 1 PUMPING RADIUS=3.048M
FLOWRATE=957.3 CM**3/MIN FOR 0.2 RADIANS
FLOWRATE=0.50126X10**-3/SEC FOR FULL CIRCLE

TEMPERATURE IN DEGREES KELVIN

HEIGHT ABOVE BOTTOM OF FLOW LAYER IN METERS

TIME	0.0762	0.3048	0.6096	0.7520	0.9144	1.2192	1.4478	AVG
0.0	300.42	303.10	306.78	314.65	309.46	312.59	313.49	309.27
25.0	300.58	302.86	306.21	314.28	309.06	312.31	313.39	309.02
50.0	300.69	302.53	305.54	313.48	308.39	311.91	313.28	308.65
115.0	300.75	301.71	303.96	311.40	306.77	310.92	312.86	307.67
175.0	300.60	301.03	302.78	309.59	306.08	309.97	312.26	306.85
235.0	300.33	300.43	301.77	307.93	304.35	308.92	311.45	305.87
295.0	300.01	299.92	300.96	306.47	303.44	307.89	310.57	305.03
355.0	299.70	299.52	300.31	305.47	302.78	306.99	309.71	304.33
475.0	299.10	298.87	299.26	303.51	301.61	305.42	306.52	302.67
595.0	298.50	298.32	298.41	302.16	300.73	303.98	305.50	301.71
730.0	298.06	297.88	297.68	300.94	300.10	302.95	305.11	301.05
850.0	297.68	297.58	297.27	300.18	299.68	302.12	304.04	300.40
970.0	297.38	297.38	296.91	299.59	299.24	301.39	303.07	299.83
1090.0	297.17	297.17	296.67	299.14	298.94	300.82	302.30	299.38
1210.0	297.04	297.01	296.48	298.80	298.69	300.32	301.64	299.01
1330.0	296.94	296.91	296.28	298.52	298.46	299.92	301.10	298.71
1450.0	296.87	296.82	296.15	298.29	298.29	299.60	300.67	298.47

RUN 1 PUMPING RADIUS=4.572M
FLOWRATE=957.3 CM**3/MIN FOR 0.2 RADIANS
FLOWRATE=0.50126X10**-3/SEC FOR FULL CIRCLE

TEMPERATURE IN DEGREES KELVIN

HEIGHT ABOVE BOTTOM OF FLOW LAYER IN METERS

TIME	0.0762	0.3048	0.6096	0.7520	0.9144	1.2192	1.4478	AVG
0.0	295.72	295.91	295.72	296.35	298.48	298.07	300.38	297.71
10.0	295.72	295.93	295.72	296.39	298.53	298.12	300.43	297.74
40.0	295.72	295.93	295.72	296.42	298.55	298.18	300.61	297.80
70.0	295.72	295.88	295.72	296.42	298.48	298.21	300.75	297.82
100.0	295.72	295.93	295.72	296.45	298.58	298.28	300.91	297.90
130.0	295.72	295.93	295.72	296.46	298.59	298.35	301.06	297.95
160.0	295.72	295.93	295.72	296.49	298.60	298.40	301.16	297.99
190.0	295.72	295.93	295.72	296.52	298.63	298.40	301.26	298.02
220.0	295.72	295.93	295.72	296.52	298.64	298.52	301.33	298.06
280.0	295.72	295.95	295.72	296.56	298.68	298.60	301.40	298.10
340.0	295.72	295.95	295.72	296.60	298.70	298.69	301.40	298.12
430.0	295.72	295.96	295.72	296.64	298.75	298.79	301.33	298.13
520.0	295.72	295.99	295.72	296.69	298.79	298.83	301.17	298.11
610.0	295.72	296.00	295.72	296.73	298.84	298.86	301.16	298.12
670.0	295.72	296.01	295.72	296.79	298.87	298.88	301.16	298.14
790.0	295.72	296.03	295.72	296.82	298.92	298.83	300.61	298.00
910.0	295.72	296.05	295.72	296.86	298.94	298.79	300.34	297.94
1030.0	295.72	296.06	295.72	296.87	298.94	298.66	300.06	297.85
1150.0	295.72	296.08	295.72	296.87	298.94	298.54	299.83	297.78
1270.0	295.72	296.09	295.72	296.86	298.92	298.40	299.60	297.69
1390.0	295.72	296.09	295.72	296.83	299.01	298.25	299.39	297.62
1450.0	295.72	296.11	295.72	296.82	298.87	298.18	299.29	297.57

RUN 1 PUMPING RADIUS=6.096M
FLOWRATE=957.3 CM**3/MIN FOR 0.2 RADIANS
FLOWRATE=0.50126X10**-3/SEC FOR FULL CIRCLE

TEMPERATURE IN DEGREES KELVIN

HEIGHT ABOVE BOTTOM OF FLOW LAYER IN METERS

TIME	0.0762	0.3048	0.6096	0.7520	0.9144	1.2192	1.4478	AVG
0.0	295.72	296.07	296.15	298.39	296.26	297.45	297.78	296.93
10.0	295.72	296.08	296.16	298.42	296.30	297.51	297.83	296.96
40.0	295.72	296.08	296.18	298.44	296.32	297.51	297.90	296.98
70.0	295.72	296.08	296.16	298.42	296.32	297.48	297.93	296.98
100.0	295.72	296.09	296.20	298.44	296.32	297.51	297.98	297.01
130.0	295.72	296.09	296.20	298.44	296.32	297.50	298.04	297.02
160.0	295.72	296.10	296.20	298.44	296.32	297.50	298.10	297.04
190.0	295.72	296.10	296.20	298.44	296.32	297.48	298.15	297.05
220.0	295.72	296.10	296.20	298.44	296.33	297.48	298.20	297.06
280.0	295.72	296.12	296.21	298.44	296.33	297.47	298.25	297.07
340.0	295.72	299.93	296.21	298.44	296.29	297.47	298.28	297.71
430.0	295.72	296.13	296.21	298.43	296.28	297.45	298.31	297.08
520.0	295.72	296.14	296.21	298.42	296.25	297.43	298.31	297.07
347.0	295.72	296.16	296.21	298.42	296.22	297.40	298.27	297.06
670.0	295.72	296.16	296.23	298.42	296.22	297.40	298.24	297.05
790.0	295.72	296.18	296.24	298.43	296.23	297.40	298.15	297.04
910.0	295.72	296.20	296.29	298.47	296.28	297.42	298.05	297.04
1030.0	295.72	296.23	296.34	298.54	296.33	297.37	297.94	297.02
1150.0	295.72	296.28	296.42	298.59	296.39	297.31	297.82	297.01
1270.0	295.72	296.32	296.48	298.63	296.41	297.22	297.69	296.99
1390.0	295.72	296.37	296.51	298.63	296.40	297.08	297.54	296.94
1450.0	295.74	296.39	296.53	298.60	296.39	296.99	297.46	296.90

RUN 2 INJECTION 1 RADIUS=0.3048M
FLOWRATE=1482CM**3/MIN FOR 0.2 RADIANS
FLOWRATE=0.77634X10**-3 M**3/SEC FOR A FULL CIRCLE

TEMPERATURE IN DEGREES KELVIN

HEIGHT ABOVE BOTTOM OF FLOW LAYER IN METERS

TIME	0.3048	0.6096	0.7520	0.9144	1.2192	AVG
0.0	296.04	297.18	297.66	295.72	297.40	296.74
5.0	296.04	297.37	297.87	297.92	297.83	297.32
10.0	296.30	299.85	300.49	300.29	301.25	299.47
20.0	299.68	311.62	312.15	311.86	315.72	309.77
30.0	306.07	320.33	320.89	321.12	324.96	318.14
40.0	311.65	324.94	325.56	325.90	328.55	322.78
50.0	315.74	327.41	327.94	328.35	330.14	325.42
60.0	318.41	328.73	329.20	329.52	330.86	326.89
120.0	325.61	331.26	331.35	331.46	331.91	330.06
180.0	326.50	330.20	330.01	330.09	330.50	329.31
240.0	328.44	331.88	331.81	331.86	332.29	331.11
300.0	329.50	332.09	332.07	332.06	332.93	331.64
360.0	329.95	332.14	332.14	332.13	332.42	331.66
480.0	330.74	332.24	332.14	332.13	332.35	331.86
600.0	330.94	332.24	332.14	332.13	332.35	331.91
720.0	331.14	332.24	332.14	332.13	332.35	331.96
840.0	331.14	332.09	331.94	331.92	332.23	331.84
960.0	331.28	332.19	332.14	332.13	332.35	331.98
1200.0	331.48	332.35	332.21	332.19	332.42	332.10
1440.0	331.35	332.24	332.07	332.13	332.35	332.00
1680.0	330.08	331.36	331.15	331.32	331.91	331.14
1920.0	330.81	332.19	332.14	332.13	332.42	331.88
2160.0	331.21	332.19	332.07	332.06	332.29	331.93

RUN 2 INJECTION 1 RADIUS=0.6096M
FLOWRATE=1482CM**3/MIN FOR 0.2 RADIANS
FLOWRATE=0.77634X10**-3 M**3/SEC FOR A FULL CIRCLE

TEMPERATURE IN DEGREES KELVIN

HEIGHT ABOVE BOTTOM OF FLOW LAYER IN METERS

TIME	0.0762	0.3048	0.6096	0.7520	0.9144	1.2192	AVG
0.0	297.07	297.19	296.39	297.25	297.34	297.31	297.10
5.0	297.10	297.19	296.42	297.25	297.33	297.48	297.15
10.0	297.10	297.19	296.39	297.25	297.33	298.16	297.29
20.0	297.10	297.22	296.42	297.26	297.37	299.62	297.64
30.0	297.12	297.69	296.60	297.42	297.62	301.11	298.16
40.0	297.25	299.04	297.18	298.04	298.36	302.74	299.13
50.0	297.56	301.25	298.43	299.47	299.84	304.80	300.73
60.0	297.98	303.70	300.13	301.56	301.83	306.92	302.64
80.0	299.38	310.20	305.32	308.02	307.88	311.98	307.95
100.0	296.60	314.63	310.88	314.47	314.02	316.48	312.29
120.0	303.02	318.47	315.46	319.19	318.69	319.97	316.70
180.0	308.96	323.94	323.22	326.02	325.89	325.46	323.05
240.0	313.64	326.19	325.89	328.01	328.23	327.83	325.65
300.0	317.11	327.52	327.73	329.57	329.94	329.45	327.46
360.0	319.33	328.47	328.62	330.35	330.71	330.15	328.43
420.0	321.01	329.22	329.21	330.78	331.13	330.55	329.09
480.0	322.53	329.77	329.65	331.08	331.50	330.86	329.62
540.0	323.50	330.16	329.98	331.33	331.66	331.04	329.97
600.0	324.07	330.33	330.04	331.89	331.77	331.08	330.17
660.0	324.28	330.22	329.98	331.20	331.66	330.99	330.04
720.0	324.82	330.55	330.20	331.51	331.87	331.17	330.32
780.0	325.03	330.61	330.20	331.51	331.93	331.17	330.37
840.0	325.25	330.66	330.26	331.51	331.93	331.13	330.40
960.0	325.36	330.66	330.20	331.51	331.87	331.22	330.41
1080.0	325.47	330.78	330.26	331.51	331.93	331.26	330.48
1200.0	325.74	330.83	330.31	331.58	331.98	331.26	330.55

RUN 2 INJECTION 1 RADIUS=0.6096M
FLOWRATE=1482CM**3/MIN FOR 0.2 RADIANS
FLOWRATE=0.77634X10**-3 M**3/SEC FOR A FULL CIRCLE

TEMPERATURE IN DEGREES KELVIN

HEIGHT ABOVE BOTTOM OF FLOW LAYER IN METERS

TIME	0.0762	0.3048	0.6096	0.7520	0.9144	1.2192	AVG
1320.0	325.80	330.89	330.31	331.64	331.98	331.31	330.59
1440.0	325.91	330.89	330.37	331.64	332.03	331.31	330.62
1560.0	325.96	331.17	330.59	331.89	332.25	330.63	330.63
1740.0	326.07	330.49	329.82	331.14	331.50	330.90	330.22
1920.0	325.85	329.77	329.11	330.17	330.66	330.28	329.53
2130.0	325.80	330.61	330.15	331.27	331.61	330.95	330.31

RUN 2 INJECTION 1 RADIUS=1.524M
FLOWRATE=1482CM**3/MIN FOR 0.2 RADIANS
FLOWRATE=0.77634X10**-3 M**3/SEC FOR A FULL CIRCLE

TEMPERATURE IN DEGREES KELVIN

HEIGHT ABOVE BOTTOM OF FLOW LAYER IN METERS

TIME	0.0762	0.3048	0.6096	0.7520	0.9144	1.2192	1.4478	AVG
0.0	296.97	296.31	297.38	297.82	297.50	297.44	297.50	297.26
60.0	297.06	296.33	297.38	297.87	297.92	306.89	300.70	299.70
120.0	297.21	296.61	297.50	298.31	299.71	311.75	304.05	301.68
180.0	298.15	297.21	297.88	299.34	302.27	314.82	306.90	303.54
240.0	298.57	298.23	298.66	300.90	305.02	315.47	308.97	304.94
300.0	299.57	299.32	299.94	302.77	307.55	316.67	310.71	306.47
360.0	300.81	300.61	301.90	305.16	310.25	318.34	312.56	308.31
420.0	302.45	302.73	296.17	308.25	313.45	320.34	314.39	309.54
480.0	304.44	306.01	308.73	312.04	316.87	322.34	316.51	313.43
540.0	306.80	309.23	313.47	316.28	320.36	324.17	318.45	316.33
600.0	308.84	311.98	317.48	273.16	322.94	325.38	319.77	314.72
660.0	310.53	314.55	320.53	322.18	324.66	326.06	320.92	320.37
720.0	312.57	317.91	323.30	324.52	326.32	326.91	322.07	322.28
780.0	314.37	320.27	325.29	326.15	327.39	327.40	322.89	323.63
840.0	315.80	321.85	326.62	327.23	328.05	327.78	323.55	324.58
900.0	317.01	323.09	327.57	327.93	328.56	328.00	324.07	325.29
960.0	317.99	323.60	328.32	328.47	328.95	328.22	324.56	325.81
1020.0	318.76	321.61	328.76	328.83	329.18	328.33	324.90	325.76
1080.0	319.47	322.10	329.09	329.07	329.29	328.45	325.19	326.06
1140.0	319.94	324.33	329.26	329.20	329.41	328.56	325.44	326.60
1200.0	320.28	325.39	329.48	329.32	329.52	328.61	325.69	326.93
1260.0	320.72	325.84	329.59	329.44	329.58	328.67	325.84	327.12
1320.0	320.94	326.07	329.70	329.51	329.64	328.73	326.05	327.27
1380.0	321.21	325.75	329.76	329.57	329.64	328.78	326.20	327.29
1440.0	321.12	325.53	329.82	329.63	329.64	328.84	326.30	327.30
1500.0	321.29	325.44	329.87	329.57	329.69	328.84	326.40	327.33

RUN 2 INJECTION 1 RADIUS=1.524M
FLOWRATE=1482CM**3/MIN FOR 0.2 RADIANS
FLOWRATE=0.77634X10**-3 M**3/SEC FOR A FULL CIRCLE

TEMPERATURE IN DEGREES KELVIN

HEIGHT ABOVE BOTTOM OF FLOW LAYER IN METERS

TIME	0.0762	0.3048	0.6096	0.7520	0.9144	1.2192	1.4478	AVG
1560.0	321.47	325.43	329.93	329.63	329.75	328.95	326.50	327.41
1620.0	321.56	325.21	329.99	329.69	329.81	329.07	326.66	327.46
1680.0	321.75	325.44	329.93	329.69	329.81	328.95	326.66	327.48
1740.0	321.97	325.48	330.04	329.75	329.58	328.95	326.76	327.52
1800.0	321.84	325.57	330.11	329.82	329.81	328.95	326.81	327.58
1860.0	321.61	326.03	330.10	329.82	329.81	329.01	326.87	327.67
1920.0	321.79	326.26	330.10	329.75	329.81	328.84	326.87	327.68
1980.0	321.84	326.26	330.04	329.69	329.69	328.84	326.87	327.66
2040.0	321.84	326.12	329.99	329.63	329.64	328.84	327.13	327.69
2100.0	321.75	325.98	329.93	329.57	329.64	328.90	326.97	327.61
2160.0	321.56	325.94	329.93	329.57	329.64	328.95	327.07	327.62

RUN 2 INJECTION 1 RADIUS=3.048M
FLOWRATE=1482CM**3/MIN FOR 0.2 RADIANS
FLOWRATE=0.77634X10**-3 M**3/SEC FOR A FULL CIRCLE

TEMPERATURE IN DEGREES KELVIN

HEIGHT ABOVE BOTTOM OF FLOW LAYER IN METERS

TIME	0.0762	0.3048	0.6096	0.7520	0.9144	1.2192	1.4478	AVG
0.0	296.87	296.97	295.56	297.10	297.01	297.32	297.46	296.98
240.0	296.91	297.04	295.73	297.41	295.31	306.25	299.74	298.89
360.0	296.97	297.10	296.71	299.74	303.09	314.23	303.03	302.35
480.0	297.06	297.20	298.87	303.69	308.67	319.40	305.85	305.23
600.0	297.22	297.82	302.36	308.82	313.79	322.70	308.56	308.08
720.0	297.46	298.96	306.32	313.88	318.16	324.47	311.06	310.67
840.0	297.92	300.80	310.40	318.11	321.02	325.46	313.19	312.94
900.0	298.31	302.13	312.95	320.20	322.60	325.92	314.27	314.23
960.0	298.91	303.83	315.26	322.19	323.70	326.33	315.36	315.49
1020.0	299.61	305.67	317.41	323.68	324.52	326.64	316.28	316.64
1080.0	300.49	307.82	319.31	325.05	325.68	327.01	317.28	317.88
1140.0	301.58	310.23	321.19	326.17	326.38	327.27	318.14	319.04
1200.0	302.73	312.59	322.72	327.01	326.84	327.48	318.91	320.08
1260.0	304.16	315.11	324.18	327.60	327.41	327.70	319.37	321.07
1320.0	305.61	317.23	325.03	328.09	327.62	327.59	319.92	321.84
1380.0	307.39	319.50	326.21	328.47	328.54	328.13	321.10	323.05
1440.0	308.91	321.06	327.17	328.75	328.54	328.29	321.64	323.74
1500.0	310.53	322.49	327.43	328.86	328.42	328.34	322.19	324.28
1560.0	312.01	323.47	327.59	328.80	328.29	328.29	322.56	324.65
1620.0	313.48	324.43	328.06	328.97	328.50	328.45	322.88	325.14
1680.0	314.73	325.02	328.22	328.86	328.89	328.62	323.45	325.57
1740.0	315.87	325.47	328.38	329.16	328.93	328.62	323.79	325.88
1800.0	316.83	325.98	328.54	329.25	328.33	328.51	324.08	326.05
1860.0	317.72	326.29	328.64	329.31	328.97	328.67	324.43	326.39
1920.0	318.49	326.60	328.75	329.37	328.63	328.78	324.67	326.56
1980.0	319.09	327.06	328.70	329.31	327.58	328.62	324.82	326.55

RUN 2 INJECTION 1 RADIUS=3.048M
FLOWRATE=1482CM**3/MIN FOR 0.2 RADIANS
FLOWRATE=0.77634X10**-3 M**3/SEC FOR A FULL CIRCLE

TEMPERATURE IN DEGREES KELVIN

HEIGHT ABOVE BOTTOM OF FLOW LAYER IN METERS

TIME	0.0762	0.3048	0.6096	0.7520	0.9144	1.2192	1.4478	AVG
2040.0	319.63	326.91	328.75	329.20	328.21	328.56	325.07	326.70
2100.0	319.86	326.29	327.85	328.64	328.00	327.37	324.18	326.01

RUN 2 INJECTION 1 RADIUS=4.572M
FLOWRATE=1482CM**3/MIN FOR 0.2 RADIANS
FLOWRATE=0.77634X10**-3 M**3/SEC FOR A FULL CIRCLE

TEMPERATURE IN DEGREES KELVIN

HEIGHT ABOVE BOTTOM OF FLOW LAYER IN METERS

TIME	0.0762	0.3048	0.6096	0.7520	0.9144	1.2192	1.4478	AVG
0.0	293.91	296.75	295.02	296.67	298.42	296.57	296.87	296.50
180.0	293.91	296.75	295.02	296.67	298.42	296.57	296.88	296.50
240.0	293.97	296.79	295.06	296.72	298.45	296.60	296.90	296.54
300.0	294.00	296.83	295.11	296.77	298.50	296.67	296.95	296.59
360.0	294.06	296.87	295.15	296.80	298.58	296.82	297.02	296.66
420.0	294.13	296.90	295.20	296.86	298.71	297.09	297.15	296.77
480.0	294.21	296.93	295.28	296.97	298.99	297.57	297.36	296.97
540.0	294.28	296.98	295.40	297.17	299.49	298.30	297.68	297.28
600.0	294.30	297.00	295.55	297.42	300.15	299.20	298.06	297.65
660.0	294.37	297.06	295.85	297.92	301.14	300.42	298.59	298.21
720.0	294.47	297.15	296.27	298.58	302.36	301.83	299.22	298.88
780.0	294.50	297.26	296.79	299.33	303.70	303.29	299.89	299.61
840.0	294.54	297.40	297.44	300.33	305.28	304.97	300.70	300.48
900.0	294.62	297.60	298.18	301.37	306.83	306.53	301.57	301.37
960.0	294.73	297.86	299.04	302.50	308.47	308.11	302.41	302.31
1020.0	294.84	298.15	299.88	303.66	309.91	309.43	303.24	303.17
1080.0	295.05	298.51	300.78	304.81	311.33	310.65	304.06	304.04
1140.0	295.26	298.93	293.57	305.99	312.68	311.81	304.90	303.90
1200.0	295.51	299.37	302.55	307.02	313.88	312.76	305.63	305.69
1260.0	295.84	299.91	303.49	308.11	315.07	313.73	306.40	306.52
1320.0	296.27	300.54	304.52	309.27	316.32	314.66	307.18	307.39
1380.0	296.78	301.24	305.50	310.37	317.48	315.70	307.96	308.28
1440.0	297.30	301.93	306.45	311.38	318.48	316.29	308.64	309.04
1500.0	297.90	302.79	307.50	312.50	319.51	317.06	309.35	309.89
1560.0	298.53	303.68	308.47	313.59	320.45	317.67	309.94	310.67
1620.0	299.23	306.19	309.42	314.67	321.28	318.21	310.51	311.69

RUN 2 INJECTION 1 RADIUS=4.572M
FLOWRATE=1482CM**3/MIN FOR 0.2 RADIANS
FLOWRATE=0.77634X10**-3 M**3/SEC FOR A FULL CIRCLE

TEMPERATURE IN DEGREES KELVIN

HEIGHT ABOVE BOTTOM OF FLOW LAYER IN METERS

TIME	0.0762	0.3048	0.6096	0.7520	0.9144	1.2192	1.4478	AVG
1680.0	300.20	305.89	310.79	315.73	322.32	319.07	311.38	312.47
1740.0	301.18	307.15	312.04	316.84	323.29	319.76	312.02	313.41
1800.0	302.24	308.54	313.25	318.00	324.20	320.37	312.75	314.37
1860.0	303.37	310.07	314.61	319.17	325.02	320.99	313.42	315.36
1920.0	304.46	311.48	315.80	320.14	325.72	321.46	314.00	316.23
1980.0	305.64	313.00	317.01	321.10	326.32	321.90	314.57	317.10
2040.0	306.77	313.85	317.81	321.67	326.73	322.07	314.97	317.67
2100.0	307.73	315.25	318.59	322.23	326.83	322.28	315.30	318.25
2160.0	308.98	316.91	319.79	323.50	327.46	322.84	315.99	319.24

RUN 2 INJECTION 1 RADIUS=0.096M
FLOWRATE=1482CM**3/MIN FOR 0.2 RADIANS
FLOWRATE=0.77634X10**-3 M**3/SEC FOR A FULL CIRCLE

TEMPERATURE IN DEGREES KELVIN

HEIGHT ABOVE BOTTOM OF FLOW LAYER IN METERS

TIME	0.0762	0.3048	0.6096	0.7520	0.9144	1.2192	1.4478	AVG
0.0	295.84	296.22	296.18	298.11	295.83	295.99	296.09	296.22
180.0	295.84	296.22	296.18	298.11	295.83	295.99	296.09	296.22
240.0	295.88	296.28	296.26	298.19	295.90	296.03	296.11	296.27
300.0	295.92	296.33	296.31	298.24	295.97	296.07	296.14	296.32
360.0	295.96	296.37	296.37	298.29	296.03	296.11	296.16	296.36
420.0	296.00	296.41	296.42	298.35	296.07	296.15	296.20	296.40
480.0	296.04	296.47	296.50	298.42	296.14	296.20	296.22	296.45
540.0	296.10	296.52	296.56	298.47	296.21	296.24	296.25	296.50
600.0	296.13	296.56	296.59	298.54	296.28	296.27	296.26	296.53
660.0	296.19	296.60	296.67	298.60	296.31	296.32	296.30	296.58
720.0	296.25	296.68	296.77	298.69	296.37	296.38	296.37	296.66
780.0	296.28	296.72	296.81	298.71	296.44	296.42	296.40	296.70
840.0	296.30	296.76	296.86	298.75	296.48	296.46	296.42	296.73
900.0	296.36	296.84	296.93	298.84	296.55	296.52	296.50	296.80
960.0	296.39	296.89	296.99	298.91	296.64	296.58	296.53	296.86
1020.0	296.41	296.93	297.06	298.97	296.69	296.63	296.57	296.90
1100.0	296.46	296.98	297.12	299.07	296.82	296.71	296.61	296.97
1140.0	296.50	297.02	297.20	299.21	296.96	296.79	297.15	297.17
1200.0	296.52	297.09	297.30	299.36	297.16	296.89	296.73	297.14
1260.0	296.56	297.12	297.41	299.60	297.43	297.03	296.82	297.26
1320.0	296.62	297.20	297.59	299.93	297.65	297.21	296.84	297.40
1380.0	296.65	297.28	297.80	300.35	298.30	297.51	296.97	297.64
1440.0	296.71	297.33	298.05	300.82	298.83	297.81	297.09	297.87
1500.0	296.77	297.43	298.36	301.40	299.48	298.21	297.26	298.17
1560.0	296.76	297.46	298.72	301.99	300.19	298.67	297.42	298.47
1620.0	296.87	297.68	299.12	302.79	301.02	299.24	297.64	298.89

RUN 2 INJECTION 1 RADIUS=6.096M
FLOWRATE=1482CM**3/MIN FOR 0.2 RADIANS
FLOWRATE=0.77634X10**-3 M**3/SEC FOR A FULL CIRCLE

TEMPERATURE IN DEGREES KELVIN

HEIGHT ABOVE BOTTOM OF FLOW LAYER IN METERS

TIME	0.0762	0.3048	0.6096	0.7520	0.9144	1.2192	1.4478	AVG
1680.0	296.94	297.86	299.63	303.50	301.80	299.82	297.93	299.31
1740.0	297.07	298.07	300.20	304.40	302.74	300.58	298.28	299.83
1800.0	297.20	298.31	300.78	305.27	303.68	301.34	298.62	300.36
1860.0	297.38	298.63	301.47	306.22	304.67	302.21	299.10	300.98
1920.0	297.56	298.94	302.12	307.10	305.60	303.01	299.53	301.56
1980.0	297.76	299.29	302.81	308.03	306.56	303.88	300.00	302.18
2040.0	297.97	299.65	303.45	308.93	307.45	304.71	300.48	302.78
2100.0	298.14	299.93	304.06	309.57	308.15	305.47	300.89	303.29
2160.0	298.46	300.37	304.80	310.56	306.69	306.31	301.37	303.64

RUN 2 PUMPING RADIUS=0.3048M
FLOWRATE=1482CM**3/MIN FOR 0.2 RADIANS
FLOWRATE=0.77634X10**-3 M**3/SEC FOR A FULL CIRCLE

TEMPERATURE IN DEGREES KELVIN

HEIGHT ABOVE BOTTOM OF FLOW LAYER IN METERS

TIME	0.3048	0.6096	0.7520	0.9144	1.2192	AVG
0.0	331.08	332.19	332.07	332.06	331.91	331.80
55.0	327.66	330.50	331.03	330.99	329.36	329.66
115.0	325.67	329.07	330.13	330.09	328.84	328.49
175.0	324.45	328.16	329.45	329.52	328.43	327.72
235.0	323.39	327.36	328.90	329.02	327.97	327.02
295.0	322.48	326.72	328.42	328.59	327.63	326.45
355.0	321.48	325.95	327.88	328.17	327.24	325.81
415.0	320.69	325.29	327.42	327.81	326.91	325.28
475.0	320.02	324.68	326.95	327.39	326.52	324.77
555.0	319.21	323.91	326.33	326.93	326.19	324.17
615.0	318.71	323.37	325.78	326.47	325.82	323.70
675.0	318.22	322.85	325.18	326.07	325.18	323.17
735.0	317.89	322.39	324.86	325.68	324.70	322.77
795.0	317.60	321.99	324.38	325.29	324.28	322.38
855.0	317.35	321.56	323.71	324.87	323.73	321.94
915.0	317.07	321.17	323.51	324.43	323.27	321.57
975.0	316.83	320.78	323.05	324.01	322.78	321.18
1035.0	316.49	320.33	322.56	323.54	322.19	320.72
1095.0	316.19	319.88	322.07	323.08	321.66	320.28
1155.0	315.93	319.44	321.55	322.57	321.05	319.82
1215.0	315.71	318.82	320.94	321.98	320.40	319.29
1275.0	315.36	318.26	320.35	321.45	319.81	318.78
1335.0	314.66	317.64	319.64	320.79	319.10	318.10
1395.0	314.19	317.03	319.03	320.19	318.41	317.51
1455.0	313.70	316.37	318.32	319.52	317.73	316.88
1515.0	313.13	315.63	317.55	318.74	316.95	316.16

RUN 2 PUMPING RADIUS=0.3048M
FLOWRATE=1482CM**3/MIN FOR 0.2 RADIANS
FLOWRATE=0.77634X10**-3 M**3/SEC FOR A FULL CIRCLE

TEMPERATURE IN DEGREES KELVIN

HEIGHT ABOVE BOTTOM OF FLOW LAYER IN METERS

TIME	0.3048	0.6096	0.7520	0.9144	1.2192	AVG
1575.0	312.62	314.94	316.80	318.03	316.23	315.49
1635.0	312.15	314.30	316.11	317.33	315.57	314.87
1695.0	311.65	313.62	315.38	316.58	314.89	314.22
1755.0	311.14	312.93	314.67	315.86	314.19	313.56
1815.0	310.60	312.21	313.88	315.08	313.44	312.86
1875.0	310.07	311.49	313.13	314.30	312.71	312.17
1935.0	309.58	310.83	312.46	313.62	312.08	311.56
1995.0	309.07	310.16	311.76	312.93	311.40	310.92
2055.0	308.56	309.47	311.05	312.20	310.71	310.26
2115.0	308.10	308.89	310.40	311.52	310.07	309.67
2160.0	307.77	308.40	309.94	311.05	309.60	309.23

RUN 2 PUMPING RADIUS=0.6096M
FLOWRATE=1482CM**3/MIN FOR 0.2 RADIANS
FLOWRATE=0.77634X10**-3 M**3/SEC FOR A FULL CIRCLE

TEMPERATURE IN DEGREES KELVIN

HEIGHT ABOVE BOTTOM OF FLOW LAYER IN METERS

TIME	0.0762	0.3048	0.6096	0.7520	0.9144	1.2192	AVG
5.0	325.74	330.27	329.09	331.27	331.61	330.99	330.06
55.0	324.71	328.15	329.32	330.65	330.97	329.53	329.02
155.0	323.55	326.85	328.46	329.99	330.40	328.85	328.14
175.0	322.58	325.89	327.83	329.46	329.99	328.42	327.49
235.0	321.59	324.95	327.16	328.99	329.53	327.96	326.83
295.0	320.68	324.18	326.60	328.58	329.17	327.59	326.27
355.0	319.70	323.57	326.04	328.12	328.82	327.17	325.73
415.0	327.93	322.73	325.50	327.72	328.48	326.81	326.19
475.0	318.27	322.15	325.06	327.33	328.13	326.45	324.73
555.0	317.49	321.48	324.39	326.78	327.64	325.93	324.13
615.0	316.99	321.00	323.91	326.29	327.26	325.54	323.68
675.0	316.61	320.57	323.40	325.86	326.92	325.15	323.27
735.0	316.33	320.15	322.99	325.43	326.50	324.73	322.86
795.0	316.17	319.81	322.54	325.01	326.17	324.31	322.50
855.0	316.01	319.44	322.09	324.54	325.71	323.86	322.09
915.0	315.81	319.15	321.69	324.18	325.34	323.41	321.74
975.0	315.57	318.75	321.26	323.73	324.93	322.98	321.34
1035.0	315.25	318.35	320.79	323.23	324.48	322.47	320.89
1095.0	315.10	317.92	320.24	322.73	324.00	321.94	320.43
1155.0	314.87	317.49	319.74	322.25	323.52	321.42	319.98
1215.0	314.41	316.89	319.21	321.54	322.91	320.80	319.39
1275.0	313.82	316.33	318.50	320.98	322.36	320.23	318.80
1335.0	313.42	315.79	317.80	320.29	321.66	319.51	318.17
1395.0	312.81	315.18	317.23	319.62	321.09	318.84	317.55
1455.0	312.26	314.56	316.49	318.93	320.41	318.18	316.89
1515.0	311.59	313.85	315.67	318.12	319.64	317.42	316.13

RUN 2 PUMPING RADIUS=0.6096M
FLOWRATE=1482CM**3/MIN FOR 0.2 RADIANS
FLOWRATE=0.77634X10**-3 M**3/SEC FOR A FULL CIRCLE

TEMPERATURE IN DEGREES KELVIN

HEIGHT ABOVE BOTTOM OF FLOW LAYER IN METERS

TIME	0.0762	0.3048	0.6096	0.7520	0.9144	1.2192	AVG
1576.0	311.06	313.23	314.94	317.38	318.88	316.71	315.45
1635.0	310.62	312.63	314.26	316.66	318.17	316.07	314.81
1695.0	310.03	311.95	313.48	315.88	317.38	315.37	314.09
1755.0	309.45	311.29	312.75	315.13	316.61	314.68	313.40
1815.0	308.96	310.62	312.02	314.33	315.83	313.97	312.69
1875.0	308.33	309.95	311.22	313.52	315.01	313.22	311.95
1935.0	307.81	309.35	310.57	312.80	314.27	312.57	311.30
1995.0	307.33	308.72	309.85	312.08	313.53	311.90	310.64
2055.0	306.79	308.09	309.16	311.32	312.75	311.19	309.95
2115.0	306.31	307.55	308.53	310.61	312.03	310.55	309.33
2160.0	306.04	307.17	308.10	310.13	311.50	310.07	308.89

RUN 2 PUMPING RADIUS=1.524M
FLOWRATE=1482CM**3/MIN FOR 0.2 RADIANS
FLOWRATE=0.77634X10**-3 M**3/SEC FOR A FULL CIRCLE

TEMPERATURE IN DEGREES KELVIN

HEIGHT ABOVE BOTTOM OF FLOW LAYER IN METERS

TIME	0.0762	0.3048	0.6096	0.7520	0.9144	1.2192	1.4478	AVG
5.0	321.07	325.57	329.87	329.51	329.64	328.90	327.02	327.49
30.0	320.32	325.08	329.70	329.38	329.52	328.67	326.82	327.21
65.0	319.77	324.20	329.42	329.20	329.35	328.39	326.56	326.83
115.0	319.26	323.34	329.04	328.95	329.18	328.11	326.35	326.46
175.0	318.72	322.59	328.65	328.65	328.95	327.84	326.10	326.08
235.0	318.39	321.89	328.16	328.23	328.67	327.51	325.79	325.67
295.0	317.83	321.21	327.73	327.87	328.33	327.24	325.49	325.26
355.0	317.44	320.66	327.20	327.52	328.00	326.91	325.10	324.85
415.0	316.93	320.12	326.78	327.00	327.67	326.59	324.80	324.45
475.0	316.47	319.70	326.31	326.60	327.34	326.27	324.46	324.07
555.0	316.21	319.14	325.70	325.98	326.80	325.85	324.02	323.58
615.0	315.84	318.73	325.19	325.54	326.43	325.49	323.64	323.18
675.0	315.55	318.30	324.65	324.94	325.95	325.13	323.31	322.76
735.0	315.36	317.91	324.16	324.52	325.53	324.77	322.99	322.40
795.0	315.15	317.55	323.63	323.99	325.07	324.42	322.66	322.01
855.0	314.93	317.14	323.06	323.43	324.56	324.02	322.34	321.59
915.0	314.65	316.73	322.55	322.92	324.11	323.63	322.07	321.21
1035.0	313.36	315.60	321.23	321.65	322.94	322.76	321.44	320.19
1155.0	312.61	314.52	319.84	320.26	321.67	321.78	320.79	319.18
1275.0	311.85	313.19	318.27	318.77	320.23	320.69	320.06	318.03
1395.0	310.71	312.15	316.56	317.05	318.52	319.34	319.14	316.73
1515.0	309.41	310.79	314.88	315.39	316.75	317.89	318.05	315.31
1635.0	308.35	309.52	313.27	313.78	315.13	316.48	316.55	313.86
1755.0	306.96	308.23	311.68	312.29	313.55	315.10	315.78	312.59
1825.0	305.95	306.59	310.15	310.80	311.94	313.63	314.47	311.14
1995.0	305.04	305.93	308.83	309.51	310.51	312.35	313.30	310.00

RUN 2 PUMPING RADIUS=1.524M
FLOWRATE=1482CM**3/MIN FOR 0.2 RADIANS
FLOWRATE=0.77634X10**-3 M**3/SEC FOR A FULL CIRCLE

TEMPERATURE IN DEGREES KELVIN

HEIGHT ABOVE BOTTOM OF FLOW LAYER IN METERS

TIME	0.0762	0.3048	0.6096	0.7520	0.9144	1.2192	1.4478	AVG
2055.0	304.60	305.46	308.16	308.85	309.79	311.66	312.65	309.38
2160.0	304.02	304.49	307.09	307.81	308.66	310.55	311.66	308.38

RUN 2 PUMPING RADIUS=3.048M
FLOWRATE=1482CM**3/MIN FOR 0.2 RADIANS
FLOWRATE=0.77634X10**-3 M**3/SEC FOR A FULL CIRCLE

TEMPERATURE IN DEGREES KELVIN

HEIGHT ABOVE BOTTOM OF FLOW LAYER IN METERS

TIME	0.0762	0.3048	0.6096	0.7520	0.9144	1.2192	1.4478	AVG
0.0	320.57	326.97	328.97	329.25	328.12	328.40	325.33	326.85
30.0	320.61	326.75	328.75	329.14	328.42	328.51	324.97	326.74
65.0	320.69	326.29	328.48	328.97	327.91	327.96	324.77	326.42
115.0	320.41	325.42	327.79	327.01	327.17	327.32	324.18	325.66
175.0	320.69	325.17	327.95	328.47	328.04	327.11	324.23	325.87
235.0	320.29	324.23	327.33	328.53	327.66	326.95	323.84	325.43
295.0	320.14	323.70	326.71	327.81	327.05	326.48	323.41	324.93
355.0	319.71	323.09	326.16	327.33	326.20	326.02	323.03	324.41
415.0	319.28	322.35	325.86	327.06	326.20	325.36	322.65	323.98
475.0	318.71	321.46	325.08	326.33	325.72	324.76	322.00	323.31
555.0	318.08	320.34	323.85	325.35	324.79	323.98	321.50	322.46
615.0	317.54	318.11	321.92	324.66	323.25	322.75	319.16	320.76
675.0	316.94	318.50	321.90	323.97	321.68	322.52	320.66	320.86
735.0	316.25	317.45	320.53	322.88	321.32	321.79	320.09	320.05
795.0	315.51	316.45	319.25	321.51	320.45	320.94	319.58	319.17
855.0	314.79	315.42	317.44	320.76	319.56	319.99	319.04	318.25
915.0	314.09	314.67	317.12	319.91	318.41	319.49	318.75	317.66
1035.0	312.56	312.60	314.89	317.76	316.54	317.71	316.69	315.71
1155.0	311.17	311.20	312.79	314.89	314.18	315.71	316.05	314.04
1275.0	309.83	309.66	310.98	313.75	312.42	314.06	315.00	312.59
1395.0	308.26	308.14	309.10	311.34	309.93	312.43	313.79	310.89
1515.0	306.37	306.39	307.23	309.89	307.58	308.92	311.98	308.75
1635.0	306.06	305.58	305.52	307.95	310.75	309.48	310.65	308.37
1755.0	305.05	304.87	304.81	307.09	305.69	308.19	310.19	307.05
1875.0	304.07	303.48	303.56	305.79	304.43	306.85	308.82	305.75
1995.0	303.28	303.05	302.42	304.67	303.15	305.71	307.99	304.82

RUN 2 PUMPING RADIUS=3.048M
FLOWRATE=1482CM**3/MIN FOR 0.2 RADIANS
FLOWRATE=0.77634X10**-3 M**3/SEC FOR A FULL CIRCLE

TEMPERATURE IN DEGREES KELVIN

HEIGHT ABOVE BOTTOM OF FLOW LAYER IN METERS

TIME	0.0762	0.3048	0.6096	0.7520	0.9144	1.2192	1.4478	AVG
2055.0	302.81	302.65	301.95	304.09	302.94	305.19	304.44	303.60
2160.0	302.21	302.02	301.21	303.06	302.30	304.38	306.61	303.60

RUN 2 PUMPING RADIUS=4.572M
FLOWRATE=1482CM**3/MIN FOR 0.2 RADIANS
FLOWRATE=0.77634X10**-3 M**3/SEC FOR A FULL CIRCLE

TEMPERATURE IN DEGREES KELVIN

HEIGHT ABOVE BOTTOM OF FLOW LAYER IN METERS

TIME	0.0762	0.3048	0.6096	0.7520	0.9144	1.2192	1.4478	AVG
0.0	309.33	317.05	320.09	323.60	327.61	322.87	316.11	319.39
60.0	309.58	315.71	319.22	322.60	326.78	322.14	315.63	318.65
120.0	309.33	313.78	317.48	321.32	324.29	320.66	315.06	317.28
180.0	309.25	312.70	317.01	319.80	324.01	320.02	314.68	316.67
240.0	308.93	311.65	315.65	318.40	322.83	319.16	314.14	315.76
300.0	308.57	310.70	315.03	317.41	321.87	318.30	314.17	315.15
360.0	307.99	309.56	313.48	316.24	320.32	317.23	313.72	314.14
420.0	307.92	309.31	313.38	315.59	319.72	316.74	313.56	313.83
480.0	307.38	308.35	312.29	314.26	318.48	318.68	312.99	313.40
535.0	306.73	307.68	311.29	313.20	317.09	314.63	312.53	312.06
595.0	306.29	307.04	309.86	311.86	315.54	313.55	312.12	311.15
655.0	305.68	306.34	309.34	310.91	314.47	312.64	311.53	310.40
715.0	305.21	305.32	308.45	309.92	313.31	311.64	311.06	309.57
775.0	304.72	305.17	307.52	308.88	312.07	310.69	310.51	308.85
835.0	304.24	304.64	306.68	307.86	311.02	309.72	309.94	308.10
895.0	303.74	304.12	305.91	306.90	309.94	308.82	309.39	307.37
955.0	303.22	303.57	305.09	306.06	308.81	307.87	308.75	306.60
1015.0	302.79	303.17	304.45	305.27	307.98	307.11	308.25	306.00
1075.0	302.15	302.14	303.24	304.35	306.78	305.83	307.30	304.95
1135.0	301.94	302.30	303.14	303.93	306.32	305.60	307.16	304.78
1195.0	301.47	301.85	302.50	303.33	305.52	304.82	306.61	304.17
1255.0	301.12	301.50	301.86	302.56	304.86	304.16	306.09	303.61
1315.0	300.72	301.04	301.34	302.14	304.18	303.53	305.63	303.10
1375.0	300.16	300.62	300.62	301.57	303.53	302.92	305.04	302.51
1435.0	299.83	300.41	300.20	300.87	303.07	302.47	304.57	302.09
1500.0	299.47	300.05	299.66	300.54	302.51	301.78	304.08	301.60

RUN 2 PUMPING RADIUS=4.572M
FLOWRATE=1482CM**3/MIN FOR 0.2 RADIANS
FLOWRATE=0.77634X10**-3 M**3/SEC FOR A FULL CIRCLE

TEMPERATURE IN DEGREES KELVIN

HEIGHT ABOVE BOTTOM OF FLOW LAYER IN METERS

TIME	0.0762	0.3048	0.6096	0.7520	0.9144	1.2192	1.4478	AVG
1560.0	298.27	299.73	298.94	299.36	301.62	300.86	303.73	300.90
1620.0	298.78	299.40	298.51	299.65	301.41	300.99	303.24	300.73
1680.0	298.33	299.41	298.23	299.58	301.28	300.79	302.80	300.50
1740.0	298.19	299.16	298.33	299.32	301.18	300.51	302.70	300.35
1800.0	297.96	299.02	298.06	299.13	300.96	300.23	302.39	300.11
1860.0	297.60	298.81	297.79	298.88	300.62	299.94	302.01	299.80
1920.0	297.32	298.64	297.40	298.64	300.43	299.69	301.72	299.54
1980.0	297.10	298.50	297.28	298.46	300.27	299.41	301.44	299.33
2040.0	296.84	298.28	297.04	298.29	300.01	299.23	301.20	299.11
2100.0	296.68	298.19	296.90	298.05	299.87	299.01	300.85	298.90
2160.0	296.27	298.01	296.54	297.76	299.68	298.74	300.61	298.64

RUN 2 PUMPING RADIUS=6.096M
FLOWRATE=1482CM**3/MIN FOR 0.2 RADIANS
FLOWRATE=0.77634X10**-3 M**3/SEC FOR A FULL CIRCLE

TEMPERATURE IN DEGREES KELVIN

HEIGHT ABOVE BOTTOM OF FLOW LAYER IN METERS

TIME	0.0762	0.3048	0.6096	0.7520	0.9144	1.2192	1.4478	AVG
0.0	298.48	300.50	304.95	310.83	309.28	306.38	301.57	304.09
60.0	298.67	300.40	304.61	309.78	308.07	305.56	301.53	303.66
120.0	298.50	300.16	304.18	308.64	306.87	304.49	301.30	303.08
180.0	298.64	299.89	303.59	307.39	305.64	303.67	301.15	302.54
240.0	298.56	299.76	302.86	306.70	304.77	302.77	301.05	302.08
300.0	298.68	299.68	302.75	306.03	303.70	302.46	300.97	301.80
360.0	298.62	299.50	302.27	305.23	303.12	301.87	300.75	301.41
420.0	298.54	299.31	301.71	304.49	302.32	301.34	300.48	300.98
480.0	298.42	299.06	301.13	303.72	301.37	300.70	300.31	300.53
535.0	298.38	298.96	300.87	303.27	300.97	300.35	300.17	300.29
695.0	298.23	298.77	300.10	302.54	299.98	299.59	299.77	299.74
655.0	298.19	298.64	300.06	302.23	299.86	299.59	299.77	299.67
715.0	298.04	298.48	299.68	301.69	299.40	299.25	299.56	299.37
760.0	297.95	298.39	299.46	301.42	299.10	299.06	299.45	299.20
835.0	297.81	298.22	299.17	301.07	298.78	298.76	299.23	298.95
850.0	297.85	298.20	299.07	300.95	298.68	298.47	299.10	298.84
965.0	297.85	298.24	299.05	300.93	298.59	298.69	299.17	298.88
1025.0	297.76	298.07	298.02	300.67	298.35	298.47	299.04	298.60
1085.0	297.72	298.03	298.66	300.49	298.19	298.33	298.91	298.58
1145.0	297.20	297.64	298.33	299.81	297.81	297.43	298.51	298.07
1195.0	297.59	297.91	298.30	300.11	297.76	297.96	298.64	298.29
1255.0	297.53	297.79	298.11	299.97	297.56	298.50	298.48	298.25
1315.0	297.36	297.73	297.98	299.70	297.36	297.57	298.29	297.96
1375.0	297.39	297.62	297.75	299.60	297.05	297.38	298.21	297.82
1435.0	297.35	297.64	297.72	299.39	297.03	297.25	298.07	297.74
1495.0	297.19	297.47	297.04	299.18	296.64	297.03	297.83	297.45

RUN 2 PUMPING RADIUS=6.096M
FLOWRATE=1482CM**3/MIN FOR 0.2 RADIANS
FLOWRATE=0.77634X10**-3 M**3/SEC FOR A FULL CIRCLE

TEMPERATURE IN DEGREES KELVIN

HEIGHT ABOVE BOTTOM OF FLOW LAYER IN METERS

TIME	0.0762	0.3048	0.6096	0.7520	0.9144	1.2192	1.4478	AVG
1555.0	297.23	297.25	297.27	298.85	296.57	297.01	296.86	297.16
1615.0	296.96	296.77	297.17	297.55	296.05	296.18	297.50	296.89
1675.0	297.19	297.23	296.90	298.85	295.90	296.14	297.49	297.04
1750.0	297.15	297.21	297.11	298.65	296.40	296.78	297.57	297.23
1810.0	297.12	297.25	297.04	298.71	296.35	296.82	297.51	297.22
1870.0	297.10	297.18	296.99	298.69	296.40	296.86	297.49	297.20
1930.0	297.03	297.15	296.93	298.70	296.39	296.86	297.46	297.18
1990.0	296.96	297.14	296.83	298.66	296.37	296.73	297.42	297.12
2050.0	296.88	297.06	296.94	298.74	296.40	296.88	297.42	297.15
2110.0	296.90	297.09	296.93	298.78	296.50	296.92	297.34	297.16

RUN 2 INJECTION 2 RADIUS=0.3048M
FLOWRATE=1482CM**3/MIN FOR 0.2 RADIANS
FLOWRATE=0.77634X10**-3 M**3/SEC FOR A FULL CIRCLE

TEMPERATURE IN DEGREES KELVIN

HEIGHT ABOVE BOTTOM OF FLOW LAYER IN METERS

TIME	0.3048	0.6096	0.7520	0.9144	1.2192	AVG
4.0	307.71	308.38	309.67	310.56	310.40	309.29
10.0	307.79	309.74	310.17	311.65	312.71	310.41
14.0	307.98	312.40	313.00	313.92	316.43	312.66
20.0	308.29	316.60	316.76	317.61	321.85	316.04
30.0	310.43	322.55	322.41	323.54	328.26	321.12
40.0	312.78	325.55	325.51	326.53	330.20	323.70
50.0	315.49	327.50	327.70	328.47	331.05	325.59
60.0	317.92	328.73	328.90	329.58	331.42	326.88
80.0	321.00	329.90	330.07	330.47	331.67	328.25
100.0	323.05	330.50	330.51	330.93	331.91	329.07
120.0	324.40	330.95	331.28	331.32	331.60	329.59
180.0	327.19	331.62	331.68	331.72	332.04	330.64
240.0	328.56	332.04	332.07	332.80	332.10	331.33
300.0	329.06	331.41	331.35	331.26	331.48	330.80
420.0	329.50	331.41	331.28	329.32	331.60	330.57
540.0	330.34	332.04	331.94	331.92	332.29	331.64
660.0	330.74	331.01	330.77	330.60	330.62	330.74
780.0	329.18	328.16	328.59	328.41	328.37	328.57
900.0	328.32	332.35	332.41	332.81	334.29	331.92

RUN 2 INJECTION 2 RADIUS=0.6096M
FLOWRATE=1482CM**3/MIN FOR 0.2 RADIANS
FLOWRATE=0.77634X10**-3 M**3/SEC FOR A FULL CIRCLE

TEMPERATURE IN DEGREES KELVIN

HEIGHT ABOVE BOTTOM OF FLOW LAYER IN METERS

TIME	0.0762	0.3048	0.6096	0.7520	0.9144	1.2192	AVG
10.0	305.92	307.14	307.86	309.96	311.11	310.37	308.82
20.0	305.90	307.19	307.88	309.99	311.03	311.35	309.04
30.0	305.87	307.29	307.96	309.99	311.03	312.54	309.33
40.0	305.92	307.60	308.23	310.31	311.33	313.86	309.83
50.0	305.97	308.23	308.80	310.41	311.97	315.45	310.54
60.0	306.09	309.32	309.80	313.08	313.14	317.30	311.87
80.0	306.51	311.86	312.17	314.87	315.90	320.30	314.20
100.0	307.28	314.83	315.11	318.25	319.10	322.94	316.93
120.0	308.22	317.49	317.99	321.35	321.99	325.07	319.41
180.0	311.75	323.47	324.33	327.39	327.74	328.63	324.60
240.0	314.83	325.64	326.34	329.57	329.22	329.71	326.49
300.0	317.88	327.78	328.62	330.71	331.08	330.72	328.35
420.0	321.40	328.58	328.89	330.47	330.97	330.63	328.90
540.0	322.99	329.22	329.32	330.90	331.29	330.99	329.47
660.0	324.07	330.22	330.04	331.64	331.98	331.26	330.19
780.0	325.41	329.88	329.48	330.90	331.18	330.01	329.68
900.0	324.60	327.62	327.31	328.52	328.97	329.06	327.88

RUN 2 INJECTION 2 RADIUS=1.524M
FLOWRATE=1482CM**3/MIN FOR 0.2 RADIANS
FLOWRATE=0.77634X10**-3 M**3/SEC FOR A FULL CIRCLE

TEMPERATURE IN DEGREES KELVIN

HEIGHT ABOVE BOTTOM OF FLOW LAYER IN METERS

TIME	0.0762	0.3048	0.6096	0.7520	0.9144	1.2192	1.4478	AVG
60.0	304.14	304.73	307.36	308.18	309.06	310.96	311.45	308.56
120.0	304.32	305.07	307.90	308.80	310.05	312.87	312.15	309.36
240.0	304.98	306.14	309.51	311.26	314.77	319.00	315.81	312.53
300.0	306.06	307.36	311.17	313.71	318.11	322.10	318.18	314.76
360.0	307.22	308.84	313.34	316.36	320.94	324.12	320.35	316.83
420.0	308.63	310.93	316.29	319.29	323.33	325.59	322.11	318.89
480.0	310.16	313.39	321.63	321.99	325.17	326.70	323.54	321.10
540.0	311.88	315.89	322.45	324.36	326.64	327.40	324.65	322.53
600.0	313.42	317.77	324.55	325.87	327.61	328.06	325.59	323.83
660.0	315.20	320.16	326.42	327.34	328.56	328.78	326.51	325.20
720.0	317.40	322.51	327.89	328.47	329.41	329.29	327.34	326.45
780.0	318.97	323.50	328.76	329.14	329.69	329.41	327.81	327.09
840.0	319.47	324.16	328.96	329.19	329.58	328.84	327.65	327.12
900.0	319.38	323.90	329.09	329.19	329.46	328.61	327.65	327.03

RUN 2 INJECTION 2 RADIUS=3.048M
FLOWRATE=1482CM**3/MIN FOR 0.2 RADIANS
FLOWRATE=0.77634X10**-3 M**3/SEC FOR A FULL CIRCLE

TEMPERATURE IN DEGREES KELVIN

HEIGHT ABOVE BOTTOM OF FLOW LAYER IN METERS

TIME	0.0762	0.3048	0.6096	0.7520	0.9144	1.2192	1.4478	AVG
60.0	301.90	302.22	301.40	303.59	302.44	304.83	306.61	303.76
120.0	301.88	302.66	301.99	303.77	302.88	306.38	306.96	304.33
180.0	301.92	303.01	302.52	304.77	304.04	310.43	307.89	305.59
240.0	302.14	303.21	303.38	306.15	306.27	315.17	309.58	307.35
300.0	302.42	304.01	304.29	307.15	308.63	318.75	311.27	309.02
360.0	302.59	304.22	305.31	308.90	311.82	321.03	312.29	310.38
420.0	302.91	304.89	306.80	313.91	312.62	321.74	314.23	311.82
480.0	303.19	305.43	308.67	313.91	316.40	323.36	315.11	313.13
540.0	303.49	313.06	310.54	316.43	318.10	324.03	314.51	315.05
600.0	303.69	306.50	312.11	318.03	319.01	324.37	317.08	315.11
660.0	304.18	306.70	312.43	319.53	320.89	325.41	316.13	315.52
720.0	304.09	307.35	314.50	322.05	321.37	324.86	318.34	316.62
780.0	305.11	309.98	318.04	323.02	324.22	326.53	320.57	318.85
840.0	305.65	311.29	319.20	324.36	325.14	326.85	321.37	319.74
900.0	306.23	311.96	320.36	324.51	325.45	327.01	321.55	320.17

RUN 2 INJECTION 2 RADIUS=4.572M
FLOWRATE=1482CM**3/MIN FOR 0.2 RADIANS
FLOWRATE=0.77634X10**-3 M**3/SEC FOR A FULL CIRCLE

TEMPERATURE IN DEGREES KELVIN

HEIGHT ABOVE BOTTOM OF FLOW LAYER IN METERS

TIME	0.0762	0.3048	0.6096	0.7520	0.9144	1.2192	1.4478	AVG
120.0	296.30	298.39	296.96	298.23	300.20	299.34	300.94	299.05
240.0	296.64	298.88	297.51	298.85	300.88	300.08	301.34	299.58
480.0	297.40	299.93	298.64	300.31	302.44	301.74	302.41	300.82
600.0	297.88	300.40	299.64	301.21	303.77	302.94	302.83	301.61
720.0	298.67	301.25	300.73	302.82	306.62	305.39	303.77	303.09
840.0	299.76	302.39	302.73	304.99	310.67	309.16	305.63	305.40
900.0	300.16	302.54	301.41	306.03	311.05	309.60	306.17	305.64

RUN 2 INJECTION 2 RADIUS=6.096M
FLOWRATE=1482CM**3/MIN FOR 0.2 RADIANS
FLOWRATE=0.77634X10**-3 M**3/SEC FOR A FULL CIRCLE

TEMPERATURE IN DEGREES KELVIN

HEIGHT ABOVE BOTTOM OF FLOW LAYER IN METERS

TIME	0.0762	0.3048	0.6096	0.7520	0.9144	1.2192	1.4478	AVG
120.0	296.79	296.99	296.98	298.67	296.53	296.76	297.26	297.08
240.0	296.85	297.23	297.06	298.39	296.64	296.95	297.36	297.19
360.0	296.72	297.20	297.22	298.85	296.15	296.88	296.49	296.94
480.0	296.93	297.39	297.44	299.33	297.13	297.32	514.27	351.70
600.0	296.97	297.41	297.56	299.53	297.85	297.41	297.53	297.65
720.0	296.97	297.48	297.56	299.66	297.55	297.60	297.61	297.69
840.0	297.31	297.72	298.00	300.19	298.04	298.11	297.97	298.09
900.0	297.48	297.98	298.55	300.74	298.62	298.46	298.25	298.47

LIST OF SYMBOLS

Symbol	Definition	Units
a	$\sqrt{\frac{K_2\rho_1 C_1}{K_1\rho_2 C_2}}$	———
A	Area	L^2
A_t	Total area out top, bottom, and sides of laboratory model	L^2
A_b	Area for heat transfer out the top and bottom = $2r\ \Delta\theta\ \Delta r$	L^2
A_s	Area for heat transfer out the sides of the model = $2\Delta rh$	L^2
b	Flow layer thickness	L
C	Specific heat	$FLM^{-1}deg^{-1}$
C_f	Specific heat of flowing fluid	$FLM^{-1}deg^{-1}$
C_r	Specific heat of the porous media	$FLM^{-1}deg^{-1}$
C_w	Specific heat of water	$FLM^{-1}deg^{-1}$
C_2	Specific heat of confining layer	$FLM^{-1}deg^{-1}$
d_b	Bulk density	ML^{-3}
d_p	Mean particle diameter	L
f	Subscript denoting flowing fluid properties	———
g	Accelleration of gravity	LT^{-2}
h	Flow layer thickness	L
h_1	Water level measured at radius r_1	L
h_2	Water level measured at radius r_2	L
k_i	Intrinsic permeability	L^2

LIST OF SYMBOLS (continued)

Symbol	Definition	Units
K	Thermal conductivity	$FT^{-1}deg^{-1}$
K_0	Stagnant thermal conductivity	$FT^{-1}deg^{-1}$
K_1	Thermal conductivity of combined porous media and flowing fluid	$FT^{-1}deg^{-1}$
K_2	Thermal conductivity of confining layers	$FT^{-1}deg^{-1}$
n	Summation counter	____
P	Hydraulic conductivity	LT^{-1}
Pe	Peclet number = $\frac{Vd_p}{\alpha_1}$	____
Q	Injection flowrate	L^3T^{-1}
r	Subscript denoting porous media	____
r	Radial distance from well	L
R	Dimensionless radius = $\frac{2r}{h}$	____
t	Time	T
T	Temperature	deg
T_i	Fluid injection temperature	deg
T_o	Average initial aquifer temperature	deg
$\overline{T}$	Dimensionless temperature = $\frac{T-T_o}{T_i-T_o}$	____
$\overline{V}$	Fluid pore water velocity vector	LT^{-1}
V	Fluid pore water velocity	LT^{-1}
Vol	Incremental volume of an incremental radius (Δr) = $r\ \Delta\theta\ \Delta r$	L^3
w	Subscript denoting water properties	____
x	Horizontal distance	L

LIST OF SYMBOLS (continued)

Symbol	Definition	Units
y	Integration parameter	———
z	Vertical distance above or below aquifer midplane	L
0	Subscript referring to initial aquifer conditions	———
1	Subscript referring to total porous media, combined fluid properties	———
2	Subscript referring to properties of caprock and bedrock	———
α	$\frac{\lambda a-1}{\lambda a+1}$	———
α_1	Thermal diffusivity of the flow layer $\frac{K_o}{\rho_1 C_1}$	L^2T^{-1}
ν	Dimensionless flowrate = $\frac{Q\rho_f C_f}{4\pi h K_1}$	———
ϵ	Thermal efficiency	———
η	$\frac{2z}{h}$ for $z \geq h/2$	———
η	1 for $z \leq h/2$	———
θ	$\frac{\rho_1 C_1}{\rho_2 C_2}$	———
λ	$\frac{K_1}{K_2}$	———
μ	Viscosity of fluid	$FL^{-2}T$
ξ	$\frac{4K_2 x}{h^2 \rho_f C_f V}$ (for cartesian coordinates)	———

LIST OF SYMBOLS (continued)

Symbol	Definition	Units
ξ	$\frac{4K_2\pi r^2}{h\rho_f C_f Q}$ (for cylindrical coordinates)	———
π	3.14159	———
ρ	Density	ML^{-3}
ρ_f	Density of flowing fluid	ML^{-3}
ρ_p	Particle density	ML^{-3}
ρ_r	Porous media density	ML^{-3}
ρ_w	Water density	ML^{-3}
ρ_2	Confining layer density	ML^{-3}
$\rho_1 C_1$	Specific heat capacity of flow layer = $\phi\rho_w C_w + (1-\phi)\rho_r C_r$	$FL^{-2}deg^{-1}$
τ	$\frac{4K_2 t}{h^2\rho_1 C_1}$	———
ϕ	Porosity	———
erfc	Complimentary Error Function	———
Γ	Gamma Function	———
U	Unit Step Function defined as $U(\tau-\xi)=0$ when $(\tau-\xi)\leq 0$ and $U(\tau-\xi) = 1$ when $(\tau-\xi) > 0$	———
∇	Vector "del" operator	L^{-1}
Δr	Incremental radius	L
$\Delta\theta$	Incremental angle	radians